Low-Temperature Effects on Sandwich Composites under Low-Velocity Impact

By

Alejandra G. Castellanos

A dissertation submitted in partial fulfillment of

the requirements for the degree of

Doctor of Philosophy

(Civil and Environmental Engineering)

at the

UNIVERSITY OF WISCONSIN-MADISON

2019

Date of final oral examination: 04/19/2019

The dissertation is approved by the following members of the Final Oral Committee:

Pavana Prabhakar, Assistant Professor, Civil and Environmental Engineering
Hannah Blum, Assistant Professor, Civil and Environmental Engineering
Bu Wang, Assistant Professor, Civil and Environmental Engineering
Tim Osswald, Professor, Mechanical Enginereering

TABLE OF CONTENTS

Page

Page

LIST OF TABLES

Table Page

LIST OF FIGURES

Figure Page

Figure Page

Figure Page

Figure Page

ABSTRACT

Recent interest in Arctic exploration has brought new challenges concerning the mechanical behavior of light weight materials for offshore structures. Polymeric sandwich composites have become an attractive option for such applications due to their lightweight, high stiffness and high strength to weight ratios. However, exposure to seawater and cold temperatures are known to degrade the mechanical properties of several materials, thus, compromising the safety of personnel and structures. Therefore, it is critical to establish a detailed understanding of the mechanical behavior and damage mechanisms of sandwich composites and its constituents under these harsh conditions to enable their use in these situations. This work addresses the fundamental challenges of damage mitigations, failure mechanisms and life of composites in extreme environments through computational and experimental investigations. In particular, the low-temperature effects on the sandwich and laminated composites under low-velocity impacts. The single and repeated impact response of woven carbon/vinyl ester composites under Arctic temperatures was investigated. The main damage mechanisms were identified to elucidate the damage by the variation in temperature and impact energy. Then a computational model was developed to predict the failure mechanisms under the single low-velocity impact. After identifying the dominant failure mechanisms, a novel printed reinforcement was proposed to increase the fracture toughness under quasi-static loading on woven carbon/epoxy laminates. After that, the single impact response of woven carbon/vinyl ester sandwich composites with Polyvinyl chloride (PVC) foam core at low temperatures (25 °C, 0 °C, -25 °C and -50 °C) was investigated. Key failure mechanisms were identified to understand how temperature and impact energy affected the sandwich composite. Finally, a printed reinforcement design was studied to mitigate the damage during a low-velocity impact on sandwich composites. A computational model of a woven carbon/epoxy sandwich composite was developed

to study parameters such as reinforcement spacing, pattern design, and damage mitigation to select the optimal reinforcement design. Finally, the novel reinforcement was incorporated to woven carbon/epoxy sandwich composites with Polyvinyl chloride (PVC) foam core and the single impact response was investigated.

Chapter 1

Introduction

Economic and environmental demands have forced different industries such as marine, aerospace, and automobile to use lightweight structures to reduce their fuel consumption. At the same time, these structures must maintain their stiffness, strength, and damage tolerance. Lightweight structures require the use of high-performance materials, such as composite materials and the use of geometrically efficient structure, such as sandwich composites [3]. *In this chapter, we introduce the readers to fiber reinforced composites, sandwich composites, dynamic impact loading and general organization of the thesis.*

1.1 Composite Materials

Composite materials consist of two or more materials that are superior to those of the individual constituents [4]. There are two general phases of the constituent materials: the matrix phase and the reinforcing phase. The matrix phase is responsible for binding the reinforcements and transferring the loads between the reinforcing phase [5]. The most common matrix phases are metal, ceramic and polymer. Although the matrix phase is weak as compared to the reinforcing phase, it offers compressive strength, thermal resistance and fatigue resistance, which influences many mechanical properties of the overall composite [6]. The reinforcing phase is responsible for providing stiffness and strength to the composite. Typical reinforcing phases are particulate (spherical, platelets or any other geometry [7]) or fiber reinforcement (discontinuous or continuous). Continuous fiber reinforcements can be unidirectional (Figure 1.1(a)), bi-directional (Figure 1.1(b)) or randomly oriented (Figure 1.1(c)). The fibers are arranged in layers known as lamina, which are stacked to create a laminate. Woven fabric with fibers arranged in plain weave is the most commonly used bi-directional reinforcement in which each warp yarn crosses alternatively under an

over each weft yarn [8]. This configuration prevents a crack from propagating due to the change of direction of the yarns.

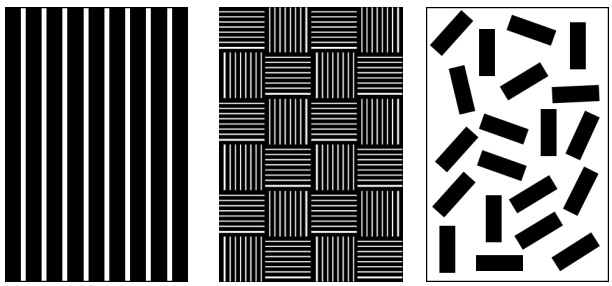

(a) (b) (c)

Figure 1.1: Schematics of different fibers: (a) Uni-directional orientation; (b) Bi-directional orientation; (c) Random orientation.

1.1.1 Fiber Reinforced Polymer Composites (FRPCs)

Fiber reinforced polymer composites consist of fibers reinforced in a polymer matrix (Figure 2.3(b)), where the laminas are stacked to create a laminate (Figure 1.2(b)). The mechanical properties along the fibers are strong and stiff; however, the region between the layers of fiber is a matrix-rich region known as the interlaminar region, which is very weak (Figure 1.2(c)). The mechanical performance of FRPC does not depend only on the constituents, but also on the interactions at the fiber-matrix interface and interlaminar regions. FRPCs offer tailorable mechanical properties, with high stiffness and high strength-to-weight ratio [9, 10, 11]. *Despite several advantages that FRPCs offer, a significant drawback is their low resistance to impact damage.*

1.2 Sandwich Composites

Sandwich composites consist of two thin, but very stiff facesheets (FRPCs), which are bonded to a lightweight core (honeycomb, foam or metallic) by an adhesive (Figure 1.3). The facesheets carry transverse loads or bending moments while the core carries the transverse shear loads [12]. The separation of the facesheets increases the moment of inertia of the panel with little increase of weight, which results in an efficient structure that can resist bending and buckling loads [13].

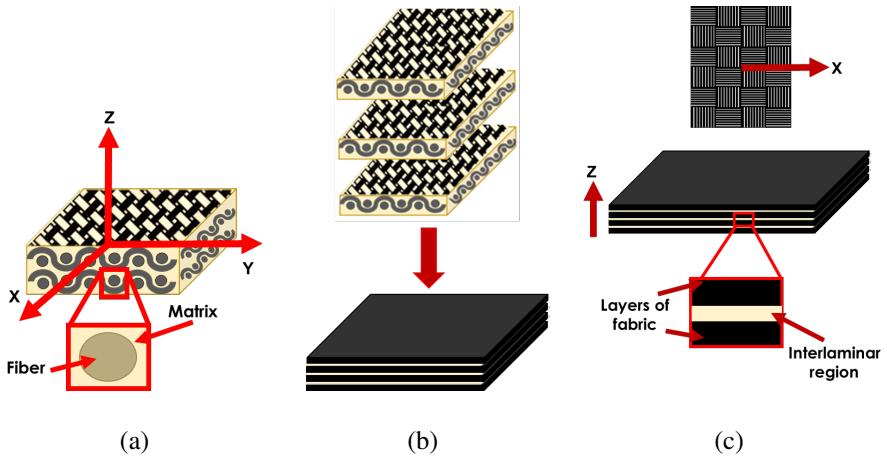

(a) (b) (c)

Figure 1.2: Fiber reinforced polymer composites

Despite several advantages of sandwich composites, a significant drawback is their low resistance to impact damage.

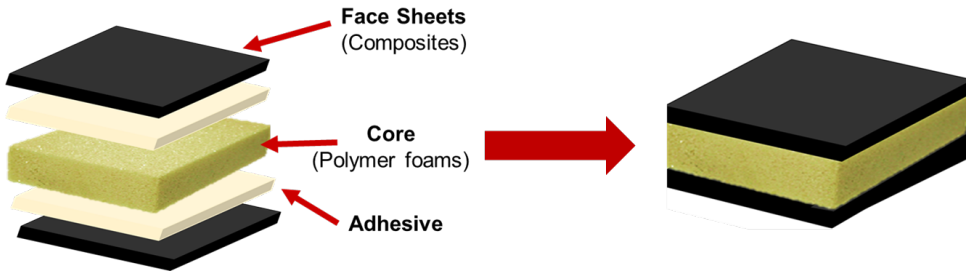

Figure 1.3: Sandwich composites

1.3 Impact Damage

Dynamic impacts on structures can occur under different scenarios, including but not limited to, tool dropping during maintenance, hail strikes, iceberg collision, debris from runways or bird strikes [14, 15, 16], etc. Impact loading is typically divided into low-velocity (Figure 1.4(a)) and high-velocity [17, 18] impact (Figure 1.4(b)), where the velocity less than 10 m/s is termed as low-velocity. Low-velocity impacts produce barely visible damage (BVD) on composite surfaces, with the possibility of significant internal damage that could result in catastrophic failure of the structure without prior warning. Common failure modes observed during low-velocity impacts are matrix cracking (Figure 1.5(a)), fiber breakage (Figure 1.5(b)) and delamination [19, 20, 21]

(Figure 1.5(a)). Of these, delamination, which is the separation of the layers of fabric, is one of the most common failure mechanisms [22]. This often results in the reduction of stiffness, strength, durability and stability of a composite [23, 24]. *Therefore, low-velocity impact studies on FRPCs and sandwich composites is critical for material certification.*

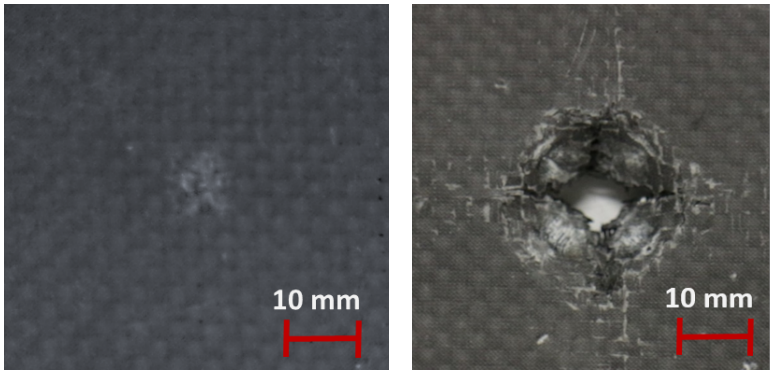

(a) (b)

Figure 1.4: (a) Low-velocity impact damage; (b) High-velocity impact damage

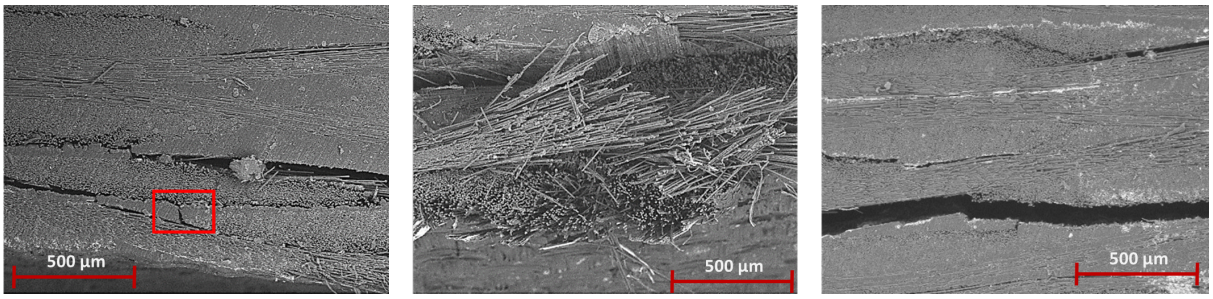

(a) (b) (c)

Figure 1.5: Common failure mechanisms under low-velocity impacts: (a) matrix cracking; (b) Fiber fracture; (c) Delamination

1.4 Main Contributions and Organization of the Thesis

An assessment by the U.S. Geological Survey (USGS) of the Arctic circle has revealed that approximately 22% of the world's undiscovered oil and natural gas resources are located in this region [25]. Due to ice melting in the Arctic, new passages (Northwest and Northeast) have been created, which can become viable transportation routes [26] in the future. Therefore, there has been a great interest in Arctic exploration, which has necessitated the investigation of the mechanical behavior and damage mechanisms of current and future materials when exposed to low temperatures. Offshore structures, such as ship vessels, are typically subjected to adverse environments including but not limited to sea water, wave impacts and extremely low temperatures, which can cause surface alterations, internal damage, and degradation of their chemical and mechanical properties that may ultimately compromise their safety. Therefore, the materials used in these structures must be able to withstand harsh environmental conditions in addition to mechanical loads. Sandwich composites have become an attractive option for marine applications due to their lightweight, high stiffness and high strength to weight ratio [27]. Despite several advantages of sandwich composites, a major drawback is their low resistance to impact damage. Dynamic impact on structures can occur under different scenarios, for example, tool drop during maintenance and repair, wave slamming, iceberg collisions, bird or hail strikes [14, 28, 29]. Low-velocity impacts typically occur at velocities below 10 m/s [17], which may produce barely visible damage (BVD) on composite surfaces (facesheets), but with the possibility of significant internal damage. This is deemed very dangerous, as BVD could result in catastrophic failure of the structure without warning. Therefore, low-velocity impact studies on sandwich composites is critical for material certification and establishing allowable for structural design. In particular, *their response to dynamic impact loading at low temperatures is of main interest in this work in light of arctic applications.*

1.4.1 Objectives

The goal of this work is to address the fundamental challenges of damage mitigation, failure mechanisms and life of composites in extreme environments through computational and experimental investigation. The low-temperature effects on sandwich composites and the facesheets under low-velocity impacts are investigated in this dissertation, and it is organized as follow:

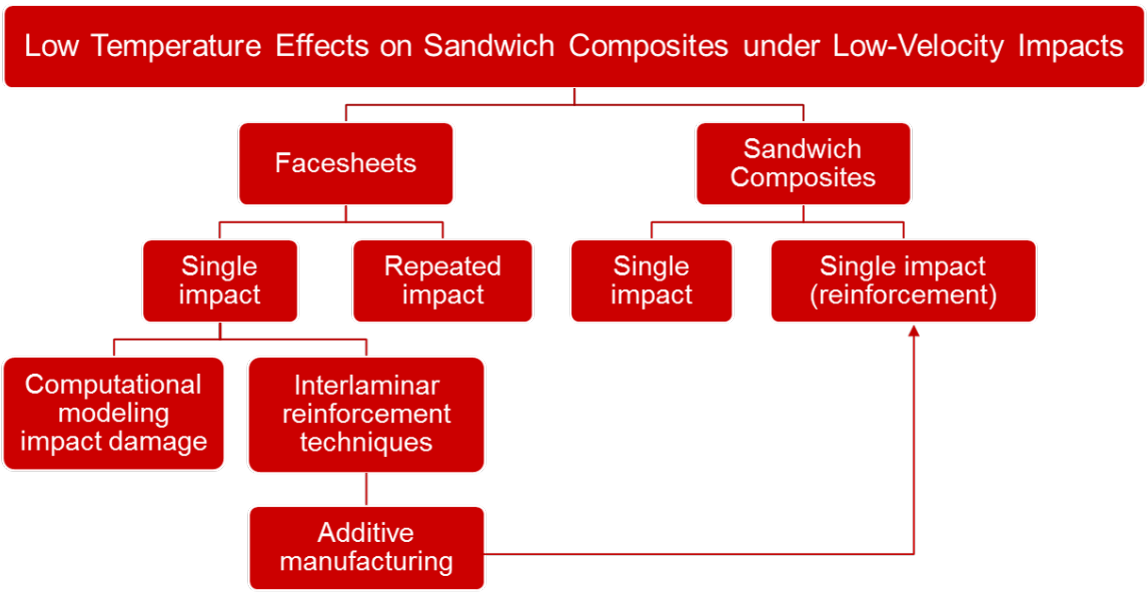

Figure 1.6: Dissertation organization

Chapter 2 explores the influence of combined arctic temperature (-50 °C) and single low-velocity dynamic impact loading on the damage and failure mechanisms of woven carbon/vinyl ester laminates. Next, Chapter 3 explores the influence of combined arctic temperature (-50 °C) and repeated low-velocity dynamic impact loading on the damage and failure mechanisms of woven carbon/vinyl ester laminates. Chapter 4 provides a detailed description of a computational model that can predict the failure mechanisms during a single low-velocity impact event at room temperature. These predictions are found to agree with experimental observations and account for the failure mechanisms of fiber fracture and delamination. Chapter 5 proposes a novel technique for improving the interlaminar fracture toughness of unidirectional carbon fiber reinforced polymeric composites using polymer additive manufacturing (PAM). In Chapter 6, the mechanical response and damage mechanisms of woven/carbon vinyl ester laminated sandwich composites with polyvinyl chloride (PVC) foam core subjected to a range of single low-velocity impact loadings at four different temperatures are investigated. Chapter 7 provides a detailed description of a computational model that can predict delamination during a single low-velocity impact event of woven/carbon vinyl ester laminated sandwich composites with polyvinyl chloride (PVC) foam

core. Also, a PAM pattern design that aids in increasing the damage tolerance of sandwich composites during a low-velocity impact event is proposed. Finally, Chapter 8 provides a summary of the main findings and suggestions for future work.

Chapter 2

Low-Velocity Impact Response of Woven Carbon Composites in Arctic Conditions

2.1 Introduction

Fiber reinforced polymeric composite (FRPC) materials have become an attractive alternative to metals for lightweight applications, such as in aerospace, automobile, and marine structures. FRPCs offer tailorable mechanical properties, with high stiffness and high strength-to-weight ratio [9, 10, 11]. Despite several advantages that FRPCs offer, a major drawback is their low resistance to impact damage due to their layered nature. Further, with increasing interests in arctic explorations, composites used in offshore platforms and vessels are required to withstand harsh environmental conditions of extreme low temperatures along with mechanical loads. Therefore, the motivation of this paper is to explore the influence of combined arctic temperature (-50 °C) and low-velocity dynamic impact loading on the damage and failure mechanisms of woven carbon/vinyl ester laminates.

Dynamic impacts on structure can occur under several different scenarios, including but not limited to, tool dropping during maintenance, hail strikes, iceberg collision, debris from runways or bird strikes [14, 15, 16], etc. Impact loading is typically divided into low-velocity and high-velocity [17, 18] impact, where the velocity less than 10 m/s is termed as low-velocity. Low-velocity impacts produce barely visible damage (BVD) on composite surfaces, with the possibility of significant internal damage that could result in catastrophic failure of the structure without prior warning. Common failure modes observed during low-velocity impacts are matrix cracking, fiber breakage and delamination [19, 20, 21]. Of these, delamination is one of the most common failure mechanisms [22], which often results in the reduction of stiffness, strength, durability and stability of a composite [23, 24].

To establish the durability of composite materials, researchers have studied the effect of impact and temperature on their structural integrity. However, most of the impact studies have focused on low-velocity impact at room temperature on several types of composites. Siow et al. [30] investigated the response of woven carbon fiber/epoxy laminates subjected to impact energies ranging from 4.5 to 10.5 J, and found that the delaminated area increases linearly with increasing impact energy. Liu et al. [31] studied glass/epoxy plates and reported that high-velocity impacts are characterized by penetration-induced fiber breakage, and low-velocity impacts are characterized by delamination and matrix cracking. Sultan et al. [32] studied woven carbon fiber reinforced prepreg laminates with impact energies ranging from 0.4 to 42 J, and reported that matrix cracking occurred below 21 J and fiber breakage manifested in the range of 21 to 31 J of impact energies. Murat et al. [33] tested woven carbon/epoxy prepreg laminates at different impact energy levels in the range of 1 J - 10 J. They observed that thicker samples manifested higher resistance to impact damage and the damage area increased with increasing impact energies.

Despite the extensive amount of research conducted at room temperature (RT), seldom work has been reported on impact under arctic temperatures (AT). Gomez-del Rio et al.[34] measured the response of carbon FRPC under low-velocity impact loading for different stacking sequence (unidirectional, cross-ply, quasi-isotropic and woven) composites and temperatures ranging from 20 °C to -150 °C. They reported that the extent of damage and absorbed energy increased with the decrease in temperature for all tape laminates, however, woven laminates did not exhibited this trend. Badawy [35] investigated the impact behavior of unidirectional and cross-ply glass fiber reinforced polyester (GFRP) under different temperatures of -10 °C, 20 °C, 50 °C and 80 °C, and reported that the damage area increased as temperature decreased. Icten et al.[36] studied the impact behavior of unidirectional glass-epoxy composites at 20 °C, -20 °C and -60 °C with energies varying from 5 J to 70 J, and reported that the dominant failure modes were matrix cracking and delamination for energies below 20 J and fiber breakage was significant at energies above 20 J. Icten[37] also claimed that at low temperatures (-40 °C), the laminates manifested higher peak forces and lower absorbed energy than the samples impacted at room temperature. Salehi-Khojin et al. [38] investigated three combinations of fiberglass and Kevlar woven composites. Three different impact energies were tested (8 J, 15 J, and 25 J) for temperatures ranging from -50 °C to

120 °C. They reported that the deflection, maximum force and energy absorption increases with increasing temperature (from -50 °C to 120 °C) and impact energy (from 8 J to 25 J).

There have been mixed observations with respect to the extent of damage under low-velocity impact loading at low temperatures for woven carbon fiber composites. Therefore, in the current study, the response and failure mechanisms of woven carbon/vinyl ester laminates subject to low-velocity impact at room (25 °C) and arctic temperature (-50 °C) for a range of impact energies are investigated. Vinyl ester is considered in the current study due to superior UV resistance and low water absorption as compared to polyester resins [39, 40], which makes it attractive for ship hull applications. The variations in impact response in terms of force, displacement, energy and damage mechanisms is studied in detail in the current study.

2.2 Methods

2.2.1 Laminate Fabrication

Carbon fiber reinforced composite samples tested at 25 °C and -50 °C were manufactured by vacuum assisted resin transfer molding (VARTM) process [41]. Woven plain weave carbon fabric and vinyl ester resin were purchased from Fibre Glast (www.fibreglast.com). Laminates with 16 layers of dry fabric were manufactured according to the ASTM Standard D7136/D7136M [42]. The layers of fabric were placed between 2 layers of flow-media, 2 layers of breather and 4 layers of nylon peel ply. All layers were cut to dimensions of 305 mm x 305 mm. The arrangement of fabrics was placed between 2 aluminum molds, wrapped with Stretchlon 800 bagging film and sealed with vacuum-sealant tape, ensuring spaces for both inlet and outlet connectors. The woven dry fabrics were reinforced with a mixture of vinyl ester resin and Methyl Ethyl Ketone Peroxide (MEKP) hardener. The resin was catalyzed with 1.25% MEKP by weight and mixed thoroughly as recommended by the manufacturer. The resin/hardener mixture was placed in a desiccator first to remove bubbles from the mixture. The outlet was then connected to a vacuum pump until the vacuum bag achieved a pressure of approximately 80 MPa. The inlet of the vacuum bag was then submerged in the resin/hardener mixture for transferring resin through the laminate. Upon completion of the resin transfer process, the laminate was cured at room temperature for 24 hours. A total of 6 plates of 305 mm length by 305 mm width were manufactured, and six samples were

obtained from each plate. Half the samples from each plate were set aside in a box for testing at room temperature and the other half for arctic temperature. Then, for each combination of temperature and impacted energy, 4 samples were picked from each box for testing. This was done to randomly distribute any manufacture induced effects on impact tests.

2.2.2 Impact Tests

Drop-weight impact tests were performed using a CEAST 9340 Drop Tower Impact System on rectangular laminate samples of 150 mm length x 100 mm width (refer to Figure 4.1(a)) with an average thickness of 4±0.1 mm. These samples were clamped between two metal fixtures with a uniform pressure of 0.2 MPa from the impact machine (refer to Figure 4.1(b)). The test area was a circular opening of 46 cm^2. A hemispherical striker with a mass of 3.0 kg and diameter of 12.7 mm was used to impact the samples at their centers in the out-of-plane direction [42] with kinetic energies of 20 J, 25 J, 30 J, and 35 J for both temperatures (25 °C and -50 °C). The impact velocity was calculated based on the mass of the striker and kinetic energy, using the equation:

$$E_k = \frac{1}{2}m^2 = mgh \tag{2.1}$$

where, E_k is the impact energy or kinetic energy, v is the impact velocity and m is the mass of the impacting striker, h is the height of the striker measured from the surface of a samples in the impact drop tower and g is the gravitational acceleration.

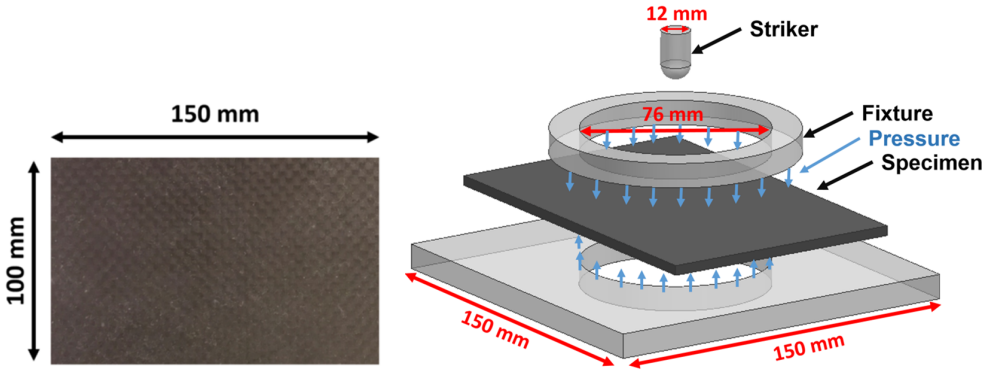

(a) (b)

Figure 2.1: (a) Woven carbon vinyl ester sample; (b) Impact fixture.

For a particular impact energy (20 J, 25 J, 30 J or 35 J), the impact velocity and the striker falling height were adjusted accordingly by the Drop Tower Impact System. For 20 J, 25 J, 30 J and 35 J impact energies, the corresponding impact velocities were 3.64 m/s, 4.07 m/s, 4.46 m/s and 4.82 m/s, respectively. All the tests were low-velocity impacts, that is, below 10 m/s [43]. Robinson et al. [44] investigated the influence of impactor mass and velocity on the low velocity impact performance of woven carbon and glass fiber reinforced laminates for impact energy range from 0.25 J to 12 J. The impactor mass was varied from 1.15 kg to 2.10 kg and the velocity was adjusted to obtain desired impact energies. They reported that the extent of impact damage predominantly depended on the magnitude of the impact energies and not on the mass or velocity individually. Based on this finding, the impactor mass was held constant and the velocity was allowed to vary for prescribed impact energies in the current paper. Force, displacement, energy and time responses were recorded by the data acquisition system "CEAST DAS 8000 Junior" of the impact machine for each test. Schematic of an impact test fixture is shown in Figure 4.1(b). Four samples were impacted for each combination of impact energy (20 J, 25 J, 30 J and 35 J) and temperature (25 °C and -50 °C). Corresponding force-time, displacement-time, energy-time and force-displacement responses were obtained for each test.

The samples planned for testing under in-situ arctic conditions were placed in a Thermo Scientific^{TM} freezer at -50 °C for a period of 90 days. Although a basic heat transfer analysis showed that a uniform temperature of -50 °C can be achieved in these samples in 15-20 min given their relatively small thickness, 90 days exposure prior to testing was chosen to subject the samples to arctic pre-conditioning. To perform the in-situ arctic tests, the samples were removed from the freezer and placed within a temperature controlled environmental chamber, which was connected to the CEAST 9340 Drop Tower Impact System. Prior to every impact test, the environmental chamber was conditioned for 15 minutes with Liquid Nitrogen (LN_2) to reach a uniform temperature of -50 °C.

2.2.3 Micro-CT Scanning

The impacted samples were examined under a micro-CT scanner to evaluate the internal damaged area in arctic and room temperature. For easier handling of the sample and for better resolution of the micro-CT scanning, the samples were reduced to a rectangle of 145 mm in length and

90 mm in width (the original dimensions were 150 mm in length by 100 mm in width). Also, this small reduction in size enabled almost the entire volume of interest to fit in the scanner chamber. Cutting around the edges did not alter the damage that occurred predominantly at the center of the samples and far away from the edges. The impact damage area was centered in this rectangle, and was ensured that no additional damage was imparted to the samples during cutting. A small hole with a diameter of 1.6 mm was drilled at the center of the impacted region of the laminates for applying a dye-penetrant at these holes, upon which the samples were held in a vacuum chamber for five minutes. This procedure was repeated three times to ensure that all damaged regions were filled with the solution. For the first 2 applications of the dye-penetrant, the solution was completely absorbed. A third application ensured that the sample was saturated with the solution, which resulted in complete solution penetration in all available openings, such as delaminations and cracks. Zinc iodide solution was used as the dye-penetrant, which has a high absorption coefficient in comparison to the constituents of the composite materials i.e. carbon fiber and vinyl ester. The Zinc iodide solution was a mixture of alcohol (10 ml), distilled water (10 ml), Kodak photo solution (1 ml) and zinc iodide powder (60 g). Excess dye-penetrant was evaporated by placing the laminates in an oven at 50 °C prior to x-ray scanning. Excess dye penetrant in its liquid phase is not preferred as its motion inside the crack during a scan adversely affects the quality of the 3-D reconstruction. This was eliminated through drying the dye penetrant, which deposits a saline residue on the crack area and in turn provides greater resolution of the damage. Hence, drying the dye penetrant is beneficial. Also, 50 C is enough to dry the samples without creating any thermal damage in the composite. All laminates were scanned with a SkyScan 1173 X-ray microtomograph with the same resolution of 35.9 μm and an angle step of 0.19. The X-ray tube voltage and current were set to 60 kV and 120 microampere, respectively. All the scans were performed using built-in Al filter, and a flat field correction was applied for each scan. The reconstruction was performed using the NRecon commercial software.

2.2.4 Compression Test

Compression tests were performed on pure vinyl ester samples at room and arctic temperatures to examine the strengthening effect of low temperature. Three samples each were tested at in-situ 25 °C and -50 °C under flat-wise compressive loading. Cylindrical specimens with a diameter of

25.4 mm and a height of 50.8 mm were tested according to ASTM D695 standard [45]. These tests were performed using an ADMET eXpert 1000 testing system with a crosshead displacement rate of 1.3 mm/min.

2.3 Results and Discussion

The impact energies considered for the impact tests were 20 J, 25 J, 30 J, and 35 J. Four samples were impacted with the same energy at temperatures of 25 °C and -50 °C each. The time, deformation, energy, force, velocity and voltage were recorded by the data acquisition system CEAST DAS 8000 Junior of the impact machine for each test conducted. In addition, the laminate impact response was evaluated in terms of visual damage, degree of damage and failure mechanisms.

2.3.1 Matrix Strengthening

Mechanical properties of woven carbon/vinyl ester composites change when cooled to arctic temperatures (AT). Prior research by Dutta [46] on the compressive response of glass-fiber-reinforced polymer composites at the U.S. Army Cold Regions Research and Engineering Laboratory (CRREL) showed that their strength and stiffness increases with reducing temperatures. But, also become brittle and are susceptible to cracks due to increase in thermal residual stresses caused by mismatch in the coefficient of thermal expansion (CTE) between the fibers and matrix. The increase in matrix strength is attributed to the binding forces between molecules, which are tightly frozen at AT [47]. Therefore, the tensile and compressive strength of vinyl ester increases at low temperatures. Garcia et al.[48] investigated the flexural response of woven carbon/vinyl ester composites in AT, and reported that dry arctic conditioned samples manifested an $\approx$23% increase in flexural strength with respect to those at room temperature. In addition, compression tests on pure vinyl ester were also conducted in-house as part of the current study to investigate the influence of low temperature. Table 3.1 shows the results from the compressive testing of vinyl ester, where the yield strength (coined as the stress value where the response starts to become non-linear), ultimate strength and elastic modulus increased by approximately 55%, 49% and 28% when cooled from 25 °C to -50 °C. Typical compressive stress-strain response of vinyl ester is shown in Figure 6.3(b), where the yield and final failure strains reduce with reduction in temperature, which implies that deformation of vinyl ester will be lower at AT as compared to those at RT.

Table 2.1: Results from compressive testing of vinyl ester at RT and AT

Mechanical Properties	Temperatures 25 °C	-50 °C	Percentage change (%)
Yield strength (MPa)	47±5	72±4	55
Ultimate strength (MPa)	85±4	126±12	49
Elastic modulus (GPa)	2.6±0.2	3.4±0.1	28

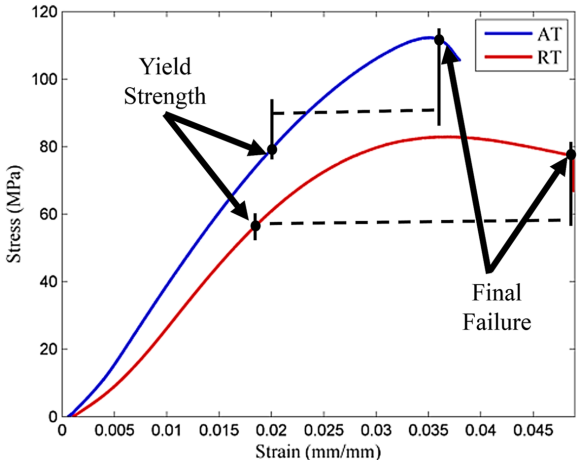

Figure 2.2: Typical compressive stress-strain plots of vinyl ester at RT and AT

2.3.2 Contact Force and Displacement

During an impact test, contact force is generated by the contact of the striker with the impacted face of a sample, which is recorded by the data acquisition system of the impact machine. Figure 2.3(a) shows a representative force-time graph of an impact event, where the maximum impact force corresponds to the peak value of the graph. Figure 2.3(b) shows the variation of maximum impact force for different impact energies for the specimens tested at room and arctic temperature. At both temperatures, the maximum impact force increased with increasing impact energies. In addition, the specimens tested at AT experienced higher impact forces as compared to those tested at RT, which is attributed to the increase in strength of composites when subject to low temperatures as discussed in the section on “Matrix strengthening”. Also, laminates became stiffer at low temperatures rendering them less flexible as compared to those at room temperature.

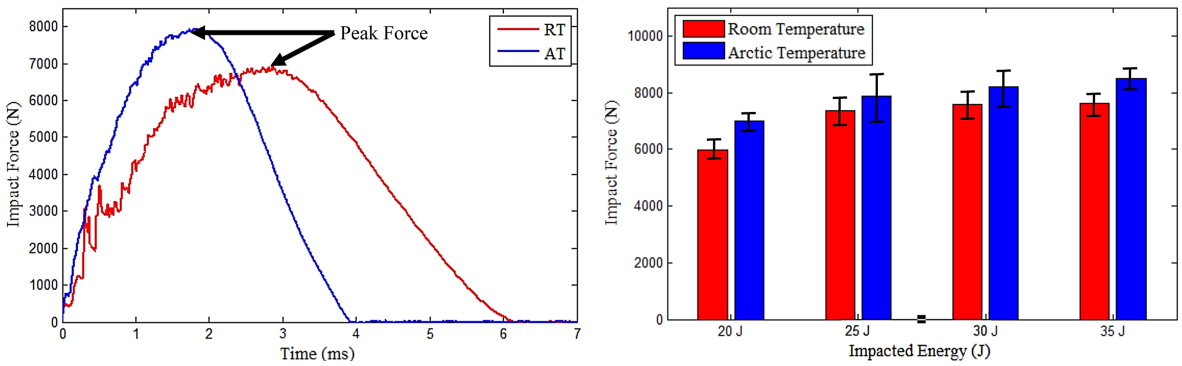

(a) (b)

Figure 2.3: (a) Representative force-time graph of an impact event at 20 J for RT and AT; (b) Impact contact force at RT and AT for 20 J, 25 J, 30 J and 35 J.

Figure 2.4(a) shows a representative force-displacement graph of an impact event. The average initial slopes of the force-displacement responses for the samples tested at different impact energies for both temperatures is shown in Figure 2.4(b), where the samples impacted at arctic temperature manifested higher stiffness values as compared to those at room temperature. This is attributed to the strength increase at low temperatures of the laminates. Due to the increased strength at arctic temperature, lower deflections were observed as compared to the samples tested at room temperature. Figure 3.6 shows the deflection with varying impact energies. As expected, the deflections at both temperatures increased with the increasing impact energies.

Figure 3.11 shows the impacted face and back face of two samples after testing. The samples impacted at 20 J in room and arctic temperature did not exhibit fiber breakage, however, exhibited small regions of matrix cracking at the impacted and back face of the laminate as seen by the enclosed blue curves. On the other hand, the samples at 35 J exhibited a combination of fiber breakage (enclosed by the red circles) and matrix cracking at the back face in both temperatures. Even though the samples at 20 J did not exhibit a significant amount of visible damage externally, there was significant internal damage. To corroborate this prediction, micro-CT scanning was performed on the impacted laminates, results of which are explained in a later section.

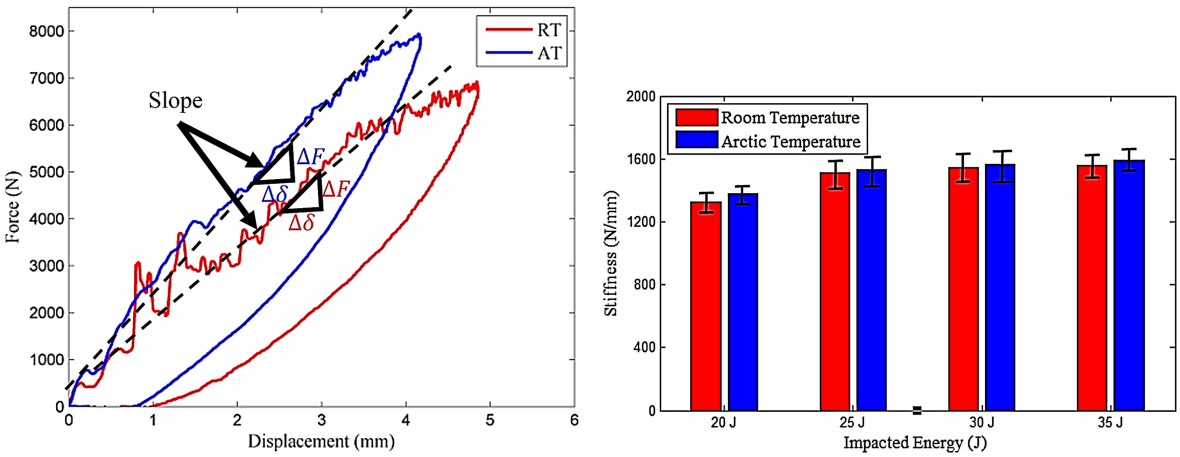

(a) (b)

Figure 2.4: (a) Representative force-displacement graph of an impact event at 20 J for RT and AT; (b) Stiffness (initial slope) at RT and AT for 20 J, 25 J, 30 J and 35 J.

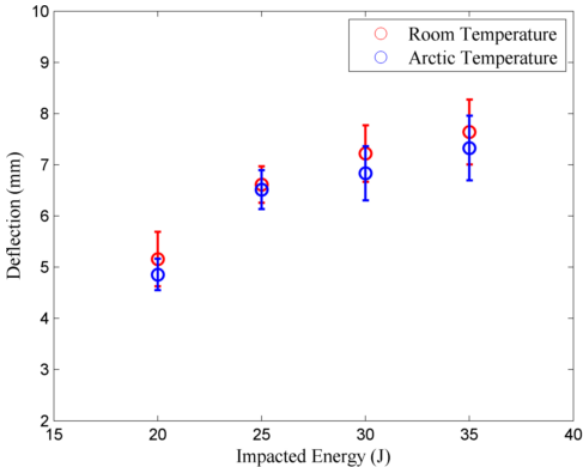

Figure 2.5: Deflection for each impacted energy at room and arctic temperature.

2.3.3 Absorbed Energy

Figure 3.7 shows a typical energy-time response obtained during an impact event on fiber reinforced laminates. The impacted energy is the peak value on the graph and the post peak response (plateau region) is the absorbed energy by the laminate that is manifested as failure mechanisms like matrix cracking, delamination or fiber fracture. The impacted laminates tested here were thin with an average thickness of 4 ± 0.1 mm. As a result, if the impact energy was equal to the absorbed

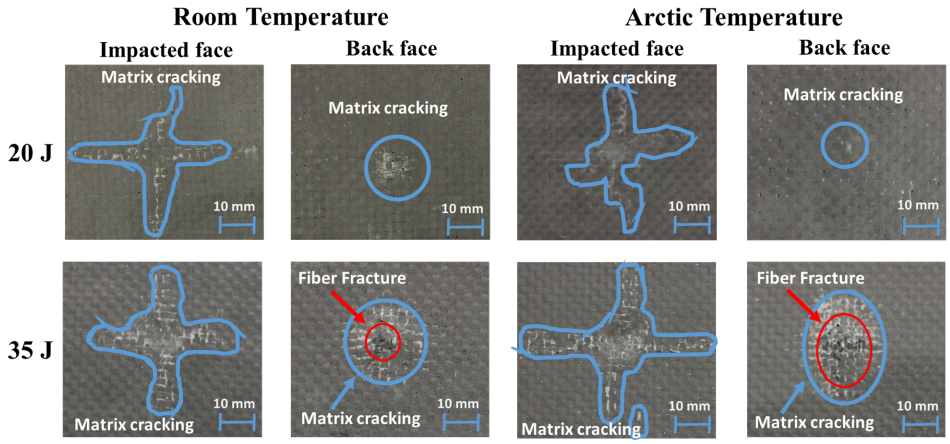

Figure 2.6: Impacted face and back face at 20 and 35 J impact energies at 25 °C and -50 °C.

energy, based on experimental observations, the laminates were deemed here to be completely perforated by the striker as a consequence of no rebound. However, in general, impact energy equals absorbed energy means that there is no rebound and all the impact energy is absorbed by the specimen typically as inelasticity or damage, which is especially true when the specimens are relatively thick or highly damping, in which case complete penetration is difficult to achieve. Increasing absorbed energy implies more damage in the laminate. Figure 2.8(a) shows representative energy-time graphs of the samples impacted at room and arctic temperature for 20 J, 25 J, 30 J and 35 J. In general, it is observed that the samples impacted at arctic temperature (blue color) absorbed less energy than the samples impacted at room temperature (red color).

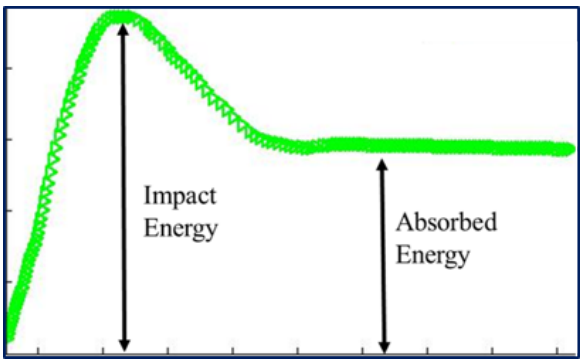

Figure 2.7: Typical energy-time response of an impact event.

To quantify the damage in the laminates, a term called degree of damage (D) coined previously by Belingardi and Vadori [49] was calculated, which is defined as the ratio between the absorbed energy and the impact energy. Figure 2.8(b) shows the degree of damage for different impact energies, where an increasing trend is observed with increasing impact energies. The samples impacted at AT recorded lower degree of damage as compared to the samples tested at RT for a specific impact energy, and is attributed to matrix strengthening at AT.

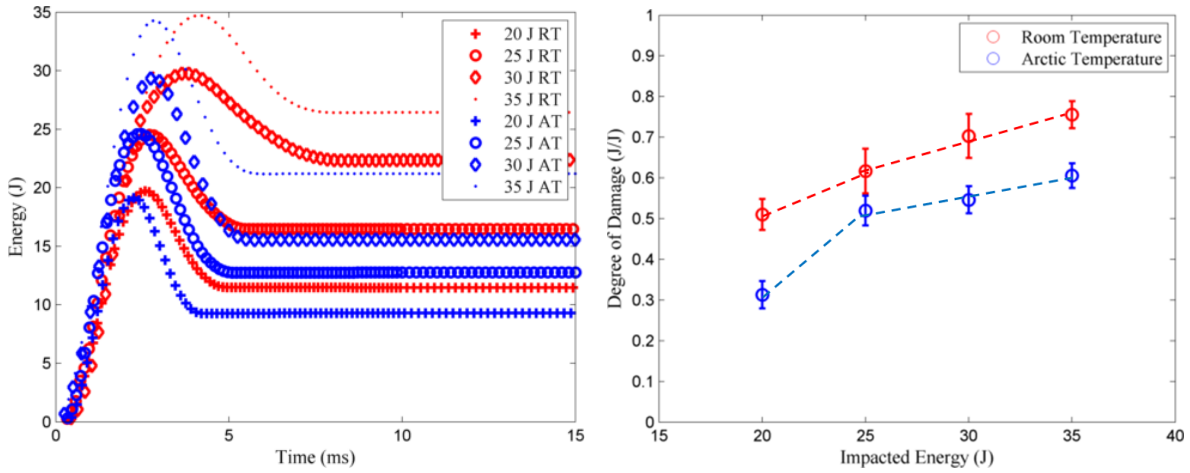

(a) (b)

Figure 2.8: (a)Representative energy-time graph for room (RT: 25 °C) and arctic temperatures (AT: -50 °C) at 20 J, 25 J, 30 J and 35 J, (b) Degree of damage for each impacted energy.

The trend lines in Figure 2.8(b) show a knee formation at 25 J, below which the slope is higher than after. It is known that for fiber reinforced laminates, matrix failure is prevalent at lower impact energies and fiber failure is dominant at higher impact energies. Therefore, the contribution of matrix cracking at lower energies to the degree of damage is significant, whereas, a combination of fiber breakage and matrix cracking contributes at higher energies. However, due to matrix strengthening at AT, the damage in the matrix is lower than damage at RT at low impact energies as explained in the "Matrix strengthening" section. Therefore, the reduction in the degree of damage measured at 20 J between RT and AT is high, about 38% for these laminates. Whereas, at higher impact energies, that is above 25 J, this difference reduces (about 15-22% here) due to lower (but not insignificant) influence of matrix cracking on the degree of damage.

2.3.4 Damage mechanisms

Figure 3.10 shows the micro-CT scan images of samples impacted at 20 J and 30 J in room and arctic temperatures. Regions identified as matrix cracking/delamination (smeared areas) and fiber breakage (sharp defined areas) are highlighted in the images. From the images shown in Figure 3.11, the samples impacted with 20 J energy at both temperatures manifested small regions of visible damage on the impacted and the back faces. However, the micro-CT scan images show considerable internal damage in terms of matrix cracking/delamination and fiber breakage through the thickness of the samples. Fiber breakage is concentrated on the impacted surface with significant matrix cracking and delamination through the thickness of the laminate impacted at 20 J energy in room temperature. On the other hand, at arctic temperature, the overall spread of damage is confined to a smaller region with higher fiber failure traversing through the thickness of the laminate. The reduction in the overall damaged area projected on to the plan of the samples is approximately 36% between RT and AT at 20 J.

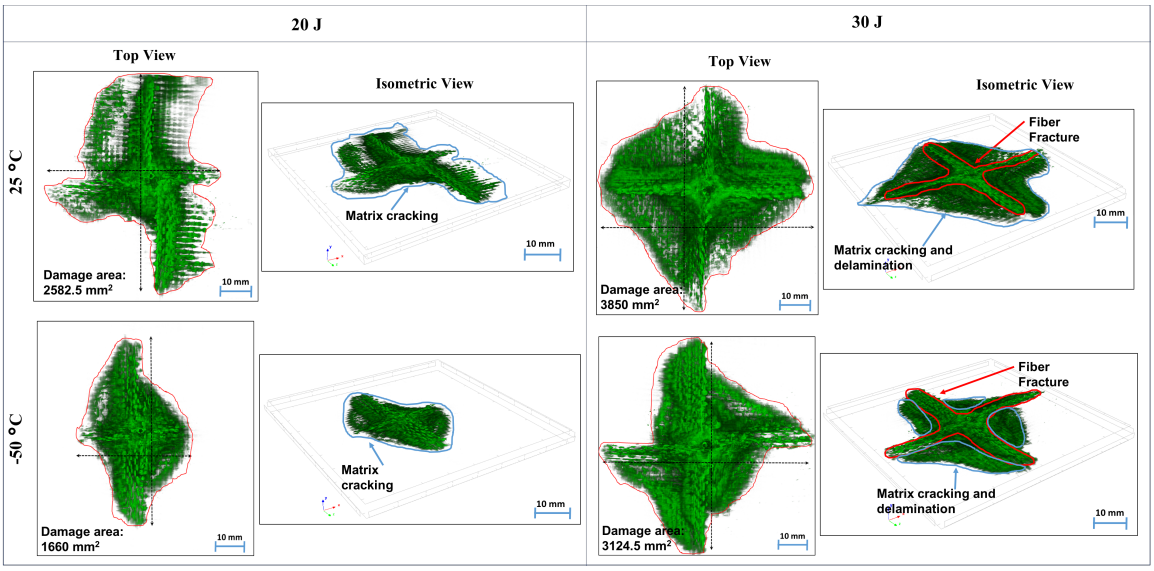

Figure 2.9: Micro-CT scan after the first impact for 20 and 30 J at 25 °C and -50 °C.

The micro-CT scan images for 30 J shown in the Figure 3.10 exhibit significant fiber failure along with matrix failure, and is representative of the samples impacted at higher energies of 25, 30 and 35 J. Fiber failure through the thickness of the samples is higher at AT as compared to RT when impacted by 30 J impact energy. Also, the reduction in the overall damaged area projected

on to the plan of the samples at 30 J is approximately 19% between RT and AT. The observed difference in percentage reduction in damaged area between RT and AT at 20 J and 30 J is due to the increase in strength when composites are subject to low temperatures. The yield strength of the vinyl ester matrix increased up to ≈55% at AT as compared to RT based on the compression tests conducted in the current study, which indicates a delay in the onset of matrix cracks at AT. Consequently, the composite manifested significantly higher fiber failure than matrix cracking as compared to RT for the same impact energy.

2.4 Conclusion

Dynamic impact behavior of woven carbon/ vinyl ester composites at room (25 °C) and arctic (-50 °C) temperatures were investigated in this paper in view of increasing interest in arctic explorations and the need to characterize these composites for arctic applications. Four different impact energies of 20 J, 25 J, 30 J and 35 J were considered for dynamic impact testing at room and in-situ arctic temperatures. Key observations in terms of the contact force, displacement, energy absorbed and failure mechanisms were reported in this paper, as follows:

1. At -50 °C, the rigidity of the laminates increased due to resin strengthening resulting in higher initial stiffness as compared to room temperature.

2. Higher peak forces manifested in laminates impacted at -50 °C for all energies.

3. Increased in strength also resulted in lower displacements in the laminates at -50 °C.

4. The laminates absorbed less energy and correspondingly the degree of damage was lower at -50 °C than at 25 °C.

5. At RT, the dominant failure mechanism was matrix failure (micro cracks/delamination) at low impact energies (20 J). Whereas, for higher impact energies (25 J, 30 J and 35 J), the dominant failure mechanism was fiber fracture along with considerable matrix failure.

6. At AT, the overall damage area projected on to the plane of the composite reduced, however, manifested significantly higher fiber failure as compared to RT for the same impact energy, due to the brittleness of the sample at AT.

7. The percentage reduction in damage area and the average degree of damage value between RT and AT exhibited a decreasing trend with increasing impact energies, as the influence of matrix failure is more dominant at lower impact energies and contribute higher to the extent of damage in a laminate.

In conclusion, failure mechanism shifts from matrix failure towards fiber failure at arctic temperature. Even though the measured degree of damage from the impact tests provide lower values at AT as compared to RT, this shift in failure mechanism can have significant detrimental effect on the residual strengths and durability of the composite.

Chapter 3

Durability and Failure Mechanics of Woven Carbon Composites under Repeated Impact Loading in Arctic Conditions

3.1 Introduction

The rise and demand in arctic exploration has necessitated an in-depth understanding of the mechanical behavior and failure mechanisms of materials exposed to arctic conditions. Structures in such applications are often subjected to adverse environments like sea water, wave impacts or extreme low temperatures, which can cause surface alterations, internal damage, and degradation of chemical and mechanical properties that may ultimately compromise the safety of the naval structure. Therefore, the materials used in these structures must be able to withstand harsh environmental conditions of extreme low temperatures in addition to mechanical loads. Fiber reinforced polymeric composite (FRPC) have become an attractive option for this type of applications due to their corrosion resistance, high strength-to-weight ratio, ability to absorb noise and vibration damping, ease of fabrication, maintenance and repair [50, 51, 52]. They have been successfully integrated in offshore applications such as offshore vessels, ships hulls, tanks or pipes [53, 54]. Despite several advantages that FRPCs offer, a major drawback is their low resistance to impact damage due to their layered nature. Therefore, the motivation of this paper is to investigate the influence of combined arctic temperature (-50 °C) and low-velocity repeated impact loading on the damage and failure mechanisms of woven carbon/vinyl ester laminates.

Dynamic impacts on structures can occur under several different scenarios, including but not limited to, tool drop during maintenance and repair, hail strikes, iceberg collision, wave slamming [14, 28, 29], etc. These impacts are divided into low- and high-velocity. Low-velocity impacts typically occur at velocities below 10 m/s [17], which may produce barely visible damage (BVD) on composite surfaces, but with the possibility of significant internal damage. This is deemed very

dangerous, as BVD could result in catastrophic failure of the structure without warning. The energy ranges vary between applications, but the velocities are always kept below 10 m/s [14, 28, 29]. The impact energies were chosen in the current paper based on the work presented by previous researchers. Common failure modes observed during low-velocity impacts are matrix cracking, fiber breakage and delamination [19, 20, 21]. Of these, delamination is one of the most common failure mechanisms [22], which often results in the reduction of stiffness, strength, durability and stability of a composite [23, 24].

To establish the life and durability of FRPC in arctic conditions, in-depth investigation into the influence of combined impact and low temperature needs to be conducted. In real applications, structures are not impacted once, but are constantly subject to repeated impacts like in the case of wave impacts, main shut-down of an off-shore platform, drifting supply vessels or ice impacts [55, 56]. Most of the previous impact studies have focused on single low-velocity and repeated impact at room temperature. Naik et al. [57] investigated the damage imparted to woven-fabric and crossply E-glass/epoxy and carbon/epoxy laminates under low-velocity (1 m/s and 3 m/s) impact. They reported that woven-fabric laminates were more resistance to in-plane impact damage than crossply lamiates. Rajkumar et al. [58] studied the effect of repeated low-velocity impacts on glass fiber metal composites, and established that the peak load, impact energy, and failure strain decreased with increasing number of impacts. Sayer et al. [59] investigated the impact response of hybrid composite plates (glass-carbon/epoxy) with different stacking sequence for impact energies ranging from 25 J to 75 J, and concluded that fiber fracture was the dominant failure mode as the impact energy increased.

Murat et al. [33] tested woven carbon/epoxy prepreg laminates at different impact energy levels in the range of 1 J - 10 J, and observed that thicker samples manifested higher resistance to impact damage and the damage area increased with increasing impact energies. Morais et al. [60] investigated the effect of repeated low energy impact response of carbon-epoxy composites with different stacking sequences, and reported that cross-ply and non-symmetric laminates have better endurance against low energy impacts than unidirectional laminates. Li et al. [61] studied the influence of the thickness of carbon fiber composites under low-velocity impact with energies of 17 and 18 J, and reported that the contact force, absorbed energy and bending stiffness decreases with reducing sample thickness. Nguyen et al. [62] investigated the influence of low, medium

and high velocity impact on carbon fiber reinforced polymeric composites with impact energies of 10 J, 40 J and 120 J, respectively. They reported that the predominant damage mode was minor delamination, large delamination and fibre fracture and perforation, corresponding to low, medium and high velocity impact, respectively. Sultan et al. [32] studied woven carbon fiber reinforced prepreg laminates with impact energies ranging from 0.4 to 42 J, and reported that matrix cracking occurred below 21 J and fiber breakage manifested of 21 to 31 J of impact energy.

Despite the extensive amount of research conducted at room temperature (RT) under single and repeated impact loading, seldom work has been reported on repeated impact in arctic temperatures (AT). Icten [63] studied the influence of temperature on single and repeated impact of woven glass-epoxy composites at room temperature and -50 °C. They observed that the laminates impacted at -50 °C recorded higher peak forces and absorbed less energy than the samples impacted at room temperature. Ibekwe et al. [64] investigated the impact response of glass fiber reinforced unidirectional and cross-ply laminated composite beams at 20 °C, 10 °C, 0 °C, -10 °C and -20 °C, and observed that more damage was induced in the specimens impacted at lower temperature than those at higher temperatures. Salehi-Khojin et al.[38] investigated three combinations of fiberglass and Kevlar woven composites. Three different impact energies were tested (8 J, 15 J, and 25 J) for temperatures ranging from -50 °C to 120 °C. They reported that the deflection, maximum force and energy absorption increases with increasing temperature (from -50 °C to 120 °C) and impact energy (from 8 J to 25 J). Lopez-Puente et al. [65] investigated the influence of low temperatures on the damage imparted in carbon fiber/epoxy laminates (tape and woven) by impact velocities ranging from 60 to 525 m/s and at three temperatures (25, -60 and -150 °C) . They reported that higher the kinetic energy and low temperature resulted in larger damage to the laminates. In addition, they concluded that as the velocity increased, damage saturation occurs and temperature will not influence the damage extension. Im et al. [66] investigated the effect of different temperatures (-30, 20, 90 and 120 °C) on carbon fiber/epoxy and carbon fiber/peek laminates with lay-up $[0_6/90_6]_s$ and $[0_4/90_4]_s$. They concluded that as the temperature increases, the delamination areas decreases. Gomez-del-Rio et al. [34] recorded the response of carbon fiber reinforced polymeric composites with different stacking sequences (unidirectional, crossply, quasi-isotropic and woven laminates) in ambient temperatures ranging from 20 °C to -150 °C. They reported that the extent of damage

and absorbed energy increased with the decrease in temperature for all tape laminates, however, woven laminates did not exhibited this trend.

There have been mixed observations with respect to the extent of damage under low-velocity impact loading at low temperatures for composites and seldom work has been reported on low-velocity repeated impact on carbon fiber reinforced polymeric composites. Therefore, in the current study, the response and failure mechanisms of woven carbon/vinyl ester laminates subject to low-velocity repeated impact loading at room (25 °C) and arctic temperature (-50 °C) for a range of impact energies are investigated. Vinyl ester is considered in the current study due to superior UV resistance and low water absorption as compared to polyester resins [39, 40], which makes it attractive for ship and offshore applications. The variations in impact response in terms of force, displacement, energy and damage mechanisms is studied in detail and presented in the paper.

3.2 Methods

3.2.1 Laminate Fabrication

Carbon fiber reinforced composite samples tested at 25 °C and -50 °C were manufactured by vacuum assisted resin transfer molding (VARTM) process [41]. Plain weave carbon fabric and vinyl ester resin were purchased from Fibre Glast (www.fibreglast.com). Laminates with 16 layers of dry fabric were manufactured according to the ASTM Standard D7136/D7136M [42]. The layers of fabric were placed between 2 layers of flow-media, 2 layers of breather and 4 layers of nylon peel ply. All layers were cut to dimensions of 305 mm x 305 mm. The arrangement of fabrics was placed between 2 aluminum molds, wrapped with Stretchlon 800 bagging film and sealed with vacuum-sealant tape, ensuring spaces for both inlet and outlet connectors. The woven dry fabrics were reinforced with a mixture of vinyl ester resin and Methyl Ethyl Ketone Peroxide (MEKP) hardener. The resin was catalyzed with 1.25% MEKP by weight and mixed thoroughly as recommended by the manufacturer. The resin/hardener mixture was placed in a desiccator first to remove bubbles from the mixture. The outlet was then connected to a vacuum pump until the vacuum bag achieved a pressure of approximately 80 MPa. The inlet of the vacuum bag was then submerged in the resin/hardener mixture for transferring resin through the laminate. Upon completion of the resin transfer process, the laminate was cured at room temperature for 24 hours.

A total of 6 plates of 305 mm length by 305 mm width were manufactured, and six samples were obtained from each plate. To ensure that the curing conditions were identical for all the samples at room and arctic temperature, half the samples from each plate fabricated were set for testing at 25 °C and the other half for -50 °C for a given impact energy.

3.2.2 Impact Tests

Drop-weight impact tests were performed using a CEAST 9340 Drop Tower Impact System on rectangular laminate samples of 150 mm length x 100 mm width (refer to Figure 4.1(b)a) with an average thickness of 4±0.1 mm. The laminates were clamped between two metal fixtures with a test area of 46 cm^2 as shown in Figure 4.1(b)b. A hemispherical striker with a mass of 3.0 kg and diameter of 12.7 mm was used to impact the samples at their centers in the out-of-plane direction [42] with kinetic energies of 20 J, 25 J, 30 J, and 35 J for both temperatures (25 °C and -50 °C). The impact velocity was calculated based on the mass of the striker and kinetic energy, using the equation:

$$E_k = \frac{1}{2}m^2 = mgh \tag{3.1}$$

where, E_k is the impact energy or kinetic energy, v is the impact velocity and m is the mass of the impacting striker, h is the height of the striker measured from the surface of a samples in the impact drop tower and g is the gravitational acceleration.

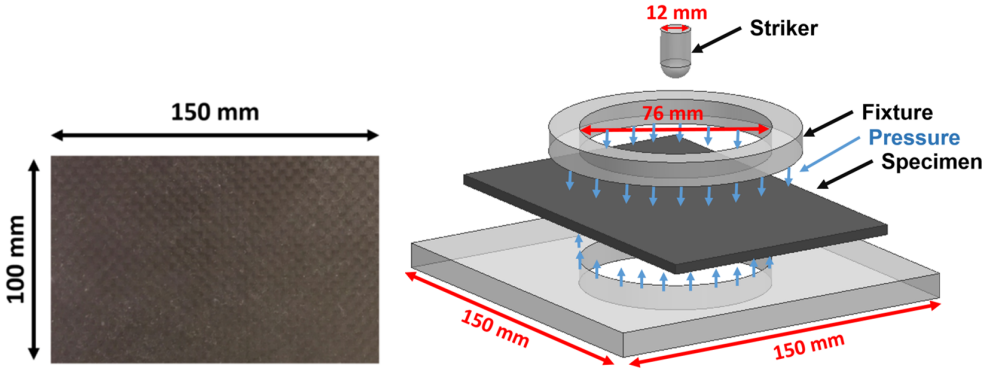

(a) (b)

Figure 3.1: (a) Woven carbon vinyl ester sample; (b) Impact fixture.

For a particular impact energy (20 J, 25 J, 30 J or 35 J), the impact velocity and the striker falling height were adjusted accordingly by the Drop Tower Impact System, where the impact velocities

were 3.64 m/s, 4.07 m/s, 4.46 m/s and 4.82 m/s, respectively. All the tests were low-velocity impacts, that is, below 10 m/s [43]. In order to establish the durability of these laminates under repeated impact loading, each sample was repeatedly impacted until complete perforation of the striker through the sample thickness. Force-time, displacement-time and energy-time responses were recorded by the data acquisition system "CEAST DAS 8000 Junior" of the impact machine for each test. Schematic of an impact test fixture is shown in Figure 4.1(b)b. Four samples were impacted for each combination of impact energy (20 J, 25 J, 30 J and 35 J) and temperature (25 °C and -50 °C). Corresponding force-time, displacement-time, energy-time and force-displacement responses were obtained for each test.

The samples planned for testing under in-situ arctic conditions were placed in a Thermo Scientific^{TM} freezer at -50 °C for a period of 90 days to reach a uniform temperature. A basic heat transfer analysis was performed which showed that a sample at room temperature can -50 °C in 15-20 min when subject to a constant ambient temperature of -50 °C. A 90 days exposure prior to testing was chosen to subject the samples to arctic pre-conditioning. To perform the in-situ arctic tests, the samples were removed from the freezer and placed within a temperature controlled environmental chamber, which was connected to the CEAST 9340 Drop Tower Impact System. Prior to every impact test, the environmental chamber was conditioned for 15 minutes with Liquid Nitrogen (LN_2) to reach a uniform temperature of -50 °C within the chamber.

3.2.3 Micro Computed Tomography (micro-CT) Scanning

Typically, low velocity impacts produce barely visible damage (BVD) on composite surfaces after a single impact. Hence, the samples were examined under a micro computed tomography (micro-CT) scanner to evaluate the internal damaged area in arctic and room temperature. The samples were reduced to a rectangle of 145 mm in length and 90 mm in width (the original dimensions were 150 mm in length by 100 mm in width), so they can fit in the scanner chamber. The impact damage was centered in this rectangle and cutting around the edges did not alter the damage that occurred predominantly at the center of the samples and far away from the edges. A small hole with a diameter of 1.6 mm was drilled at the center of the impacted region of the laminates for applying a dye-penetrant at these holes, upon which the samples were held in a vacuum chamber for five minutes. This procedure was repeated three times to ensure that all damaged regions

were filled with the solution. For the first 2 applications of the dye-penetrant, the solution was completely absorbed. A third application ensured that the sample was saturated with the solution, which resulted in complete solution penetration in all available openings, such as delaminations and cracks. Zinc iodide solution was used as the dye-penetrant, which has a high absorption coefficient in comparison to the constituents of the composite materials i.e. carbon fiber and vinyl ester. The Zinc iodide solution was a mixture of alcohol (10 ml), distilled water (10 ml), Kodak photo solution (1 ml) and zinc iodide powder (60 g). Excess dye-penetrant was evaporated by placing the laminates in an oven at 50 °C prior to x-ray scanning. Excess dye penetrant in its liquid phase is not preferred as its motion inside the crack during a scan adversely affects the quality of the 3-D reconstruction. This was eliminated through drying the dye penetrant, which deposits a saline residue on the crack area and in turn provides greater resolution of the damage. Hence, drying the dye penetrant is beneficial. Also, 50 C is enough to dry the samples without creating any thermal damage in the composite. All laminates were scanned with a SkyScan 1173 X-ray microtomograph with the same resolution of 35.9 μm and an angle step of 0.19. The X-ray tube voltage and current were set to 60 kV and 120 microampere, respectively. All the scans were performed using built-in Al filter, and a flat field correction was applied for each scan. The reconstruction was performed using the NRecon commercial software.

3.2.4 Laminate Strengthening

To examine the strengthening effect of low temperatures, compression tests were performed on pure vinyl ester samples and tension tests were performed on woven carbon/vinyl ester samples at room and arctic temperatures. A description of the tests and sample dimensions used in this study are discussed next. Compression Test: Three samples each were tested at in-situ 25 °C and -50 °C under flat-wise compressive loading. Cylindrical specimens with a diameter of 25.4 mm and a height of 50.8 mm were tested according to ASTM D695 standard [45]. These tests were performed using an ADMET eXpert 1654 testing system with a crosshead displacement rate of 1.3 mm/min. Tension Tests: Five samples each were tested at in-situ 25 °C and -50 °C under tensile loading. Rectangular specimens with a width of 15 mm, thickness of 1 mm and length of 250 mm were tested according to ASTM D3039 standard [67]. These tests were performed using an ADMET eXpert 1654 testing system with a crosshead displacement rate of 2 mm/min.

3.3 Results and Discussion

Deformation-time, energy-time and force-time responses recorded for impact energies of 20, 25, 30, and 35 J at 25 °C and -50 °C are discussed in detail in this section. Durability of laminates upon repeated impact is assessed in terms of number of impacts required to perforate a laminate through the thickness and the rate of reduction in the peak force for a combination of impact energies and temperatures. The response of the laminates in terms of visual damage, degree of damage and failure mechanisms is also evaluated and elucidated next.

3.3.1 Laminate Strengthening

Mechanical properties of woven carbon/vinyl ester composites change when cooled to arctic temperatures (AT). Prior research by Dutta [46] on the compressive response of glass-fiber-reinforced polymer composites at the U.S. Army Cold Regions Research and Engineering Laboratory (CRREL) showed that their strength and stiffness increases with reducing temperatures. But, also become brittle and are susceptible to cracks due to increase in thermal residual stresses caused by mismatch in the coefficient of thermal expansion (CTE) between the fibers and matrix.

3.3.1.1 Compression Test Results

Compression tests on pure vinyl ester were also conducted in-house as part of the current study to investigate the influence of low temperature on these composites. Table 3.1 shows the results from the compressive testing of vinyl ester, where the yield strength (coined as the stress value where the response starts to become non-linear), ultimate strength and elastic modulus increased by approximately 55%, 49% and 28% when cooled from 25 °C to -50 °C. Typical compressive stress-strain response (one sample) of vinyl ester is shown in Figure 6.3(b), where the final failure strains reduced with reduction in temperature, which implies that deformation of vinyl ester will be lower at AT as compared to those at RT. The increase in matrix strength is attributed to the binding forces between molecules, which are tightly frozen at AT [47]. Therefore, the compressive strength of vinyl ester increases at low temperatures. Garcia et al.[48] investigated the flexural response of woven carbon/vinyl ester composites in AT, and reported that dry arctic conditioned samples manifested an $\approx$23% increase in flexural strength with respect to those at room temperature.

Table 3.1: Results from compressive testing of vinyl ester at RT and AT

Mechanical Properties	Temperatures 25 °C	-50 °C	Percentage change (%)
Yield strength (MPa)	47±5	72±4	55
Ultimate strength (MPa)	85±4	126±12	49
Elastic modulus (GPa)	2.6±0.2	3.4±0.1	28

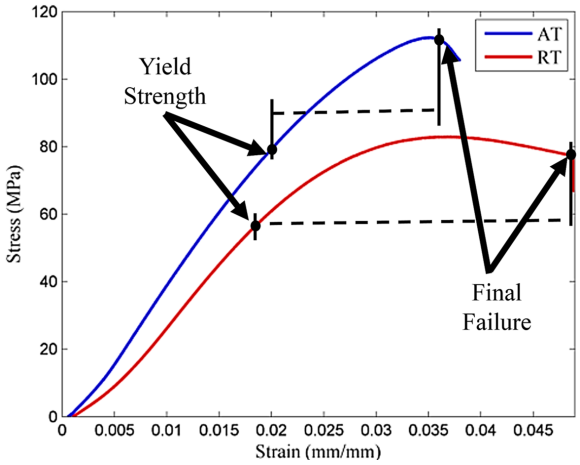

Figure 3.2: Typical compressive stress-strain plots of vinyl ester at RT and AT

3.3.1.2 Tension Test Results

Tension tests on woven/carbon vinyl ester samples were also conducted in-house as part of the current study. Table 3.2 shows the results from the tensile testing of the woven carbon/vinyl ester composite, where the Young's modulus and ultimate tensile strength increased by approximately 15% and 11% respectively when cooled from 25 °C to -50 °C. Typical tensile stress-strain response of vinyl ester is shown in Figure 6.3(a), where the final failure strains reduce with reduction of temperature. This implied that there is a reduction of ductility and increase in brittleness of the composites at low temperature [68]. Kim et al. [69] attributed such increase in brittleness at low temperatures to predominantly fibers, which increased rapidly within a temperature range from RT to -50 °C. On the other hand, the increase in the laminate strength and stiffness is attributed to the strengthening of the matrix. Therefore, there will be less damage at low temperatures initially, but it continue to increase as the load approaches a critical value where the fibers fail. However,

matrix cracking and delamination will be dominant at room temperature[70]. Figure 3.3(b) shows the failure regions of one set of specimens tested at 25 °C and -50 °C under tension. It can be seen that at AT, the damage was localized in just one region (across the transverse direction of the sample) and fiber breakage was the dominant failure mechanism. On the other hand, the samples at RT experienced a more dispersed damage (across the longitudinal direction of the sample). In addition, matrix cracks and some fiber breakage were the main failure mechanisms. The samples at RT were painted white to show this failure pattern more clearly.

Table 3.2: Results from tensile testing of woven carbon/vinyl ester samples at RT and AT

Mechanical Properties	Temperatures 25 °C	-50 °C	Percentage change (%)
Ultimate strength (MPa)	562±31	623±29	11
Youngs Modulus (GPa)	37±4	42±4	15

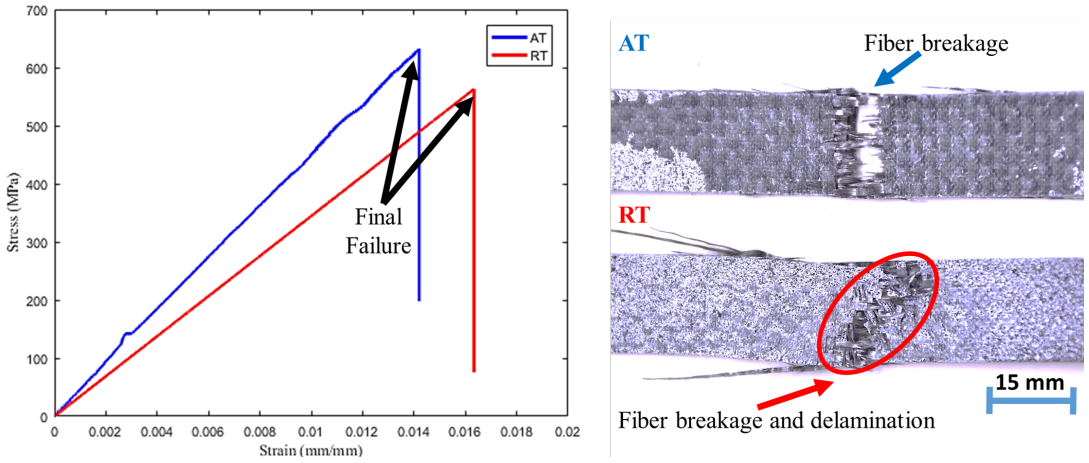

(a) (b)

Figure 3.3: (a) Typical tension stress-strain plots of woven carbon/vinyl ester at RT and AT; (b) Failure regions of the composite specimens at RT and AT under tension.

3.3.2 Contact Force and Deflection

During an impact test, contact force is generated by the contact of the striker with the impacted face of a sample, which is recorded as the force-time response by the data acquisition system of the

impact machine. Typical repeated impact responses of laminates impacted at two energies of 20J and 25J are shown in Figure 3.4(a) and Figure 3.4(b). In general, it is expected that the peak force recorded reduces with increasing number of impacts due to accumulation of damage. However, the specimens manifested two different responses at 20J and 25J. At 20J, the peak forces increased initially upon repeated impacts, but reduced after several impacts finally resulting in perforation. At 25J, the trend was as expected, where the peak force gradually reduces with increasing number of impacts.

Bienias et al. [71] categorized the repeated impact response into phases of force change. The first phase is called "stabilization", represented by letter A in Figure 3.4(a), which is the very first impact on a laminate where the impact energy is insufficient to cause damage for decreasing the stiffness of the laminate. Icten [63] attributes this to the contact of the impactor with a relatively compliant matrix material. The second phase is known as "force increase", given by letter B in Figure 3.4(a), which consists of multiple impacts before the maximum peak force is reached. In this phase, laminates experienced higher contact force after each impact due to the compaction of matrix under the striker. The third phase is "maximum force", represented by letter C, which corresponds to the number of impacts at maximum peak force beyond which force reduction occurs due to the presence of damage, such as matrix cracks, fiber breakage and delamination. The last phase is "force decrease", given by letter D, where the peak force and stiffness recorded gradually reduces with increasing number of impacts.

Specimens repeatedly impacted at 20J at room and arctic temperatures manifested all four phases of force change (Figure 3.4(a)), whereas, those impacted at 25, 30 and 35 J showed only phases C and D (Figure 3.4(b)). Lower impact energies are not sufficient to damage the laminate in the first impact, thereby, causing phases A and B, as opposed to higher impact energies that manifest only phases C and D.

3.3.2.1 Temperature Effect on Impact Force

Peak impact force is plotted against the number of impacts at room and arctic temperature in Figure 3.5. For all energies, the samples impacted at -50 °C experienced higher impact forces and required more number of impacts to perforate the laminate as compared to the samples tested at 25 °C. The samples impacted at 20 J at both temperatures experienced the four phases of force change

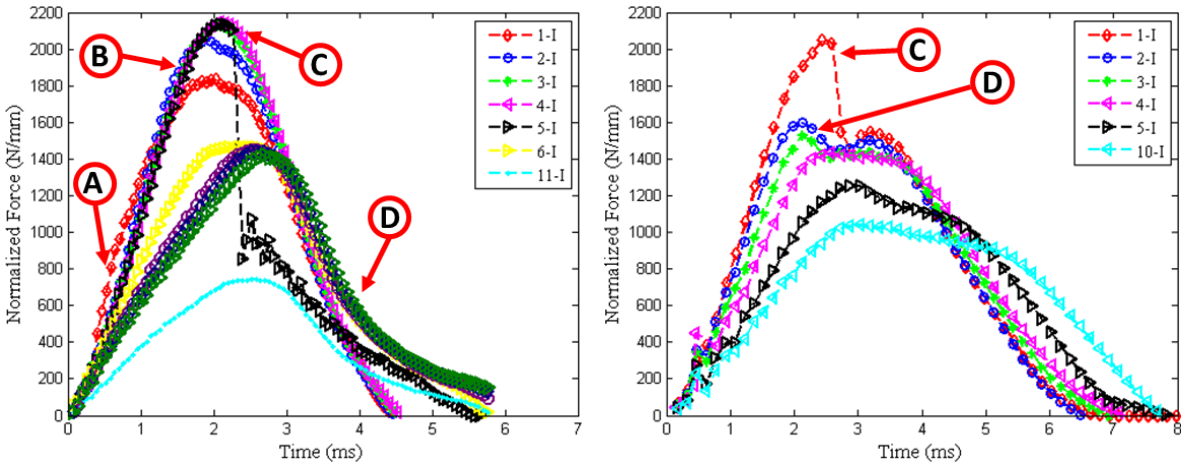

(a) (b)

Figure 3.4: Representative force-time responses for a single sample subject to repeated impact: (a) 20 J at arctic temperature; (b) 25 J at arctic temperature.

described above, which are, stabilization, force increase, maximum force and force decrease. Figure 3.5(a) shows the response for 20 J for both temperatures, where an increase in impact force after the first impact is observed corresponding to the force increase stage. Upon reaching a maximum impact force, a decrease in impact force is observed with further impacts. With increasing number of impacts, significant difference between the impact forces is observed at both temperatures. For 25, 30 and 35 J impact energies, the samples experienced only 2 phases of force change: maximum force and force decrease as shown in Figure 3.5(b), Figure 3.5(c) and Figure 3.5(d).

The slope of the force versus number of impacts plot indicates the rate of reduction in impact force with increasing number of impacts, which is higher at higher impact energies of 30J and 35J, and also similar at room and low temperature. Fiber fracture is the dominant failure mechanism at higher impact energies as opposed to matrix cracking at lower impact energies. This is attributed to two factors: 1) lesser influence of low temperature on carbon fibers and damage saturation. The influence of low temperature on carbon fiber is less significant as compared to matrix, from what is observed in the case of coefficient of thermal expansion (CTE)[72]; 2) damage saturation occurs when the temperature has no influence on damage extension. This corroborates the similar responses at low and room temperature. As expected, the impact force at both temperatures increased with the increasing impact energy.

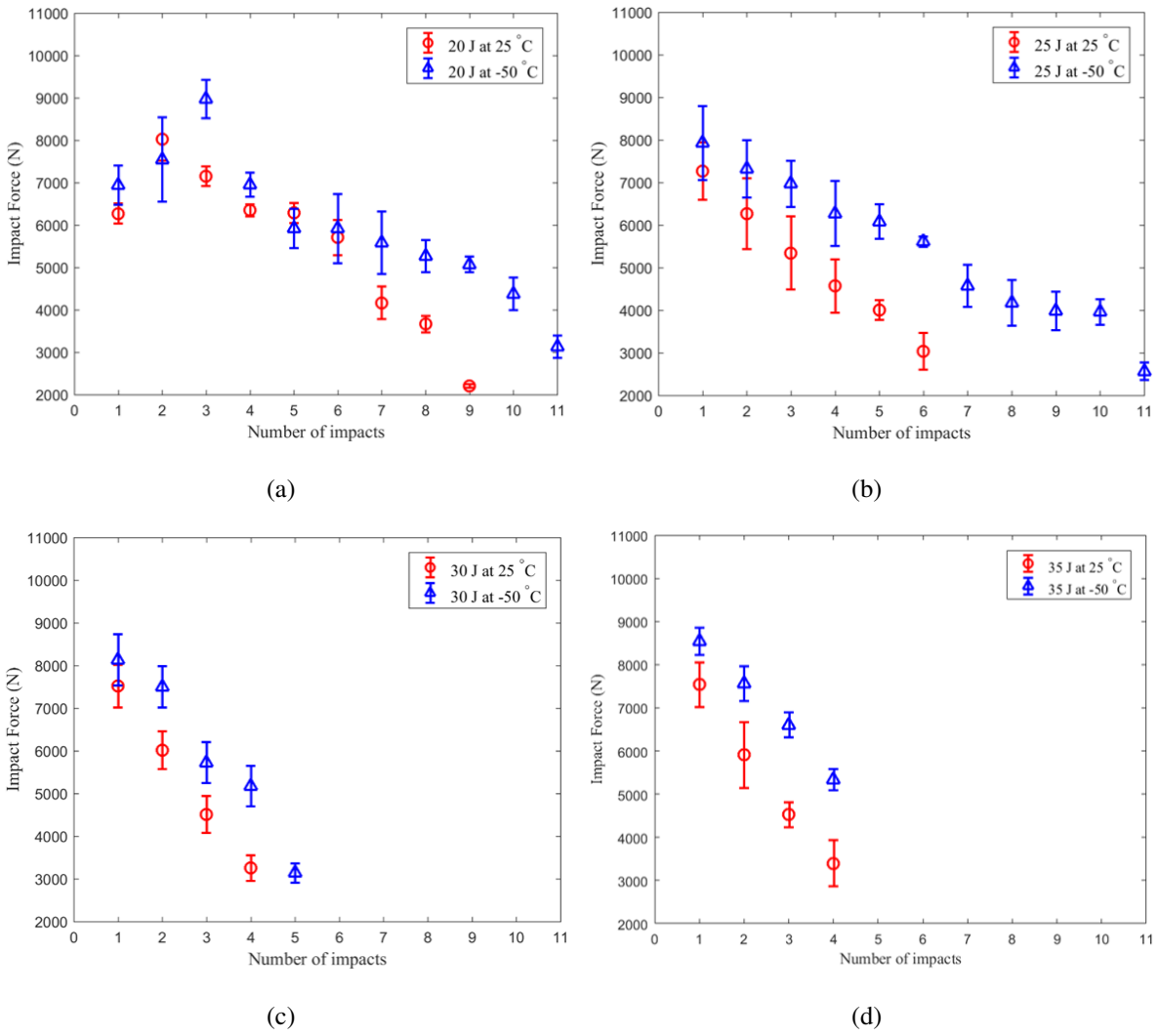

Figure 3.5: Contact force with increasing number of impacts at 25 °C and -50 °C: (a) 20 J, (b) 25 J, (c) 30 J and (d) 35 J.

3.3.2.2 Temperature Effect on Deflection

Figure 3.6 shows the deflection versus number of impacts at room and arctic temperatures. Increase in rigidity of the laminates due to matrix strengthening at arctic temperatures manifests lower deflections in samples impacted at -50 °C as compared to those at 25 °C. The deflection at both temperatures increased with the increasing impact energies. For 20 J (Figure 3.6(a)) and 25 J (Figure 3.6(b)), the difference between the deflections at room and arctic temperatures under repeated impact loading is more prominent, as compared to that observed for 30 J (Figure 3.6(c)) and 35 J (Figure 3.6(d).

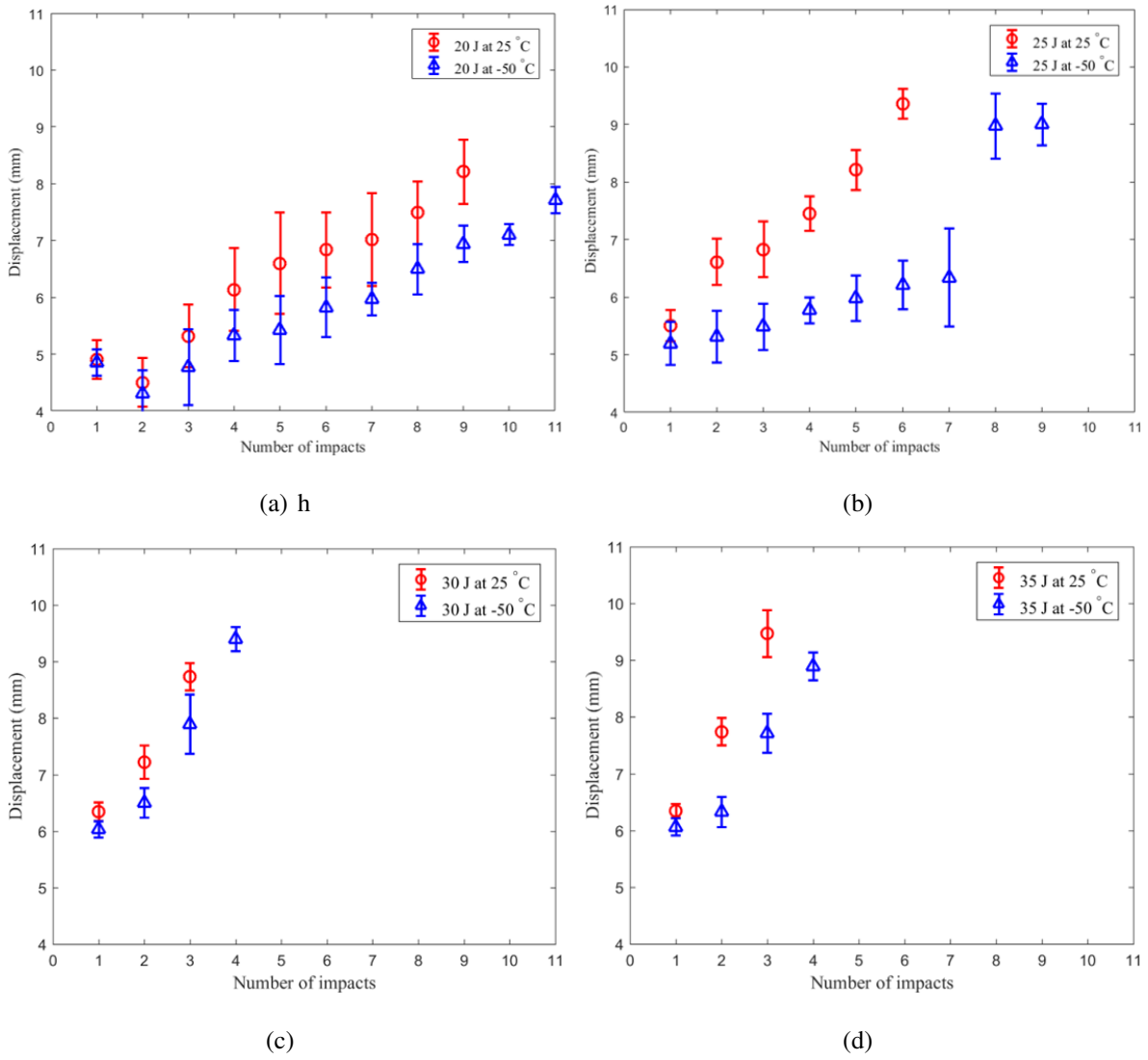

(a) h (b)

(c) (d)

Figure 3.6: Deflection with increasing number of impacts at 25 °C and -50 °C: (a) 20 J, (b) 25 J, (c) 30 J and (d) 35 J.

3.3.3 Absorbed Energy

Figure 3.7 shows a typical energy-time response obtained during an impact even on fiber reinforced laminates. The impacted energy is the peak value on the graph and the post peak plateau region is the energy absorbed by the laminate that is manifested as failure mechanisms like matrix cracking, delamination or fiber fracture. If the impact energy is equal to the absorbed energy, the laminate is deemed completely perforated by the strikers. Increasing absorbed energy implies more damage in the laminate. Hence, the degree of damage (D) for a laminate is defined as the

ratio of the absorbed energy to the impact energy, which limits the values to be between 0 (no damage) and 1 (complete damage).

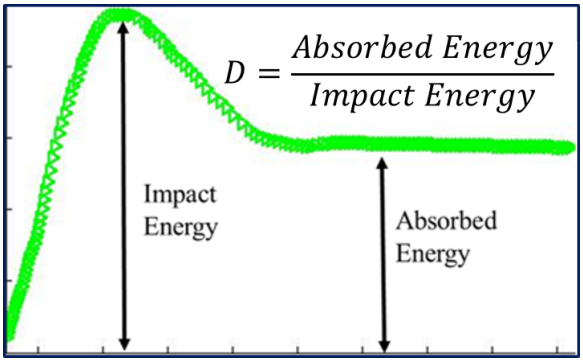

Figure 3.7: Typical energy-time response of an impact event

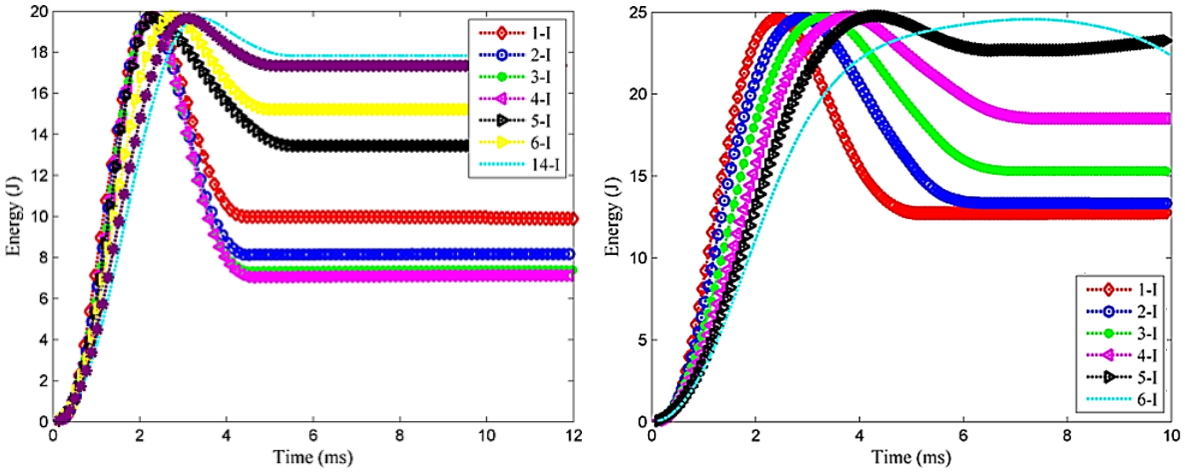

(a) (b)

Figure 3.8: Representative energy-time responses for repeated impact: (a) 20 J at arctic temperature; (b) 25 J at arctic temperature.

Figure 3.8(a) shows a representative energy-time graph for repeated impacts at 20 J, where the energy absorbed after the first impact (red) decreased first for the next three impacts (blue, green and magenta) due to the compaction of matrix during the “force change” phase as described in section 3.3.2. Upon reaching the maximum force (black graph), there was a significant increase on the absorbed energy, which continues to increase gradually after consecutive impacts until laminate

perforation. For 25 J, 30 J and 35 J, the energy absorbed increased gradually starting from the very first impact, as seen in Figure 3.8(b).

3.3.3.1 Temperature Effect on the Degree of Damage

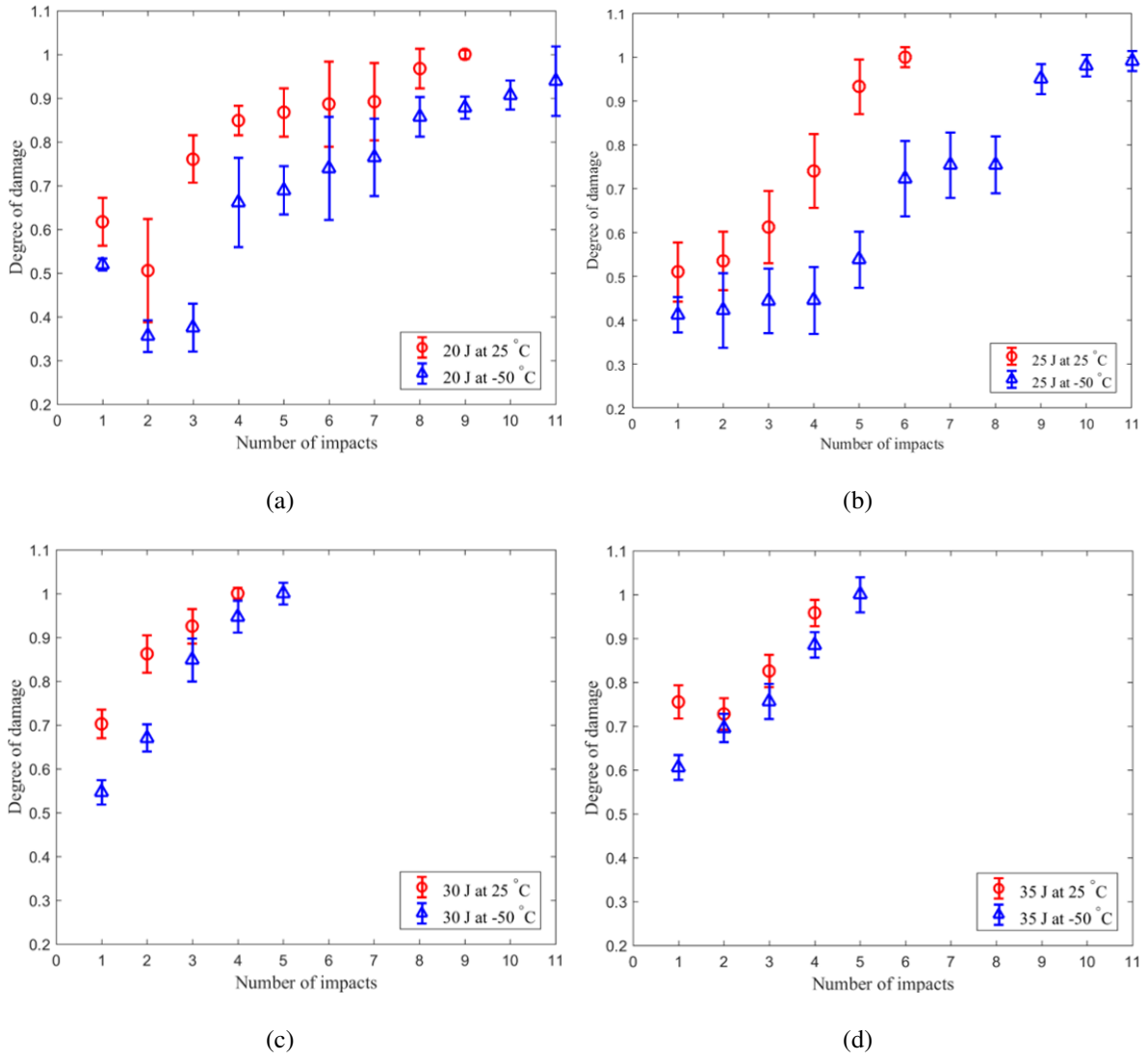

Figure 3.9: Degree of damage as a function of number of impacts at 25 °C and -50 °C: (a) 20 J, (b) 25 J, (c) 30 J and (d) 35 J.

Figure 3.9 shows the degree of damage versus number of impacts for room and arctic temperatures, where the values of D increase with increasing impact energies and also the number of impacts. In general, the samples impacted at -50 °C recorded lower degree of damage as compared

to those at 25 °C for a specific impact energy. The damage in matrix is lower at arctic temperature due to matrix strengthening than those at room temperature at low impact energies. It has been previously established the matrix failure is prevalent at lower impact energies and fiber failure is dominant at higher impact energies. Therefore, the contribution of matrix cracking at lower energies to the degree of damage is significant, whereas, a combination of fiber breakage and matrix cracking contributes at higher energies. Therefore, the difference in the degree of damage measured at 20 J Figure 3.9(a) and 25 J Figure 3.9(b) between RT and AT is high, about 21-29% for these laminates. Whereas, at higher impact energies (Figure 3.9(c) for 30 J and Figure 3.9(d) for 35 J), this difference reduces to about 10-15% due to lower (but not insignificant) influence of matrix cracking on the degree of damage.

3.3.4 Damage Mechanisms

Figure 3.10 shows the micro-CT scan images of samples impacted at 20 J and 30 J in room and arctic temperatures. Regions identified as matrix cracking/delamination (smeared areas) and fiber breakage (sharp defined areas) are highlighted in the images. From the images shown in Figure 3.11, the samples impacted with 20 J energy at both temperatures manifested small regions of visible damage on the impacted and the back faces. However, the micro-CT scan images show considerable internal damage in terms of matrix cracking/delamination and fiber breakage through the thickness of the samples. Fiber breakage is concentrated on the impacted surface with significant matrix cracking and delamination through the thickness of the laminate impacted at 20 J energy in room temperature. On the other hand, at arctic temperature, the overall spread of damage is confined to a smaller region with higher fiber failure traversing through the thickness of the laminate. The reduction in the overall damaged area projected on to the plan of the samples is approximately 36% between RT and AT at 20 J.

The micro-CT scan images for 30 J shown in the Figure 3.10 exhibit significant fiber failure along with matrix failure, and is representative of the samples impacted at higher energies of 25, 30 and 35 J. Fiber failure through the thickness of the samples is higher at AT as compared to RT when impacted by 30 J impact energy. Also, the reduction in the overall damaged area projected on to the plan of the samples at 30 J is approximately 19% between RT and AT. The observed difference in percentage reduction in damaged area between RT and AT at 20 J and 30 J is due to

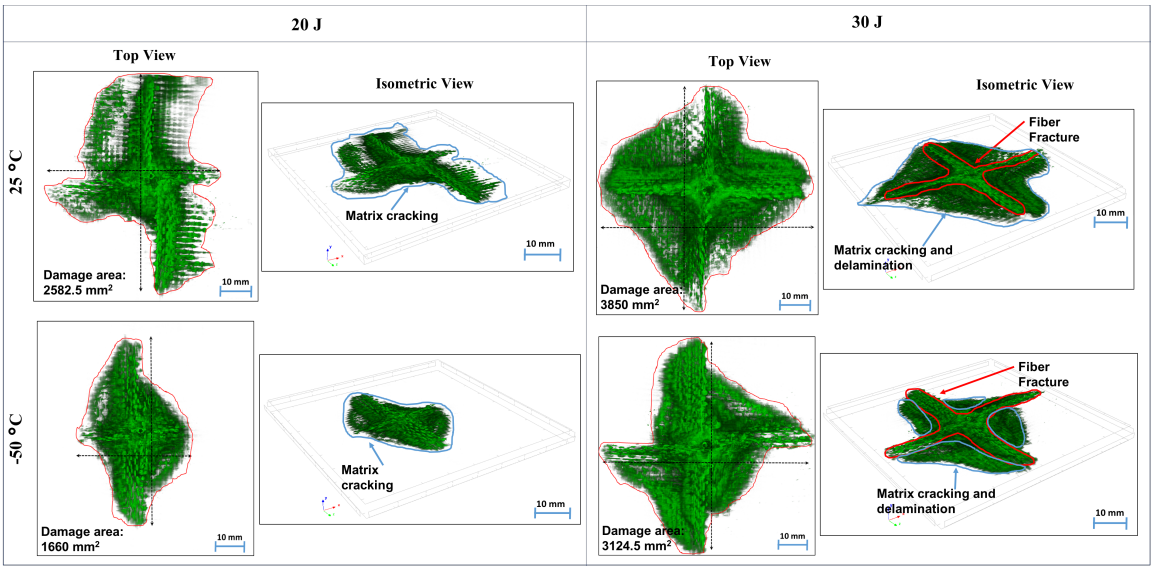

Figure 3.10: Micro-CT scan after the first impact for 20 and 30 J at 25 °C and -50 °C.

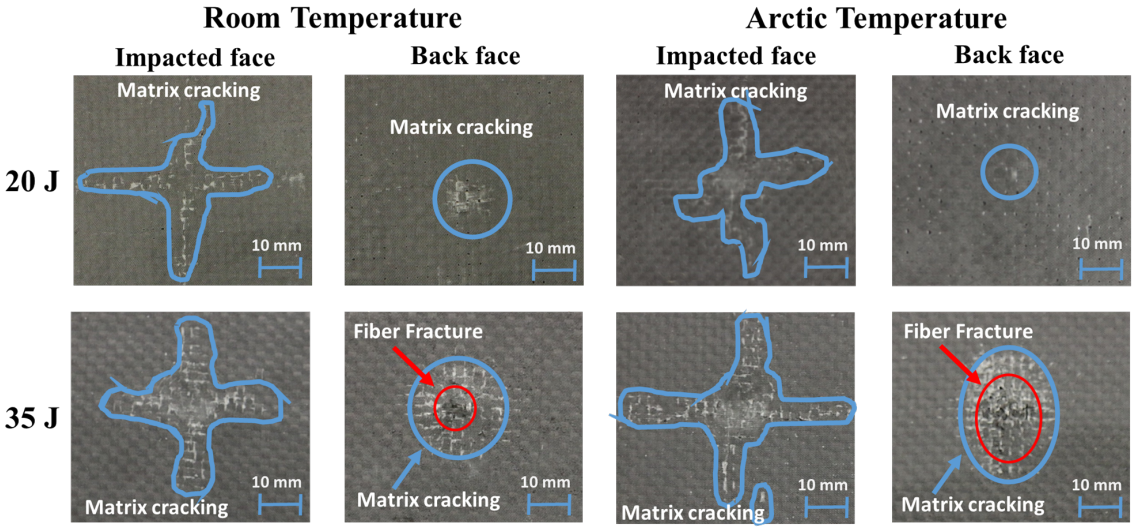

Figure 3.11: Impacted face and back face at 20 and 35 J impact energies at 25 °C and -50 °C.

the increase in strength when composites are subject to low temperatures. The yield strength of the vinyl ester matrix increased up to ≈55% at AT as compared to RT based on the compression tests conducted in the current study, which indicates a delay in the onset of matrix cracks at AT. Consequently, the composite manifested significantly higher fiber failure than matrix cracking as compared to RT for the same impact energy.

Figure 3.12 shows the impacted face and back face of samples repeatedly impacted at 20 J and 35 J to complete perforation. The samples impacted at 20 J at both temperatures experienced a combination of fiber fracture (enclosed by the red curves) and matrix cracking (enclosed by the blue curves). At 25 °C, these samples also manifested small regions of fiber bridging at the back face (enclosed by the green circles). On the other hand, at -50 °C, fiber bridging was minimal and showed predominantly fiber fracture at the back face of the laminate as predicted from the "Laminate Strengthening" section. This was also representative of the samples impacted at 25 J.

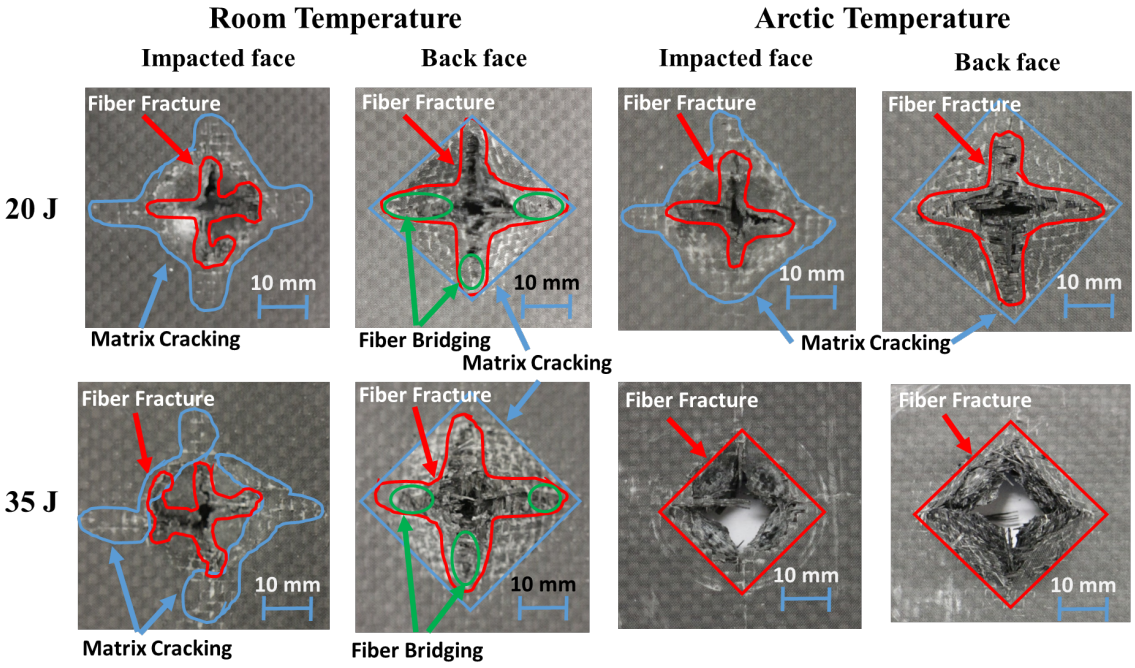

Figure 3.12: Impacted face and back face for 20 J and 35 J impact energies at 25 °C and -50 °C.

The samples impacted at 35 J at room temperature exhibited a combination of fiber breakage and matrix cracking along with fiber bridging at the back face of the laminate. On the other hand, at arctic temperature they experienced significant fiber fracture at the impacted and back face. The perforated region is sharp and well defined at 30 J in arctic temperature as compared to lower impact energies and at room temperature. The failure mechanisms were similar for the samples impacted at 30 J. Overall, arctic temperature renders the composite brittle thereby promoting more fiber fracture than matrix cracking, which is accentuated at higher impact energies.

3.4 Conclusion

Dynamic repeated impact response and failure mechanisms of woven carbon/vinyl ester composites at room (25 °C) and arctic (-50 °C) temperatures were investigated in this paper in view of increasing interest in arctic explorations and the need to characterize these composites for arctic applications. Four impact energies of 20 J, 25 J, 30 J and 35 J were considered for dynamic impact testing at room and in-situ arctic temperatures, where the samples were repeatedly impacted until perforation. Key observations in terms of the contact force, displacement, energy absorbed and failure mechanisms were reported in this paper. Key conclusions are as follows:

1. During a repeated impact event at low impact energies, a laminate experiences four phases of force change: stabilization, force increase, maximum force and force decrease. If the impact energy is sufficiently high to cause significant damage during the first impact, then only two phases of force change will be present: maximum force and force decrease.

2. At -50 °C, increase in rigidity of a laminate results in higher initial stiffness, lower defections and higher impact forces than those impacted at 25 °C for all energies.

3. The laminates absorb less energy at -50 °C due to matrix strengthening, which results in lower values of degree of damage than at 25 °C. Consequently, the number of impacts needed for complete perforation of laminates increase at low temperature.

4. At room temperature, the dominant failure mechanism is matrix cracking at low impact energies (20 J) as compared to higher impact energies (30 J and 35 J), where the dominant failure mechanism is fiber fracture with lesser matrix cracking.

5. Significant shift in failure mechanisms occurs at arctic temperature, where fiber fracture is promoted due to matrix strengthening This manifests as sharp defined perforated regions at low temperature with minimal fiber bridging at the back face of the laminate.

6. Overall, the difference in response of laminates at lower energies is more distinct with temperature change from room to arctic, whereas, if velocity increases there will be a damage saturation effect where the temperature will have lower influence on the damage extension.

In conclusion, failure mechanisms shift from matrix failure towards fiber failure at arctic temperature, even though the measured degree of damage and deflection from the impact tests provide lower value at AT as compared to RT. This shift in mechanism can have significant detrimental effect on the tensile residual strength (as fiber fracture will be the main failure mechanism at AT) and durability of the composite. Also, this study is very relevant for developing appropriate repair techniques for composites for use in arctic applications.

Chapter 4

Computational Model for the Single Low-velocity Impact Response of Woven Carbon Composites

4.1 Introduction

Fiber reinforced laminated composites have become an attractive solution in light-weight applications without sacrificing the stability or performance of a structure. Despite the several advantages that composite materials offer, a major disadvantage is their low resistance to impact damage due to their layered nature. Most of the impact loading on laminated composites are in the transverse direction. They are usually classified as low- or high-velocity impact. Low-velocity impact, like tool drop during manufacturing or repair [14, 19] or impact of debris on a ground aircraft can cause significant damage in the interior of these composites, which barely visible damage on the exterior regions. Dynamic impact is generally divided into low- or high-velocity impact [73]. Typical low-velocity impact occurs at velocities below 10 m/s [43]. Common failure mechanisms observed during low-velocity impact are fiber breakage, matrix cracking and delamination [20, 21, 16]. The objective of the research presented is to develop a computational tool capable of predicting the response of dynamic impact on woven carbon/vinyl ester laminates.

4.1.1 Impact Test

Drop-weight impact tests were performed using a CEAST 9340 Drop Tower Impact System on rectangular laminate samples of 150 mm length x 100 mm width (refer to Figure 4.1(a)) with an average thickness of 4 ± 0.1 mm. These samples were clamped between two metal fixtures with a uniform pressure of 0.2 MPa from the impact machine (refer to Figure 4.1(b)). The test area was a circular opening of 46 cm^2. A hemispherical striker with a mass of 3.0 kg and diameter of 12.7 mm was used to impact the samples at their centers in the out-of-plane direction [42] with kinetic

energies of 20 J, 25 J, 30 J, and 35 J for both temperatures (25 °C and -50 °C). The impact velocity was calculated based on the mass of the striker and kinetic energy, using the equation:

$$E_K = \frac{1}{2}mv^2 \tag{4.1}$$

where, E_k is the impact energy or kinetic energy, v is the impact velocity and m is the mass of the impacting striker, h is the height of the striker measured from the surface of a samples in the impact drop tower and g is the gravitational acceleration.

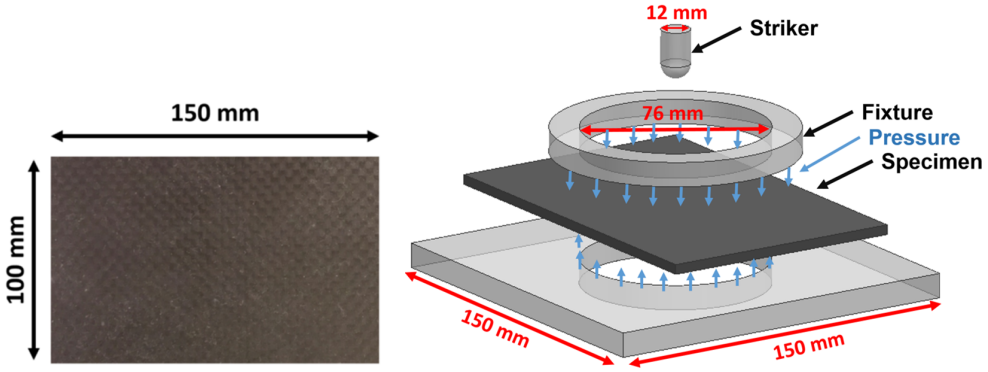

(a) (b)

Figure 4.1: (a) Woven carbon vinyl ester sample; (b) Impact fixture.

For a particular impact energy (20 J, 25 J, 30 J or 35 J), the impact velocity and the striker falling height were adjusted accordingly by the Drop Tower Impact System. For 20 J, 25 J, 30 J and 35 J impact energies, the corresponding impact velocities were 3.64 m/s, 4.07 m/s, 4.46 m/s and 4.82 m/s, respectively. All the tests were low-velocity impacts, that is, below 10 m/s [43]. Robinson et al. [44] investigated the influence of impactor mass and velocity on the low velocity impact performance of woven carbon and glass fiber reinforced laminates for impact energy range from 0.25 J to 12 J. The impactor mass was varied from 1.15 kg to 2.10 kg and the velocity was adjusted to obtain desired impact energies. They reported that the extent of impact damage predominantly depended on the magnitude of the impact energies and not on the mass or velocity individually. Based on this finding, the impactor mass was held constant and the velocity was allowed to vary for prescribed impact energies in the current paper. Force, displacement, energy and time responses were recorded by the data acquisition system "CEAST DAS 8000 Junior" of the impact machine for each test. Schematic of an impact test fixture is shown in Figure 4.1(b).

Four samples were impacted for each impact energy (20 J, 25 J, 30 J and 35 J). Corresponding force-time, displacement-time, energy-time and force-displacement responses were obtained for each test.

4.1.2 Impact Model

A 16-layer plain weave carbon laminate was modeled within the finite element method (FEM) framework using a commercially available software (ABAQUS). The laminate model consisted of 31 layers in total: 16 layers of effective plain woven carbon fabric reinforcement with matrix and 15 layers of thin pure matrix material as shown in Figure 4.2. A rectangular specimen of 6.0 in. (150 mm) long and 4.0 in. (100 mm) wide was used for experimental testing, which was clamped between a circular ring metal fixtures as shown in Figure 7.2(a). The outer diameter of the metal fixture was 4 in. (100 mm) and the inner diameter was 3 in. (76.2 mm). For the computational modeling, only the region of the laminate enclosed within the metal fixture was considered, as this was the main region influenced during low-velocity impact loading. A constant pressure of 0.2 MPa at the top and bottom of the laminate in the circular ring region was applied to simulate the clamping effect of the fixture. A cross-section of the manufactured laminate was examined under a scanning electron microscope (SEM) to obtain an average thickness of the effective woven carbon fabric layers and interlaminar matrix regions as seen in Figure 4.4. The average thickness of the matrix layer was 0.2 ± 0.01 mm. The striker was modeled as a rigid element with a diameter of 12.7 mm and a mass of 3.1 kg. The striker DOFs were all fixed, except for the displacement in the Z-direction. The element type used for the striker was R3D4 (rigid element in ABAQUS).

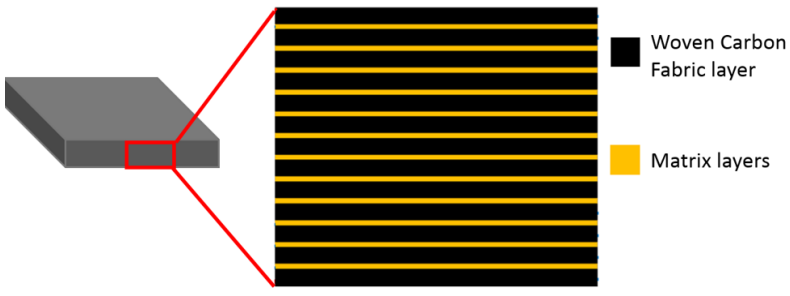

Figure 4.2: Schematic of fabric layers and interlaminar regions of the laminate

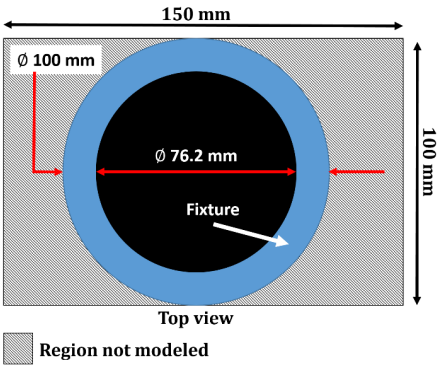

Figure 4.3: Schematic of the top view of the specimen clamped by the impact metal fixture.

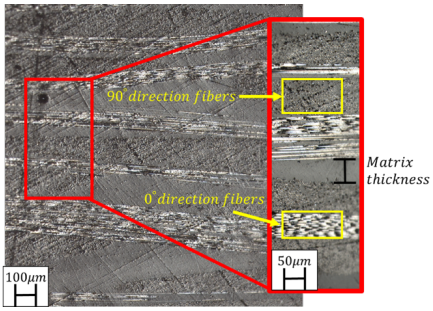

Figure 4.4: Cross-section of a laminated composite used to calculate the matrix thickness

The impact loading in the computational model was introduced in terms of impact velocity, which was calculated using the following equation:

$$E_K = \frac{1}{2}mv^2 \tag{4.2}$$

where, E_k = kinetic energy (J), m = stiker mass (kg), v = striker velocity (m/s). For each energy considered, the corresponding velocities of impact were determined. The striker was placed on the laminate model and given an impact velocity to simulate impact loading as shown in Figure 4.5. The striker was modeled as a rigid body and its motion was governed by a single reference point. A circular partition with an area of 7.0 in^2 (45.6 cm^2) (refer to Figure 4.5(a)) was created on the top and bottom faces of the laminate to simulate the circular aperture of the clamp.

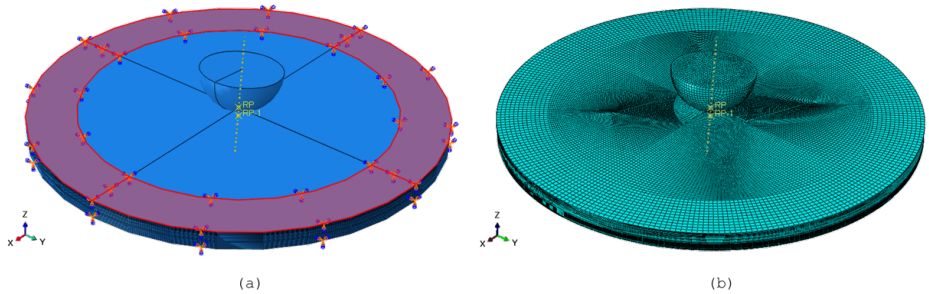

Figure 4.5: (a) Impact model of specimen with boundary conditions; (b) Meshed model using C3D8 and COH3D8 elements

4.1.2.1 Contact Interactions

The interaction between the striker and the sandwich composite was modeled using the general contact algorithm: surface-to-surface interaction available in ABAQUS/Explicit. This interaction requires two surfaces: a slave and master surface. The master surface was the striker, and the slave surface was the top surface of the laminate. The layers of matrix and laminas were partition in the Assembly module in ABAQUS. Thus, no further interactions were required between them.

4.1.2.2 Damage criteria and properties for the lamina

For the woven carbon/epoxy laminas, the element type used was quadrilateral continuum shell element (SC8R) (an 8-node hexahedron with finite membrane strains). The damage model consisted of a linear-elastic response until the onset of damage. The linear-elastic mechanical properties are shown in Table 4.1.

Table 4.1: Mechanical properties of the woven/epoxy lamina

$E_{11}(GPa)$	$E_{22}(GPa)$	$E_{33}(GPa)$	ν_{12}	ν_{13}	ν_{23}	$G_{12}(GPa)$	$G_{13}(GPa)$	$G_{23}(GPa)$
37	37	4.7	0.3	0.3	0.3	8.2	3.5	3.5

The damage onset was modeled using Hashins Failure criteria [18]. This criterion accounts for four damage initiation mechanisms: fiber tension (Equation 4.3), fiber compression (Equation 4.4), matrix tension (Equation 7.2), and matrix compression (Equation 4.6). σ^{11}, σ^{22} and τ^{12} are the

longitudinal, transverse and shear effective stress tensor in the lamina. X^T and X^C are the tensile and compressive strengths in the longitudinal direction. Y^T and Y^C are the tensile and compressive strengths in the transverse direction. S^L and S_T are the longitudinal and transverse shear strengths. The woven carbon/vinyl ester strength values are shown in Table 4.2.

$$F_f^t = \left(\frac{\sigma_{11}}{X^T}\right)^2 + \left(\frac{\tau_{12}}{S^L}\right)^2 \tag{4.3}$$

$$F_f^t = \left(\frac{\sigma_{11}}{X^c}\right)^2 \tag{4.4}$$

$$F_m^t = \left(\frac{\sigma_{11}}{Y^T}\right)^2 + \left(\frac{\tau_{12}}{S^L}\right)^2 \tag{4.5}$$

$$F_m^c = \left(\frac{\sigma_{22}}{2S^T}\right)^2 + \frac{\sigma_{22}}{Y^C}\left[\left(\frac{Y^C}{2S^T}\right)^2 - 1\right] + \left(\frac{\tau_{12}}{S^L}\right)^2 \tag{4.6}$$

Table 4.2: Woven carbon/vinyl ester lamina strengths

$X^T(MPa)$	$X^C(MPa)$	$Y^T(MPa)$	$Y^C(MPa)$	S^L	S_T
1707	1031	1707	1031	85.875	85.875

The longitudinal and transverse tensile fracture energies were taken to be 60 kJ/m^2 and 80 kJ/m^2.

4.1.2.3 Damage criteria and properties for the matrix

For the layers of the matrix, a cohesive damage model was introduced to account for delamination. The element type used was COH3D8 (an 8-node three-dimensional cohesive element in ABAQUS). Cohesive zone elements modeled the interlaminar regions. The damage model consisted of a linear-elastic response until the onset of damage. After the damage onset, the delamination process was controlled by a bilinear cohesive constitutive relation. The linear-elastic input parameters were defined as follow: t_e is the thickness of the interface cohesive element, so the penalty stiffness were approximated as: $K_3 = E/t_e$ and $K_{sh} = G/t_e$. The linear-elastic mechanical properties are shown in Table 7.5. The interface strengths dictated the damage onset for pure mode I (t_n^0) and shear modes II (t_s^0) and III (t_t^0), which are shown in Table 7.6.

Table 4.3: Linear-elastic mechanical properties of Epoxy [1]

$E(GPa)$	ν	$G(GPa)$
2.8	0.3	1.2

Table 4.4: Epoxy Interface Strengths

$t_n^0(MPa)$	$t_s^0(MPa)$	$t_t^0(MPa)$
53.78	86.88	86.88

A quadratic stress failure criterion was used for the prediction of damage onset with the following equation:

$$\left(\frac{t_n}{t_n^0}\right)^2 + \left(\frac{t_s}{t_s^0}\right)^2 + \left(\frac{t_t}{t_t^0}\right)^2 = 1 \tag{4.7}$$

The interface fracture toughness (critical strain energies) for pure mode I G_{IC} and shear modes II (G_{IIC}) and III (G_{IIIC}) are given in Table 7.7. The mode interaction parameter chosen was η=1.45 as proposed by Crews and Reeder [74].

Table 4.5: Epoxy Interface Fracture Toughness

$G_{IC}(N/mm)$	$G_{IIC}(N/mm)$	$G_{IIIC}(N/mm)$
0.4845	0.4845	0.4845

4.2 Results and Discussion

The impact energies considered for the impact tests were 20 J, 25 J, 30 J, and 35 J. The time, deformation, energy, force, velocity and voltage were recorded by the data acquisition system CEAST DAS 8000 Junior of the impact machine for each test conducted. In addition, the laminate impact response was evaluated in terms of visual damage, degree of damage and failure mechanisms.

4.2.1 Impact Model

Figure 7.12(a) shows the force-time response of an experimental and simulated impact test at 25 J.

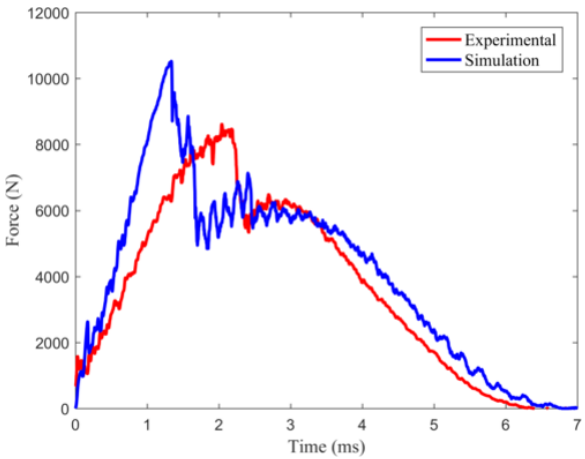

Figure 4.6: Representative force-time curve of an experimental and simulated low-velocity event

The general curve trend between the experiments and the simulation is comparable. The impact duration is well predicted. The maximum impact and stiffness are overpredicted. The accuracy of the simulation might decrease when fiber fracture appeared because not all the failure modes are taken into account such as bending or matrix/fiber crushing [75]. Figure 4.7 shows the lamina damage (fiber fracture) of the sample impacted at 25 J. As it can be seen, the model was able to capture the “plus sign damage on the surface of the laminate and the fiber fracture (red region) at the impacted and back face of the laminate. Figure 4.8 shows cross-sectional matrix damage (delamination) of the sample impacted at 25 J.

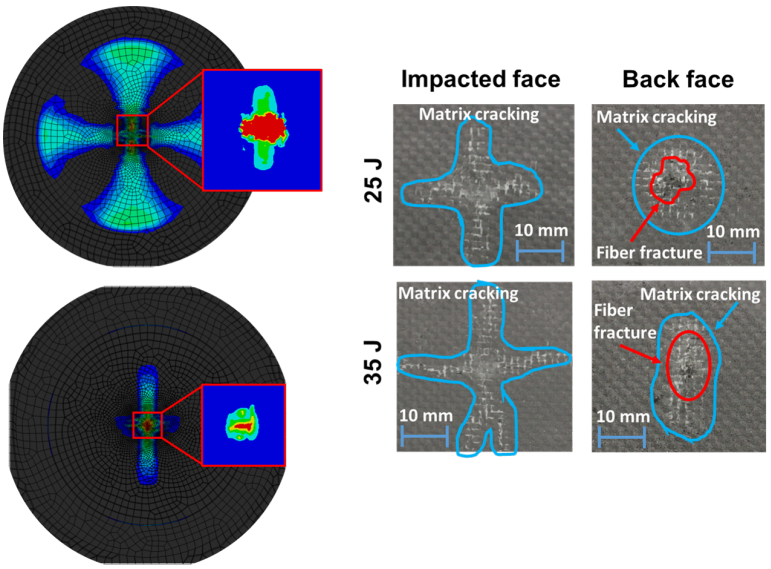

Figure 4.7: Lamina damage (Fiber fracture)

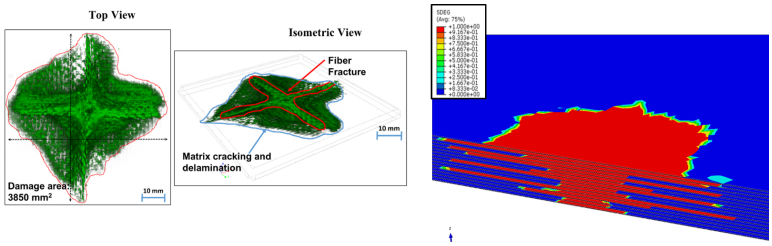

Figure 4.8: Matrix damage (delamination)

4.3 Conclusion

The single impact response of woven carbon/vinyl ester laminate was investigated. Two damage models were used one to predict fiber fracture and one to predict matrix damage (delamination). Hashins failure theory predicted the onset of fiber fracture damage. Delamination was predicted using cohesive zone modeling. The computational model was able to predict the general trend of a force-time curve. However, due to the simplicity of the model not all the failure mechanisms of the fibers were accounted such as bending or fiber/matrix crushing. Therefore, only an approximation of the experimental results was obtained. The computational model was able the “plus sign failure pattern and the delaminated area.

Chapter 5

Printed Reinforcements for Enhancing the Interlaminar Fracture Toughness of Fiber Reinforced Laminates

5.1 Introduction

Reduction of weight and maintenance cost have been two of the main goals of lightweight and energy efficient structures. A key aspect towards achieving this is to enable the materials used for such applications to be more durable, damage resistant and lighter. As a result, fiber reinforced laminated composites have become an attractive option to replace conventional materials such as steel or aluminum [76], with tailorable mechanical properties, high specific stiffness, high strength-to-weight ratios, corrosion and fatigue resistance, etc. [9, 10]. Due to such favorable properties, fiber reinforced laminates have been successfully integrated in aerospace vehicles, wind energy turbine blades, rockets, marine structures and automobiles [11].

Carbon fiber reinforced polymeric composites consist of layers of carbon fibers reinforced in a polymeric matrix (usually epoxy). The in-plane mechanical properties along the fiber direction in unidirectional laminates are strong and stiff. However, their response in the through-thickness direction is inferior due to significant contribution of resin within the layers of laminate as well as at the interface between layers of reinforcing fibers, known as “interlaminar region”. Interlaminar regions are weak regions and are highly susceptible to damage, often causing delamination type failure.

Typical failure mechanisms observed in composite structures are delamination or interlaminar fracture, matrix cracking, matrix-fiber debonding, fiber breakage, fiber pullout, etc. [22, 77]. Among these, delamination is a failure mode that can significantly reduce the residual strength of composites [78]. Delamination can occur due to manufacturing defects caused by bad layup, crack between layers, weaker matrix phase, etc. and/or under in-service conditions due to interlaminar

stresses, impact loading, compressive loading, static overload and fatigue [79, 80, 81, 82, 83, 84]. Therefore, the interlaminar properties like strength and fracture toughness should be improved for enhancing the damage resistance and residual strength of fiber reinforced laminates.

In this paper, a novel method to improve the interlaminar fracture toughness of prepreg laminates is proposed. Interlaminar fracture toughness is the amount of energy required to create new surfaces. The three fracture modes are: Mode-I (opening mode), Mode-II (sliding shear mode) and Mode-III (scissoring shear mode) [79, 85]. The focus here is on enhancing the Mode-I and Mode-II interlaminar fracture toughness values of carbon fiber reinforced unidirectional prepreg composites using polymer additive manufacturing (PAM).

Previous researchers have explored several methods to increase the interlaminar fracture toughness of polymeric composites, such as short rods (z-fibers), stitching, weaving, braiding [83], z-pins [86], carbon nanotubes [87], nanowires [88] or flocked fibers [89]. Due to the tacky resin in prepregs, most of the aforementioned reinforcement methods cannot be employed in prepreg laminates. Reinforcements that can be used with prepreg are: z-fibers, stitching, weaving and braiding and z-pins. However, any other reinforcements that requires temperature as well as aquous solutions such as carbon nanotubes and nanowires cannot be performed in prepregs. Moreover, pockets of resin rich regions tend to form around reinforcements in stitching, weaving and braiding resulting in lower in-plane properties [90]. Carbon nanotubes and ZnO nanowires were synthesized only on dry fabrics due to the temperatures and synthesizing environments needed to grow them. Carbon nanotubes can also be grown in wafers and be transferred to prepregs, but they tend to create bundles. Flocked fibers were also fabricated on dry fabrics [89]. Further, to improve matrix toughness, modifiers such as thermoplastics and rubber particles have been tested with success, but they also result in degradation of the matrix [91]. For these reasons, only short rods (z-fibers) and z-pins have been used as through-thickness reinforcements in prepreg laminates. Though an increase in through-thickness response has been observed with both the methods, the in-plane properties appear to have decreased as a result of reduction in the in-plane volume fraction, damage in the reinforcing fibers or the creation of large resin pockets [83, 92]. To avoid damage in the reinforcing fibers due to the insertion of pins or needles, polymer additive manufacturing (PAM) as an avenue for imparting interlaminar reinforcements is explored in the current study.

Most of the studies so far involving polymer additive manufacturing and composites have been focused on using fibers or particles as reinforcing phases in amorphous thermoplastics (acrylonitrile butadiene styrene (ABS) or poly lactic acid (PLA)) as matrix [93, 94, 95]. This is the very first time PAM has been used as means to provide pattern at the interlaminar regions in traditional prepreg composites with the goal of improving their interlaminar fracture toughness values. The proposed technique is particularly attractive for imparting spatially varying interlaminar reinforcements through precise computer aided design for mitigating damage at the interlaminar regions under diverse loading conditions. Carbon fiber reinforced unidirectional prepreg composites are considered here with fused deposition modeling (FDM) as the PAM technique for printing on the prepregs. Interlaminar Mode-I and Mode-II fracture toughness values with and without PAM reinforcements are compared using double cantilever beam (DCB) and end notched flexure (ENF) tests, respectively. It is hypothesized here that the PAM reinforcements constructed on the prepregs will provide resistance to the creation of new surfaces at the interlaminar regions of unidirectional prepreg laminates by locally melting the prepreg resin and fusing the pattern with the carbon fibers.

This paper is divided into the following sections: Section 5.2 describes the material system used, the process of printing onto prepregs and laminate fabrication methodology. This will be followed by the description of the tests conducted for calculating interlaminar fracture toughness values in Section 5.3. A detailed discussion comparing the fracture behavior, i.e. fracture toughness and surface morphology of interlaminar regions, of laminates with and without PAM reinforcements will be provided in Section 5.4, followed by conclusions.

5.2 Manufacturing

5.2.1 Material System

Unidirectional carbon fiber prepreg tapes were purchased from CST Composites (http://www.cstsales.com) to manufacture the laminates. The material properties of the carbon fiber prepreg are given in Table 5.1. Carbon fiber density ranges from 1.75-1.95 (g/cm^3) [96]. The resin in the prepreg is polypropylene (PP), which has a density of 0.9 (g/cm^3) [96]. Unidirectional layers of 203 mm by 203 mm were cut from the prepreg to manufacture the laminates for this study. According to

Nogueira et al. [97], unidirectional carbon fiber laminates reinforced with polypropylene have a tensile strength of ≈458.3 MPa and a modulus of elasticity of ≈43.5 GPa along the fiber direction.

Table 5.1: Prepreg properties

Properties	Prepregs
Fiber aerial weight	150 g/m^2
Resin content	35 %
Thickness	0.127-0.152 mm

Polylactic acid (PLA) was the printing filament material used for the interlaminar reinforcements, which was procured from MakerBot Industries, Brooklyn, NY, USA. According to MakerBot material data, PLA printed at high resolution (i.e. 100% infill) has compressive, tensile and flexural strengths of approximately 18 MPa, 47 MPa and 62 MPa, respectively.

5.2.2 Printing on Prepregs

Fused deposition modeling (FDM) technique was used to print interlaminar reinforcement onto the prepreg layers with a MakerBot Replicator desktop 3D printer as shown in Fig. 5.1(a). Release paper was peeled from the back of prepreg layer and then placed on a 25 cm by 25 cm bagging film, which was then attached to the printer plate with scotch tape as shown in Fig. 5.1(b). The scotch tape secured the prepreg from moving while printing and to prevent dirt from adhering to the prepreg layer from the printer plate. PLA was melted in a heated liquefier at a temperature of 210 °C and printed on top of the prepreg through a printing nozzle. This temperature was high enough to initiate partial melting of the prepreg resin in order for the PLA reinforcement to adhere to the prepreg.

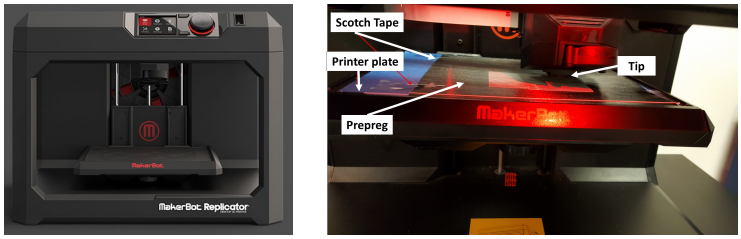

(a) (b)

Figure 5.1: (a) MakerBot Replicator desktop 3D printer and (b) 3D printing on prepregs

This machine typically prints a raft on the printer baseplate, which acts as a support on which the actual computer aided design (CAD) 3D model is printed. A raft provides a consistent build surface, which promotes better adhesion of the printed part onto it. Typical MakerBot printer raft consists of thick and wide zigzag lines as shown in Fig.5.2(a). The PAM interlaminar reinforcement design chosen for this study consisted only of thin lines perpendicular to the direction of fibers in a prepreg, as shown in Fig.5.2(b). In order to print this design directly onto the prepreg, the raft settings were modified to obtain fines line patterns. The default dimensions of the printed raft were 15 mm long x 2.5 mm wide x 0.3 mm thick at 0.8 mm spacing, which were set to 150 mm long x 1 mm wide x 0.2 mm thick at 5 mm spacing to attain the print lines of the PAM reinforcement. By default, the raft is printed in 3 layers in the thickness direction. However, the printing was restricted to a single layer to obtain fine interlaminar reinforcements.

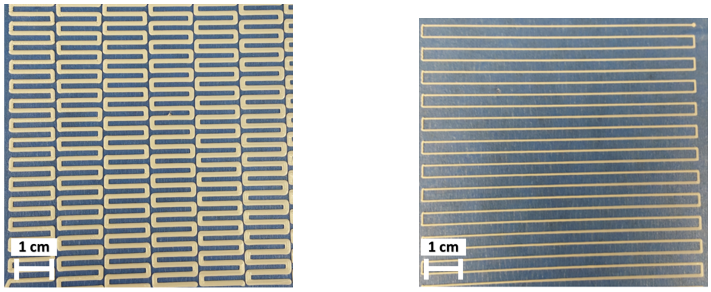

(a) (b)

Figure 5.2: Printed raft: (a) default and (b) custom

Fig. 7.7(a) shows the final result of the printed pattern on a prepreg layer. Cross-sectional dimensions of the final printed PAM reinforcements were 0.4 mm wide x 0.24 mm thick placed at 5 mm spacing as shown in Fig.5.3(b). This difference between the final printed reinforcement and the custom raft setting dimensions is attributed to the shrinkage caused by solidification during the cooling step of the printing process.

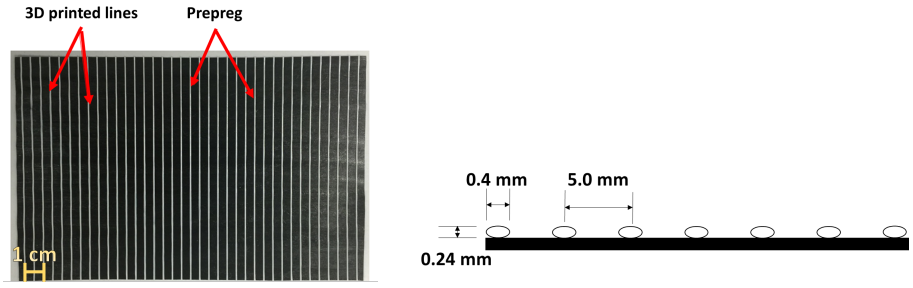

(a) (b)

Figure 5.3: (a) Printed pattern on prepreg; (b) Schematic of cross-section of 3D printed prepreg.

5.2.3 Laminate Fabrication

Hand layup procedure was followed to manufacture the unidirectional laminates with and without interlaminar reinforcements. Laminates of two thicknesses were fabricated with 28 and 32 prepreg layers corresponding to the requirements of Mode-I (DCB) and Mode-II (ENF) tests, respectively. To achieve proper compaction of the prepreg layers, a process called "debulking" was followed. This process has shown to result in higher quality laminates by ensuring that the layers are compacted sequentially as they are being placed. The debulking step involved placing release fabric and a breather layer on top of three layers of prepreg, followed by drawing it to vacuum by placing it in a vacuum bag for 15 minutes. This step was repeated until all layers were assembled. The final assembly was placed between two aluminum mold plates, along with peel ply and breather.

Figure 5.4: Laminate manufacturing setup

The entire setup was then enclosed in a vacuum bag and drawn into vacuum as shown in Fig. 5.4, which was then placed inside an oven for curing. The temperature in the oven was ramped up to 90 °C at a rate of 1.5 °C per minute and held for 20 minutes to release any trapped air. After that, the temperature was increased to 135 °C and held for 1 hour. Finally, the laminate was cooled to 120 °C prior to removing from the oven as suggested by the manufacturer. All the specimens, with and without PAM reinforcements, for DCB and ENF tests each were fabricated as one laminate as shown in Fig. 5.5(a) and in Fig. 5.5(b) to ensure identical curing conditions. A Teflon sheet of 0.05 mm thickness was placed between the 14^{th} and 15^{th} layers in DCB laminates, and 16^{th} and 17^{th} in ENF laminates to create a pre-crack along the neutral axis of the specimens. The average thickness of laminates fabricated for DCB samples was 4.38±0.03 mm for unreinforced and 4.65±0.07 mm for reinforced laminates. The same for ENF samples was 5.08±0.04 mm for unreinforced and 5.31±0.02 mm for reinforced laminates. The layers with printed patterns were staggered as shown in Fig. 5.5(c), such that the PAM reinforcements do not overlay onto each other.

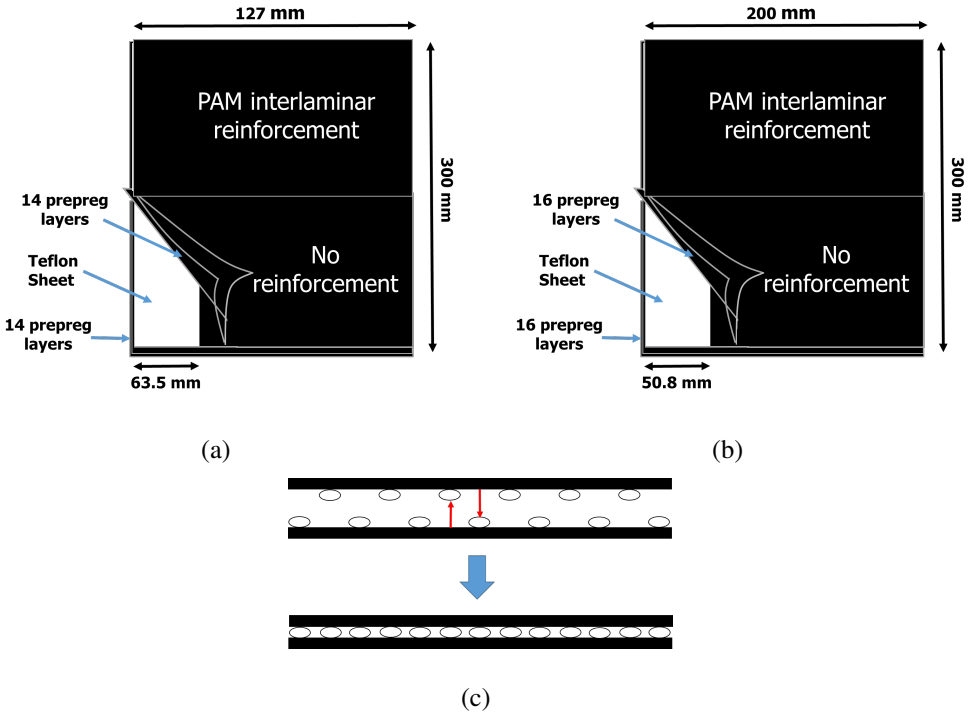

Figure 5.5: Schematic of (a) the manufactured DCB laminate, (b) the manufactured ENF laminate and (c) assembled interlaminar PAM reinforcement

5.3 Tests to Determine Interlaminar Fracture Toughness

Upon fabrication, double cantilever beam (DCB) and end-notched flexure (ENF) tests were performed to calculate Mode-I and Mode-II interlaminar fracture toughness values. The test procedures are briefly described in the sections below.

5.3.1 Mode-I Fracture Toughness: Double Cantilever Beam (DCB) Test

Mode-I interlaminar fracture toughness, which is the critical strain energy release rate in J/m^2, was determined using DCB tests. A DCB specimen typically consists of a rectangular uniform thickness laminated composite with a non-adhesive insert at the mid-plane that serves as a delamination initiator [98]. Opening forces were applied to the DCB specimen using hinges on the top and bottom surfaces at one end of the specimen by controlling the opening displacement, during which the load and delamination length were recorded [98].

According to the ASTM Standard D5528-13 [98], the dimensions (Fig. 5.6(a)) of each specimen were maintained at 127 mm long and 25.4 mm wide. The thickness of the samples with and without PAM reinforcements was 4.65$\pm$0.07 mm and 4.38$\pm$0.03 mm, respectively. A Teflon sheet inserted along the neutral axis of the laminate simulated a pre-crack of 63.5 mm long x 25.4 mm wide x 0.05 mm thick. Eight specimens were tested in total (four specimens with and four without PAM reinforcements). The initial delamination length was measured from the point where the load was applied to the end of the pre-crack. Tests were performed on an Instron 5969 machine at a loading rate of 1 mm/min (recommended loading rate was 1 - 5 mm/min by ASTM D5528-13) using a displacement control unit. During the loading, it was recorded the load point at which the visual delamination was observed on the edge of the specimen, which corresponded to a drop in load in the load-displacement graph. The crack extension was recorded and the specimens were restored to their original position at an unloading rate of 25 mm/min. About 4-5 loading-unloading cycles were conducted for each DCB specimen.

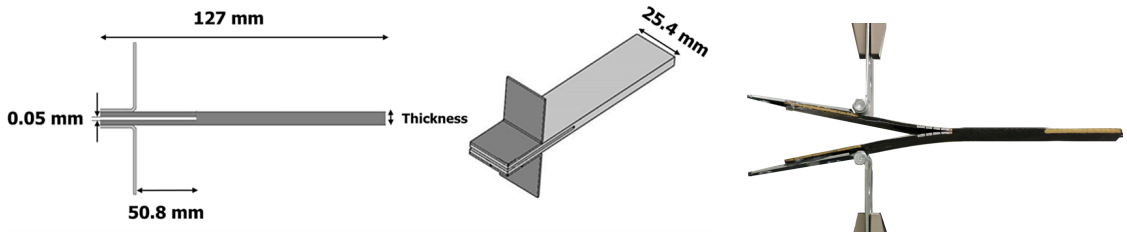

(a) (b)

Figure 5.6: (a) Dimensions of DCB specimens; (b) DCB test in progress of a carbon fiber laminate with PAM reinforcement

Data reduction methods suggested by the ASTM standard were used to calculate the Mode-I interlaminar fracture toughness, G_{IC}, which is influenced by the accuracy of the measured load, displacement, crack length and the change in compliance with crack length. Three data reduction methods were applied to the load-displacement data obtained from the tests: (1) modified beam theory (MBT), (2) compliance calibration (CC) and (3) modified compliance calibration method (MCC) as specified in ASTM D5528-13 [98]. Fig. 5.6(b) shows the DCB test in progress for one of the specimens.

5.3.2 Mode-II Fracture Toughness: End-Notched Flexure (ENF)

Mode-II interlaminar fracture toughness, which is the critical strain energy release rate in J/m^2, was calculated by conducting ENF tests. ENF specimen consists of a rectangular, uniform thickness laminated composite with a non-adhesive insert at the mid-plane that acts as a crack initiator [99]. ENF specimens were subjected to loading in a three point bend fixture that consists of two support points at the bottom and one load point at the top of the specimen at the mid-span [100]. The applied load, center point displacement and crack length were measured and recorded during displacement controlled tests.

According to the ASTM Standard D7905/D7905M-14 [99], the dimensions (Fig. 5.7(a)) of each specimen were 200 mm long and 25.4 mm wide. The thickness for the samples with and without PAM reinforcement were 5.31$\pm$0.04 mm and 5.08$\pm$0.02 mm, respectively. A Teflon sheet was inserted to simulate a pre-crack as described above. Tests were performed on an Instron 5969

machine at a loading rate of 0.5 mm/min. Eight specimens were tested in total (4 specimens with and 4 without PAM reinforcements).

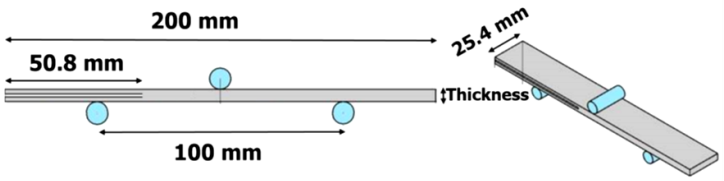

(a)

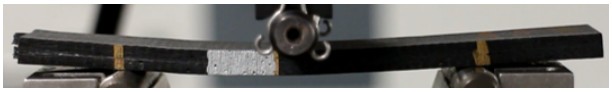

(b)

Figure 5.7: (a) Dimensions of ENF specimens; (b) ENF test in progress of a carbon fiber laminate with PAM reinforcements

In a typical test, a specimen was positioned on top of the two support rollers of the three point bending fixture. The distance between the pre-cracked tip with respect to the center of one of the support roller was 30 mm. The specimen was then subjected to three point bending until an abrupt drop in the force-displacement response was observed, which was accompanied by crack propagation. The unloading rate was held at 0.5 mm/min. Fig. 5.7(b) shows an ENF test in progress of one specimen. Compliance calibration (CC) method is described in ASTM D7905 [99] for calculating the Mode-II interlaminar fracture toughness values. The compliance (C) was determined by linear least squares regression analysis of the slope of the load-displacement response, and the fracture toughness was calculated using the compliance calibration method as described in ASTM D7905.

5.4 Discussion of Results

Interlaminar fracture toughness values of laminates with and without PAM reinforcements are compared in this section. Discussion of key observations and findings from the DCB and ENF tests are presented here with a focus on failure patterns at the interlaminar regions.

5.4.1 Mode-I Fracture Toughness: Double Cantilever Beam

Mode-I fracture toughness values were compared between the composite specimens with and without PAM reinforcements. As explained before, each specimen was loaded until an abrupt drop in load was observed. The extent of crack propagation was measured, and the specimen was unloaded to its original position. The specimen was reloaded again with the same loading rate of 1 mm/min until the next load drop occurred. The loads and displacements were recorded during each loading-unloading cycle for the entire duration of each test. The load-displacement response for four cycles of one specimen without PAM reinforcement is shown in Fig. 5.8(a) and the same for five cycles of one specimen with PAM reinforcements is displayed in Fig. 5.8(b).

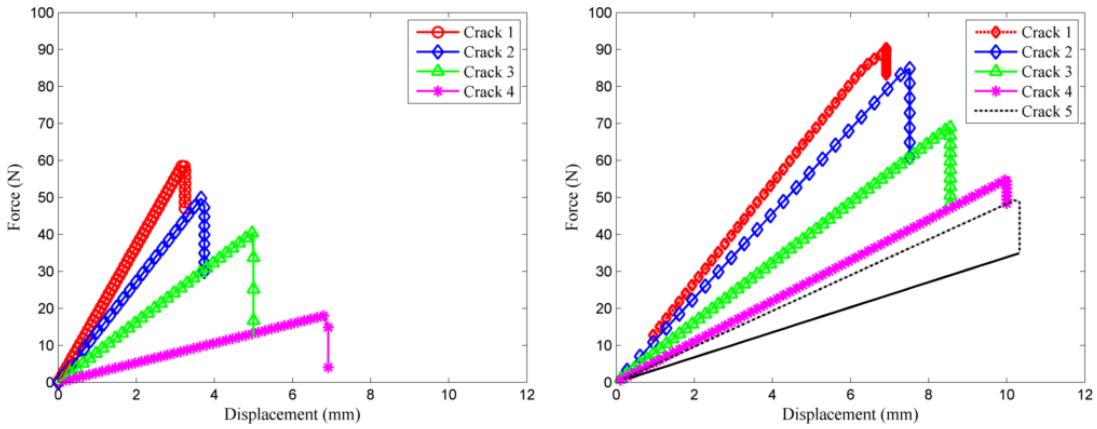

Figure 5.8: Typical load-displacement response of a single DCB test specimen (a) without and (b) with PAM reinforcement

The sample without PAM reinforcements (Fig. 5.8(a)) manifests larger drops in the peak load corresponding to each crack extension. However, the load drop is relatively gradual in the specimen with PAM reinforcements (Fig. 5.8(b)). Also, reinforced samples experience a higher average peak force (90$\pm$7 N) in comparison with the samples without (52$\pm$6 N). As stated earlier, G_{IC} values were calculated using three data reduction methods: MBT, CC and MCC. G_{IC} values corresponding to each method are given in Table 5.2 and 5.3 for specimens without and with PAM reinforcements, respectively. The crack length chosen to calculate G_{IC} corresponded to the point on which the visual onset of delamination movement was observed on the edge of the specimen.

Table 5.2: G_{IC} (kJ/m^2) without PAM reinforcements

Specimen	MBT	CC	MCC
1	0.38	0.38	0.38
2	0.34	0.34	0.34
3	0.35	0.34	0.36
4	0.41	0.41	0.41
Average	0.37±0.02	0.37±0.03	0.37±0.03

An increase of ≈27% with MBT method, ≈27% with CC method, ≈29% with MCC method is observed with interlaminar reinforcements. Thus, PAM reinforcements appear to improve the Mode-I interlaminar fracture toughness of unidirectional carbon fiber reinforced laminated composites.

Table 5.3: G_{IC} (kJ/m^2) with PAM reinforcements

Specimen	MBT	CC	MCC
1	0.53	0.52	0.54
2	0.46	0.46	0.48
3	0.45	0.43	0.43
4	0.44	0.45	0.47
Average	0.47±0.04	0.46±0.04	0.48±0.04

5.4.2 Mode-II Fracture Toughness: End-Notched Flexure

Fig. 5.9(a) and Fig. 5.9(b) show the load-displacement responses of specimens without and with PAM reinforcements from all ENF tests conducted. Reinforced specimens sustain higher peak loads (855±48 N) as compared to the ones without (563±54 N). Also, a significant change in the post peak behavior is observed, where the reinforced samples manifest a progressive post peak failure behavior as opposed to a sudden brittle type failure observed in the unreinforced samples.

Table 5.4: G_{IIC} (kJ/m^2)

Specimen	without PAM	with PAM
1	0.33	0.65
2	0.34	0.67
3	0.35	0.53
4	0.33	0.66
Average	0.34±0.02	0.63±0.07

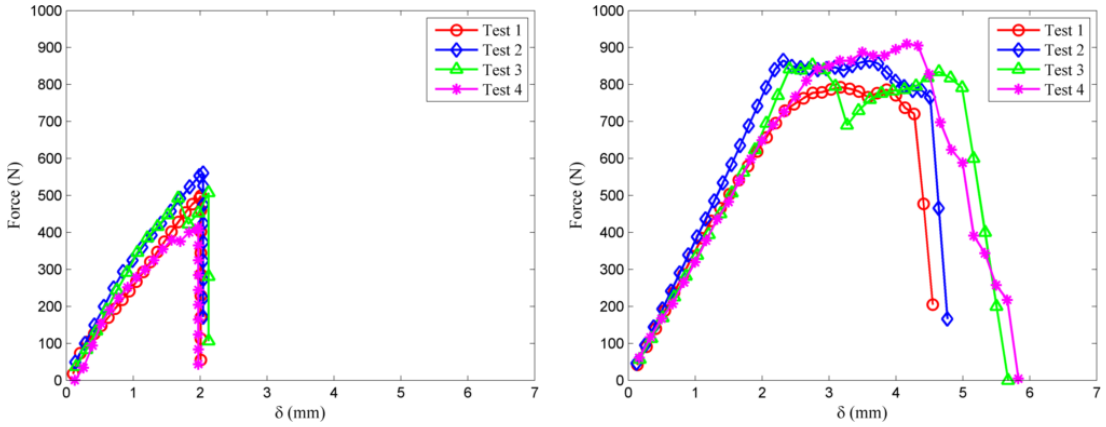

Figure 5.9: Load-displacement response of all ENF test specimens (a) without and (b) with PAM reinforcement

As stated earlier, G_{IIC} values were calculated using the CC reduction method, and are reported in Table 5.4. An increase of ≈87% is observed in PAM reinforced samples using the CC method for calculation. Also, the overall area under the load-displacement response was calculated for each test, which showed an increase of ≈434% in samples with interlaminar reinforcements. Therefore, PAM reinforcements appear to significantly improve the Mode-II interlaminar fracture toughness of unidirectional carbon fiber reinforced laminates.

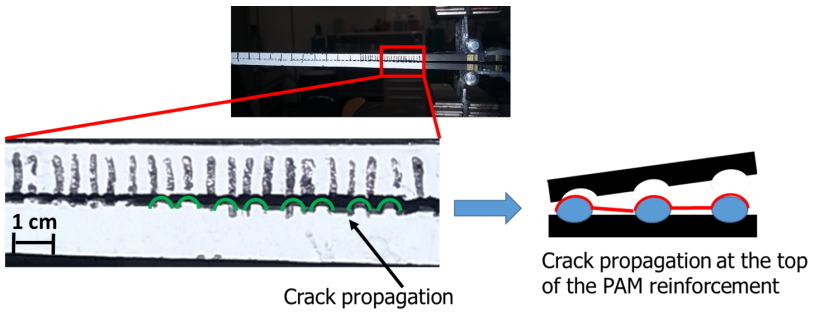

Figure 5.10: Crack path in a DCB test with PAM reinforcement

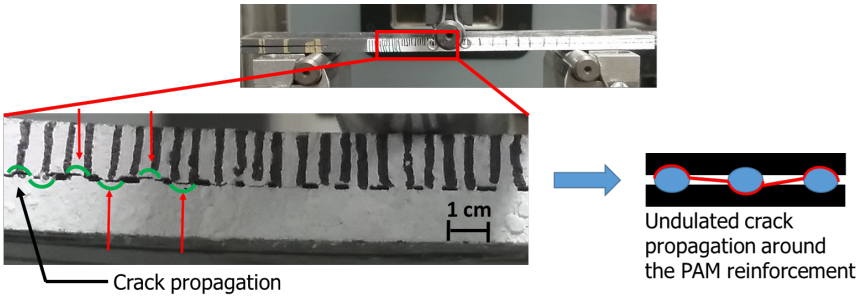

Figure 5.11: Crack path in an ENF test with PAM reinforcement

5.4.3 Visual and Fractographic Analysis of Fractured Surfaces

The newly created surfaces due to crack propagation through the mid-plane of the specimens after DCB and ENF tests were visually investigated. In reinforced samples, the crack path deviated from a straight line along the mid-plane and propagated in an undulated path upon reaching PAM reinforcements. Fig. 5.10 and Fig. 5.11 show the crack path for the DCB and ENF specimens, respectively.

As mentioned before, the increase in G_{IIC} is significantly higher than G_{IC} values. This is attributed to the undulated crack path around the PAM reinforcement along the interlaminar region. The undulated crack path increases the effective length of crack propagation resulting in longer time for the crack to propagate. The tortuosity of the crack path contributes towards increasing the fracture toughness of the interlaminar region [101, 102].

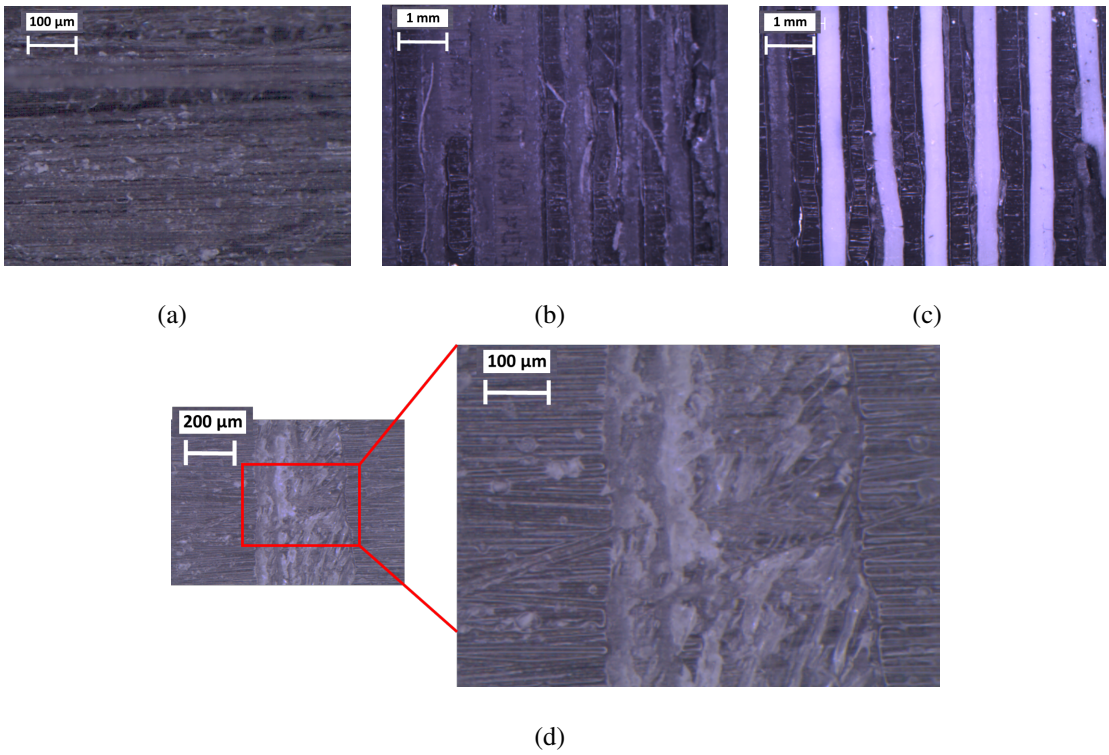

Figure 5.12: Fracture surface of a DCB specimen (a) unreinforced area, (b) debonded PAM reinforcement surface (top), (c) PAM reinforcerment surface (bottom), and (d) magnified debonded surface where PAM reinforcement was printed

The fractured surfaces of specimens with and without PAM reinforcements were also examined under an optical microscope. In both DCB and ENF specimens, these surfaces were restricted to the interlaminar region along the mid-plane of the laminate. In the unreinforced samples, the fractured surfaces appear to be smooth as shown in Fig. 5.12(a) for DCB and Fig. 5.13(a) for ENF samples. Fig. 5.12(b) and Fig. 5.12(c) display the top and bottom fracture surfaces of a DCB specimen, where the peeling effect on the reinforcements is observed. A magnified image of the bottom surface is shown in Fig. 5.12(d), where the resistance to peeling is manifested by the deformation under the printed patterns. In the ENF samples, the crack propagation was undulated around the PAM interlaminar reinforcements as shown in Fig. 5.13(b), where alternating printed reinforcements are seen on the fractured surface. Magnified image (refer to Fig. 5.13(c)) of a newly created surface displays the shear resistance promoted by the reinforcements. The friction between the resin and the interlaminar reinforcement resulted in the resin being pulled in the direction of the crack propagation. This corroborates the observed increase in Mode-II fracture toughness.

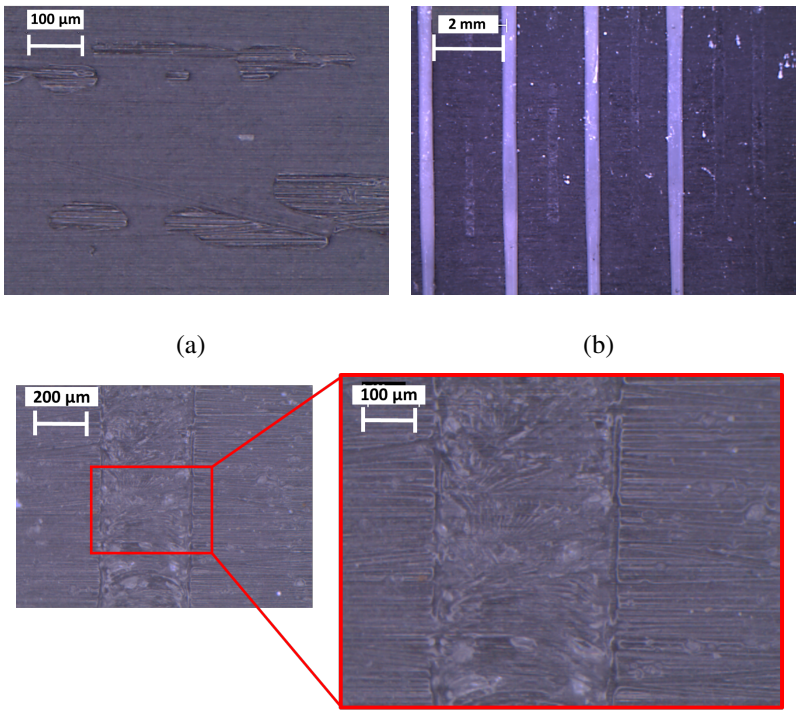

Figure 5.13: Fracture surface of an ENF specimen (a) Unreinforced area, (b) Debonded PAM reinforcement surface (top), and (c)Magnified debonded surface where PAM reinforcement was printed

5.5 Conclusion

In this paper, Mode-I and Mode-II interlaminar fracture toughness values of unidirectional carbon fiber reinforced laminates with and without polymer additive manufactured (PAM) reinforcements at the interlaminar regions were compared. Double cantilever beam (DCB) tests were conducted, and three data reduction methods: modified beam theory (MBT), compliance calibration (CC) and modified compliance calibration (MCC) were used to determine the Mode-I fracture toughness values. End-notched flexure (ENF) tests were were performed, and the Mode-II fracture toughness values were determined using compliance calibration (CC) method. Eight specimens were tested for each mode, four with and four without PAM reinforcements. This was followed by visual and fractographic analysis of the fractured surfaces. Key observations and conclusions of this paper are:

- Mode-I interlaminar fracture toughness increased by ≈27%, 27% and 29% as determined using MBT, CC and MCC date reduction methods.
- Mode-II interlaminar fracture toughness increased by ≈87%, which was determined using the CC method. The overall energy which was calculated as the area under the load-displacement responses resulted in an increase by ≈434%.
- Significantly higher increase in Mode-II fracture toughness is attributed to the tortuosity of the crack path around PAM reinforcements, which was accompanied by an effective increase in the area of the fracture surfaces created.
- It is hypothesized that finer reinforcements have the potential to increase the fracture toughness further because more surface area will be in contact with the prepreg. However, the size of the print lines was restricted by the capability of the printer used.

To summarize, the study presented in this paper showed very promising results of reinforcing interlaminar regions by introducing PAM reinforcements in carbon fiber reinforced unidirectional laminates. Significant improvement in the interlaminar fracture toughness was observed. This technique can be extended to other prepreg laminates seamlessly and is not restricted to carbon fiber reinforced laminates only.

Chapter 6

Elucidating the Mechanisms of Damage in Foam Core Sandwich Composites under Impact Loading and Low Temperatures

6.1 Introduction

An assessment by the U.S. Geological Survey (USGS) of the Arctic circle has revealed that approximately 22% of the world's undiscovered oil and natural gas resources are located in this region [25]. Due to ice melting in the Arctic, new passages (Northwest and Northeast) have been created, which can become viable transportation routes [26] in the future. Therefore, there has been a great deal of interest in Arctic exploration, which has necessitated the investigation of the mechanical behavior and damage mechanisms of current and future materials when exposed to low temperatures. Offshore structures, such as ship vessels, are typically subjected to adverse environments including but not limited to sea water, wave impacts and extremely low temperatures, which can cause surface alterations, internal damage, and degradation of their chemical and mechanical properties that may ultimately compromise their safety. Therefore, the materials used in these structures must be able to withstand harsh environmental conditions in addition to mechanical loads. Sandwich composites have become an attractive option for marine applications due to their lightweight, high stiffness and high strength to weight ratio [27]. Sandwich composites consist of two thin but very stiff facesheets that sandwich a thick lightweight core between them. The facesheets carry transverse loads or bending moments while the core carries transverse shear loads [12]. The separation of the facesheets increases the moment of inertia of the panels with little increase in weight, which results in an efficient structure that can resist bending and buckling loads [13]. Despite several advantages of sandwich composites, a major drawback is their low resistance to impact damage. Dynamic impact on structures can occur under different scenarios, for example, tool drop during maintenance and repair, wave slamming, iceberg collisions, bird or

hail strikes [14, 28, 29]. Low-velocity impacts typically occur at velocities below 10 m/s [17], which may produce barely visible damage (BVD) on composite surfaces (facesheets), but with the possibility of significant internal damage. This is deemed very dangerous, as BVD could result in catastrophic failure of the structure without warning. Therefore, low-velocity impact studies on sandwich composites is critical for material certification and establishing allowable for structural design. In particular, their response to dynamic impact loading at low temperatures is of main interest in this paper in light of arctic applications.

There is a wealth of research studies available that have focused on the dynamic impact behavior of foam core sandwich composites [103, 104, 105, 106, 107, 108, 109, 110, 111, 112, 113, 114]. Most of these prior studies have focused on low-velocity impact loading at room temperature (25 °C). Ozdemir et al. [107] investigated the effect of core material and thickness (5, 10 and 15 mm) of unidirectional E-glass/epoxy sandwich composite panel with PVC and poly(ethylene terephthalate) (PET) core with impact energies ranging from 10 J to 70 J at room temperature. They reported that the specimens absorbed more energy as the core thickness increased. Also, PVC cores had higher bending stiffness compared to PET cores. Schubel et al. [108] studied the quasi-static and low-velocity (1.6 to 5 m/s) impact behavior of woven carbon/epoxy sandwich composites with PVC foam core. They concluded that the low-velocity impact response of plates could be characterized as quasi-static based on the load-strain response and damage evaluation. Loganathan et al. [109] explored the effect of core thickness (10 and 14 mm) and density (70, 100 and 200 kg/m^3) of bi-directional woven E-glass/epoxy sandwich composite with polyurethane foam core under three different impact velocities (1.401, 2.426 and 3.123 m/s). They observed that the samples absorbed more energy with increasing core density and thickness. Park et al. [110] evaluated the impact damage resistance of unidirectional carbon/epoxy and glass epoxy sandwich composites with Nomex® honeycomb core at room temperature. They concluded that the damage resistance of sandwich structures is dependent on the facesheet material and core thickness.

Despite an extensive amount of research reported at room temperature, relative less research has been conducted at low temperatures. Gupta et al. [111] studied the blast performance of E-glass/ vinyl ester sandwich composites with Corecell™ M100 foam core at three different temperatures (22 °C, 80 °C and -40 °C) and average strain rate varied from 1600/s (-40 °C) to 2000/s (100 °C). They reported that the plateau stress reduced with increase in temperature from -40 °C to 100 °C,

which was attributed to thermal softening in the core that resulted in the collapse of cells under compression due to shock wave loading. On the other hand, the glass facesheets showed an increase in damage (delamination and fiber breakage) as the temperature increased from -40 °C to 100 °C. This was attributed to the softening of matrix in the facesheet, which led to the decrease in the compressive modulus and compressive strength of the composite. Erickson et al. [113] investigated the low-velocity impact behavior of woven E-glass/epoxy sandwich composites with filled and non-filled honeycomb core subjected to three different temperatures (-25, 25 and 75 °C) under three impact energies (12, 60 and 150 J), and concluded that the maximum impact force decreased and the energy absorption increased with increasing temperature (-25 to 75 °C). Salehi-Khojin et al. [114] explored the effects of temperature (-50 °C to 120 °C) on woven carbon fiber/epoxy, Kevlar®/epoxy and hybrid Kevlar®-carbon/epoxy sandwich composites with polyurethane foam filled with Kraft paper honeycomb core subjected to impact energies of 15, 25 and 45 J. They observed that the largest area of damage and fiber breakage occurred at -50 °C, which decreased with increasing temperature. There are more studies on the effects of temperature on fiber reinforced laminates [63, 64, 65, 66]. Castellanos et al. [115, 116] studied the single and repeated impact behavior of woven carbon/vinyl ester composites at room and arctic (-50 °C) temperatures subjected to four impact energies (20, 25, 30 and 35 J). They reported that the damage mechanisms shifted from predominantly matrix cracking to fiber fracture when the in-situ temperature was changed from room to arctic, and this shift was more noticeable at lower impact energies.

In the current study, the mechanical response and damage mechanisms of woven carbon/vinyl ester laminated sandwich composites with Polyvinyl chloride (PVC) foam core subjected to range of low-velocity impact loading at four different temperatures are investigated. Understanding the behavior of sandwich composites in these conditions is critical for the safety of structures and personnel. In addition, the identified damage mechanisms will serve as a guide for developing relevant repair and reinforcing techniques for foam core sandwich for use in such environment. The variations in impact response in terms of force, displacement, energy and damage mechanisms is studied in detail and presented here. In addition, a detailed visual damage investigation is conducted using micro-Computed tomography to identify key damage mechanisms, and support the observed responses of these sandwich composites.

6.2 Methods

6.2.1 Panel Fabrication

Woven carbon fiber/vinyl ester composite sandwiches with PVC core were manufactured by vacuum assisted resin transfer molding (VARTM) process [41] as seen in Figure 6.1(a). Woven plain weave carbon fabric and vinyl ester resin were purchased from Fibre Glast (www.fibreglast.com), and the H100 PVC foam was purchased from Aircraft Spruce (www.aircraftspruce.com). Vinyl ester was considered as the resin due to superior UV resistance and low water absorption as compared to polyester resins [39, 40]. PVC was considered due to their low cost, low density, fire retardancy and high insulation and damping properties [117]. The mechanical properties of the constituent materials are given in Table 7.4.

Table 6.1: Mechanical properties of the sandwich composite constituent materials

Mechanical properties	Woven carbon fiber	Vinyl ester resin	H100 foam	
			In-Plane	Out-of-plane
Tensile Modulus (MPa)	2275-2406	3700	111	126
Tensile Strength (MPa)	4200-4400	82.7	3	3.3
Density (kg/m^3)	1750-2000	1.800	100	100
Nominal thickness (mm)	0.3048	-	25.4	25.4

For fabricating a sandwich composite panel, PVC foam was sandwiched between two facesheets with [$(0/90)_4$/core/$(0/90)_4$] stacking sequence as per the instructions in ASTM D7766/D7766M-16 [118]. Here, $(0/90)_4$ implies 4 layers of plain weave carbon fabrics. This arrangement was placed between two layers of flow-media, two layers of breather and four layers of nylon peel ply. All the layers were cut to dimensions of 305 mm x 254 mm. This complete arrangement of fabrics was placed over an aluminum mold, then wrapped with two Stretchlon 800 bagging film and sealed with vacuum-sealant tape, ensuring spaces for both inlet and outlet connectors. The first vacuum bag was to assist in resin infusion, and the second vacuum bag was to apply continuous pressure during the curing process to obtain superior surface finish on the panels. A mixture of vinyl ester resin and Methyl Ethyl Ketone Peroxide (MEKP) hardener was used for resin infusion in the dry

woven fabrics, as well as ensuring bonding between facesheets and the core. The resin was catalyzed with 1.25% MEKP by weight and mixed thoroughly as recommended by the manufacturer. The resin/hardener mixture was placed in a desiccator first to remove any air bubbles from the mixture. The outlet was then connected to a vacuum pump until the vacuum bag achieved a pressure of approximately 80 MPa. The inlet of the vacuum bag was then submerged in the resin/hardener mixture for infusing resin through the sandwich panel. Upon completion of the resin transfer process, the panel was cured at room temperature for 24 hours under a constant pressure of ≈80 MPa by the second vacuum bag.

A total of 16 panels of 305 mm length x 254 mm width were manufactured. Four samples (shown in Figure 6.1(b)) were water jet cut from each panel. Impact test samples were randomly chosen from the set of all the samples fabricated to distribute any manufacturing induced effects on the impact response. Four samples were selected for testing for each combination of temperature and impact energy.

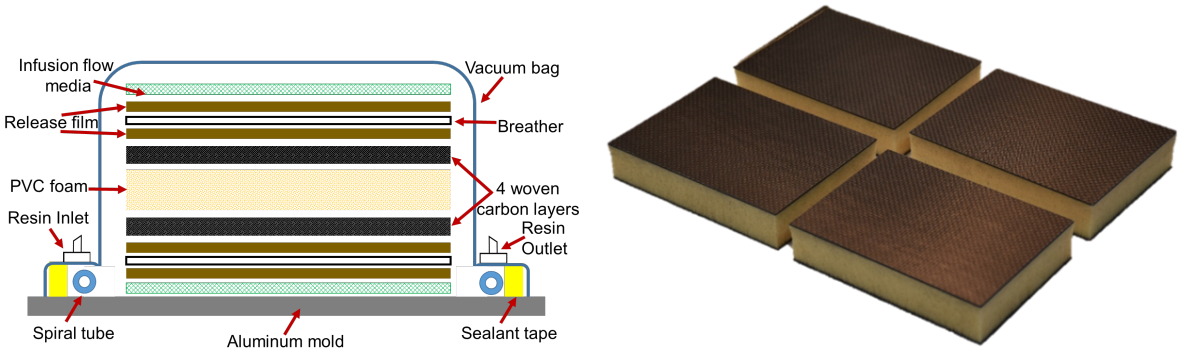

(a) (b)

Figure 6.1: (a) VARTM process configuration; (b) Samples obtained from each sandwich composite panel

6.2.2 Impact Tests

Drop-weight impact tests were performed using a CEAST 9350 Drop Tower Impact System with a load cell capacity of 22.4 kN and an in-built environmental chamber as shown on Figure 7.9. A metal fixture with a rectangular opening of 76 mm x 127 mm and toggle clamps was used. These clamps apply pressure in the vicinity of the four corners of the samples to prevent their motion during an impact event. The rectangular sandwich samples had dimensions of 150 mm length x 100

mm width (refer to Figure 7.9) with an average thickness of 27.43±0.16 mm. The core thickness was 25.4 mm, and each facesheet had an approximate thickness of 1 mm. A hemispherical striker with a fixed mass of 10 kg and a diameter of 12.7 mm was used for impacting the samples at the center of the top facesheet in the out-of-plane direction [42]. Impact velocities of 1.22 m/s, 2 m/s, 2.45 m/s and 3.46 m/s were chosen which correspond to kinetic impact energies of 7.5 J, 15 J, 30 J, and 60 J, respectively. All these tests were conducted at low-velocities, that is, below 10 m/s [119, 43]. The kinetic energies corresponding to these velocities were calculated based on the mass of the striker and the impact velocities using the equation:

$$E_k = \frac{1}{2}m^2 = mgh \tag{6.1}$$

Here, E_k is the impact energy or kinetic energy, v is the impact velocity, and m is the mass of the impacting striker, h is the height of the striker measured from the surface of a sample in the impact drop tower, and g is the gravitational acceleration.

In order to investigate the influence of temperature on the impact response of sandwich composites, four in-situ temperatures were selected: 25 °C, 0 °C, -25 °C and -50 °C. Robinson et al. [44] investigated the influence of impactor mass and velocity on the low velocity impact performance of woven carbon and glass fiber reinforced laminates for impact energy range from 0.25 J to 12 J. The impactor mass was varied from 1.15 kg to 2.10 kg and the velocity was adjusted to obtain the desired impact energies. They reported that the extent of impact damage predominantly depended on the magnitude of the impact energies and less on the mass or velocity individually. Based on this study, the impactor mass was held constant and the impact energy was varied for the prescribed velocities in the current paper.

Force-time, displacement-time and energy-time responses were recorded by the data acquisition system "CEAST DAS 8000 Junior" of the impact machine for each test. Four samples were impacted for each combination of impact energy and temperature. The samples impacted at temperatures different than 25 °C were placed in a temperature controlled environmental chamber, which was connected to the CEAST 9350 Drop Tower Impact System. A heat transfer analysis showed that uniform temperature of -50 °C for a 4 mm woven carbon fiber laminate could be achieved in 15 min given their relatively small thickness. Therefore, prior to every impact test,

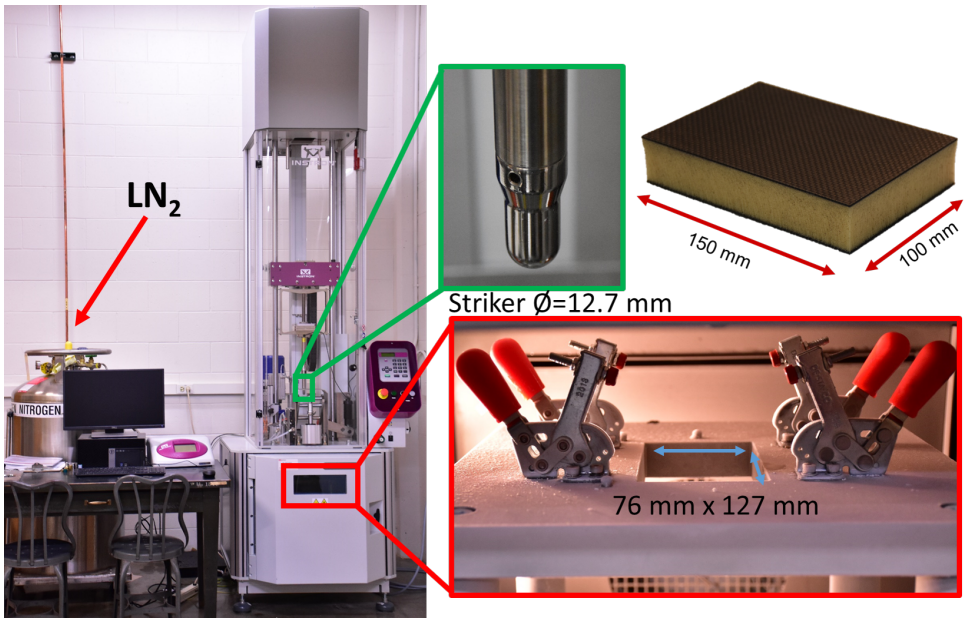

Figure 6.2: CEAST 9350 Drop Tower Impact System

the samples were conditioned in the environmental chamber for 20 minutes with Liquid Nitrogen (LN_2) to reach the desired temperature throughout the sample.

6.2.3 Micro-CT Scanning

Sandwich composite samples were examined under a micro-computed tomography (micro-CT) scanner, which is a non-destructive technique (NDT), upon subjecting to impact loading. The goal was to evaluate the internal damage incurred at different temperatures and impact energies. The samples were scanned within a Zeiss Metrotom OS 800 scanner at UW-Madison. For each sample, 1500 projections were made by rotating them until a complete revolution was obtained. The X-ray tube voltage and current were set to 80 keV and 120 μA, respectively. Reconstruction of the 3D virtual object was done with METROTOM OS software, and were further analyzed with VG Studio Max 22 software. A flat correction was applied for each scan.

6.2.4 Quasi-static tests to establish the effects of temperature on matrix and fibers

To further examine the influence of low temperature on sandwich composites, compressions tests were performed on pure vinyl ester samples and tension tests were performed on woven carbon/vinyl ester samples at 25 °C (RT) and -50 °C (AT). For the compression tests, three samples each of pure vinyl ester were tested in-situ at 25 °C and -50 °C under flat-wise compressive loading. Cylindrical samples with a diameter of 25.5 mm and a height of 50.8 mm were tested according to ASTM D695 [45]. The tests were performed using an ADMET eXpert 1654 testing system with a crosshead displacement rate of 1.3 mm/min. For the tension tests, five samples each of woven carbon/vinyl ester were tested in-situ at 25 °C and -50 °C under tensile loading. Rectangular samples with a width of 15 mm, length of 250 mm and thickness of 1 mm were tested according to ASTM D3039 [120]. These tests were also performed using the ADMET eXpert 1654 testing system mentioned above with a crosshead displacement rate of 2 mm/min.

6.3 Results and Discussion

Prior to discussing the results of dynamic impact tests, quasi-static test results on pure vinyl ester and woven carbon/vinyl ester laminates are discussed to shed light on the influence of temperature individually on the matrix and fibers.

6.3.1 Influence of temperature on the matrix and fibers under quasi-static loading

Prior research by Dutta [46] on the compressive response of glass fiber-reinforced polymer composites at the U.S. Army Cold Regions Research and Engineering Laboratory (CRREL) reported that the quasi-static strength and stiffness increased at low temperatures. However, they were also rendered brittle and manifested increased cracking due to higher residual thermal stresses caused by a mismatch in the coefficient of thermal expansion (CTE) between fibers and matrix. Similar behaviors were recorded in the current study as discussed next.

Tension tests on woven/carbon vinyl ester composite samples were conducted in the current study at 25 °C (RT) and -50 °C (AT). It was observed that the elastic modulus and ultimate tensile strength increased by approximately 15% and 11%, respectively, while the strain to failure reduced

approximately by 14% when the temperature is reduced from 25 °C to -50 °C. Representative tensile stress-strain responses at RT and AT are shown in Figure 6.3(a), which show a reduction in the ductility and increase in brittleness at AT [68]. Kim et al. [69] attributed such an increase in brittleness of a laminate under tension at low temperatures predominantly to fibers, as the brittleness of the fibers increased in the temperature range of 25 °C to -50 °C.

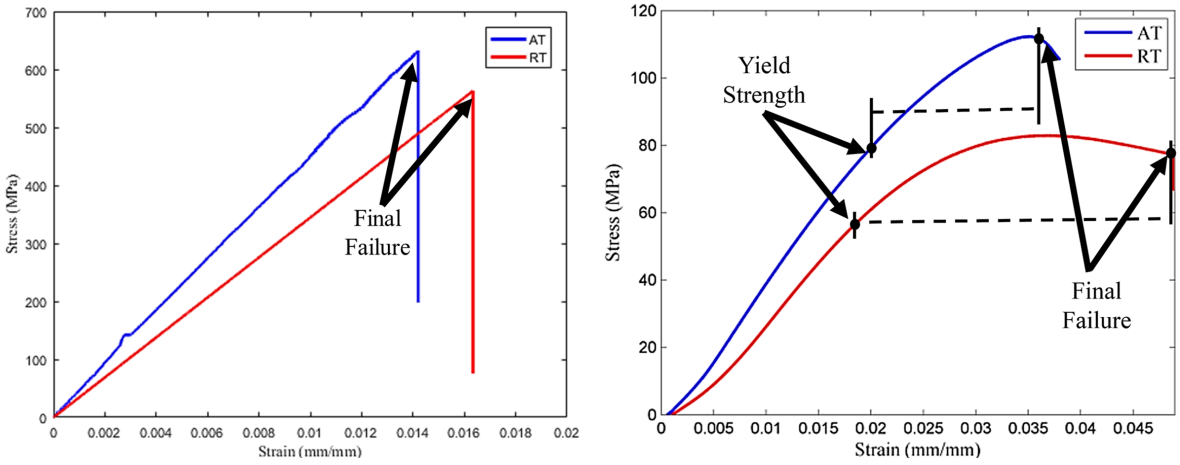

(a) (b)

Figure 6.3: (a) Typical tension stress-strain plots of woven carbon/vinyl ester at RT and AT, and (b) Typical compressive stress-strain plots of vinyl ester at RT and AT

Compression tests on pure vinyl ester were conducted in RT and AT. Representative compressive stress-strain responses of samples tested at 25 °C and -50 °C are shown in Figure 6.3(b). The yield strength (here denoted as the stress recorded at ≈0.02 strain), ultimate strength and elastic modulus increased by approximately 55, 49 and 28%, respectively, when the temperature is reduced from RT to AT. However, the strain to failure reduced by approximately 30% with decreasing temperature. This implies that the apparent elastic modulus and compressive strength of the resin increased at low temperatures. On the other hand, the resin also became more brittle at low temperatures and therefore was unable to withstand large deformations as compared to that at 25 °C.

6.3.2 Dynamic Impact Tests

Contact force-time, energy-time, and deformation-time responses were recorded by the data acquisition system of the impact machine for each combination of impact energy (7.5 J, 15 J, 30 J and 60 J) and temperature (25 °C, 0 °C, -25 °C and -50 °C) tested. In addition, the response of the laminates in terms of visual damage and damage mechanisms were established, which are discussed in detail in the following sections.

6.3.2.1 Contact Force-Displacement Response

Contact of the impact striker with the impacted face of a sandwich composite sample (top facesheet) generates the contact force and deflection during an impact test, which is recorded by the data acquisition system of the impact machine. Typically, contact force-deflection responses have an initial linear ascending region from which the initial bending stiffness [121] is determined. Three characteristic dynamic impact responses are shown in Figure 7.16, where the post-peak regimes upon reaching the maximum contact force have very different behaviors. There can be three possibilities: rebounding, penetration, and perforation of the striker. In Figure 7.16(a), the striker rebounds from the sample upon reaching a maximum contact force. A rebounding case is characterized by a gradual decrease in the displacement while the contact force diminishes to zero. Figure 7.16(b) shows a typical response of a descending regime that combines loading and unloading (rebounding). Here, there is a sudden drop in load after the maximum contact force is reached, which is typically due to damage in the top facesheet (impacted surface), such as fiber fracture, delamination or matrix cracks. This is followed by a small increase in load as the displacement increases, which is due to the crushing of the core by the striker. Finally, the striker rebounds without damaging the bottom facesheet. Figure 7.16(c) shows a representative case of striker penetration, where the striker perforates the top facesheet and the core of the sandwich composites, with no damage in the bottom facesheet. The displacement continues to increase with reduction in contact force, which implies that there is no rebound. Figure 7.16(d) shows a representative case of perforation of the sandwich composite by the striker. The striker perforates the top facesheet and penetrates the core beyond which the contact force increases resulting in a second peak contact

force which is larger than the first. This is attributed to the stiffness of the bottom facesheet which is locally subjected to local in-plane tensile loading. If the bottom facesheet is damaged, a sudden drop in contact force follows the second peak, which is typically due to fiber fracture. This is followed by an increase in displacement with reduction in contact force, which implies complete perforation of the sandwich composite.

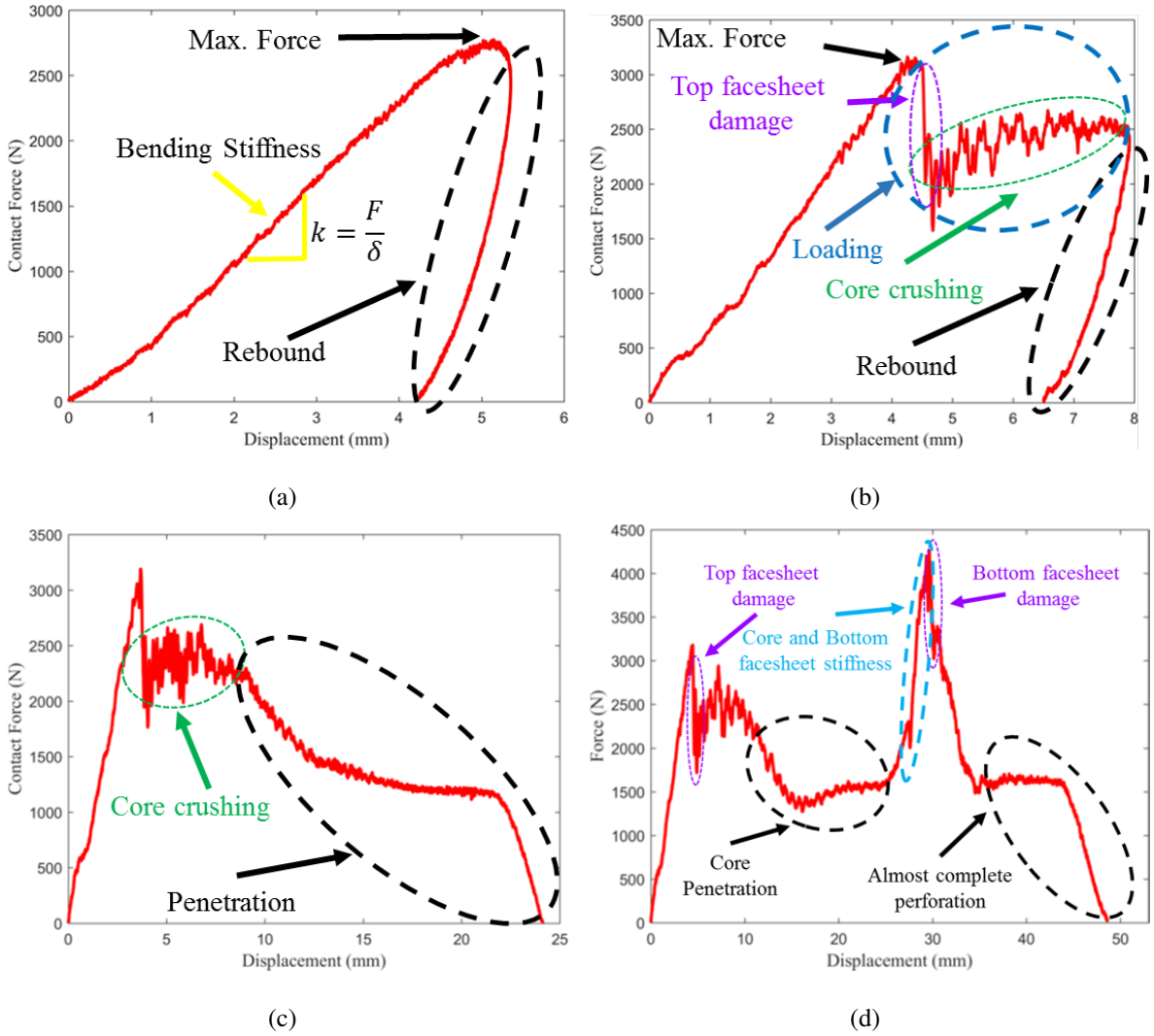

Figure 6.4: Typical load deflection responses of foam core sandwich composites under low-velocity impact loading: (a) Rebounding, (b) Partial loading and rebound, (c) Partial Perforation and (d) Complete Perforation

6.3.2.2 Influence of temperature on the contact force - displacement responses

In this section, the contact force-displacement responses were used to characterize the damage caused by an impact event at four different impact energies (7.5 J, 15 J, 30 J and 60 J) and four distinct temperatures (25 °C, 0 °C, -25 °C and -50 °C). Figure 6.5(a), Figure 6.5(b), Figure 6.5(c) and Figure 6.5(d) show the representative force-displacement responses for each case.

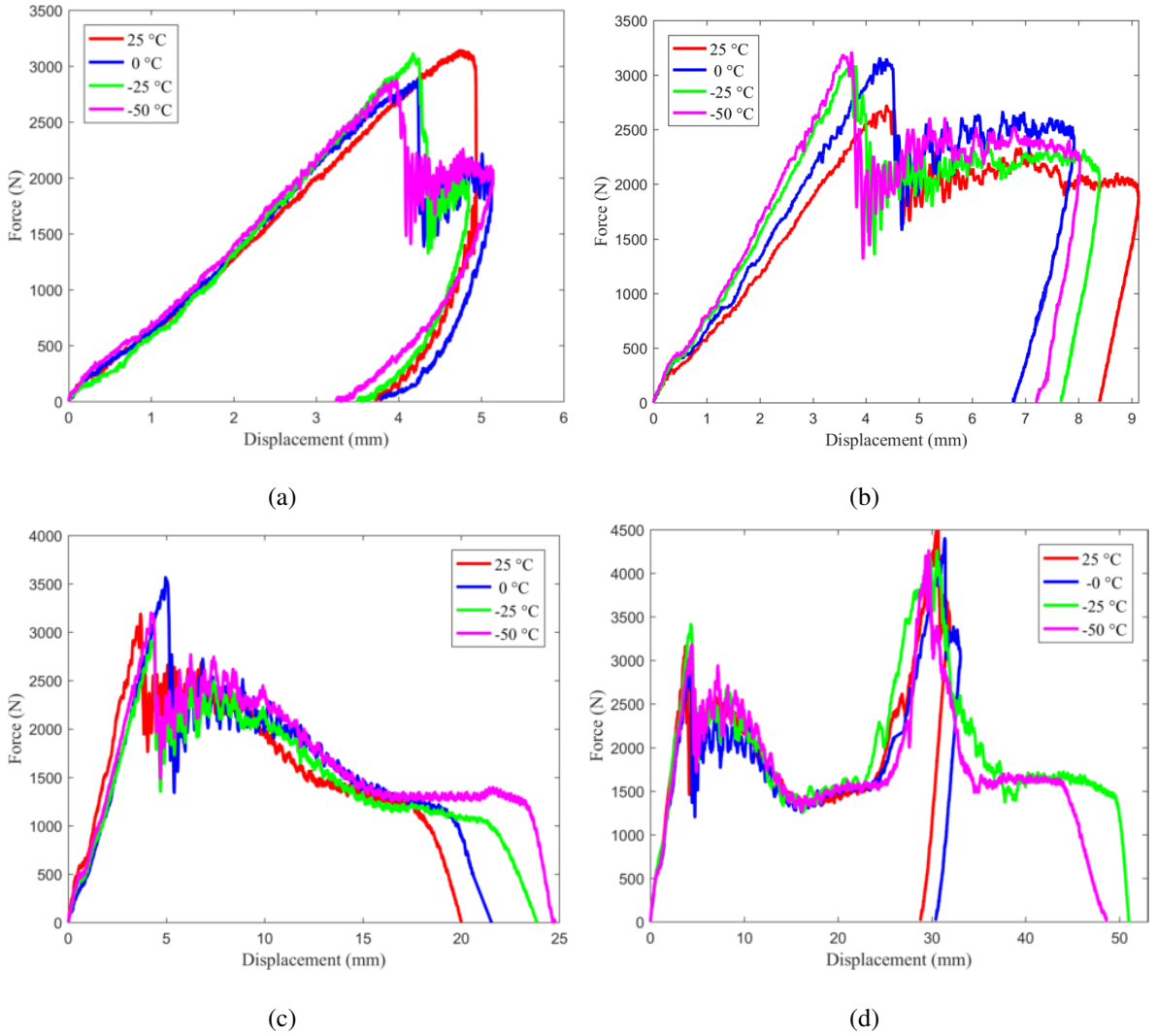

Figure 6.5: Representative contact force-displacement responses for all temperatures under impact energies of: (a)7.5 J, (b) 15 J, (c) 30 J and (d) 60 J.

Figure 6.5(a) corresponds to an impact energy of 7.5 J, where a drop in the contact force is observed upon reaching the first maximum contact force at 25 °C which indicates damage in the

top facesheet, upon which the striker rebounds from the sample. However, at 0 °C, -25 °C and -50 °C, damage in the top facesheet is accompanied with core crushing, which is indicated by the small increase in the contact force after the first vertical drop in the contact force. Finally, the striker rebounds from the specimens without further penetration into the samples. Figure 6.5(b) corresponds to an impact energy of 15 J, where all the graphs manifest a sudden drop after the maximum contact force is reached, which implies that the top facesheet experienced damage along with a noticeable amount of indentation on the impacted surface. The indentation is manifested by an increase in residual displacement of the striker after rebound. For this impact energy, only crushing of the core and perforation of the top facesheet by the striker is expected based on these responses. Figure 6.5(c) corresponds to an impact energy of 30 J, where the striker perforates the top facesheet and penetrates through the foam core at all temperatures, which is indicated by a decrease in the contact force with increasing displacement upon core crushing.

Figure 6.5(d) corresponds to an impact energy of 60 J, where the striker perforates the top facesheet, damages the core completely and perforates the bottom facesheet at all temperatures. All the responses have two peaks for contact force which correspond to the perforation of the top and damage at the bottom facesheets by the striker. The second peak is higher than the first peak due to a higher strength of the bottom facesheet under tension [122] compared to compressive strength of the top facesheet. The graphs at 25 °C and 0 °C have the same profile. That is, displacement of the striker reduces with reduction in contact force after the second peak. This implies that the striker reaches the bottom facesheet, stresses it and then rebounds from the bottom facesheet [123]. However, at -25 °C and -50 °C, the striker almost entirely perforates the samples and get lodged in the bottom facesheet with no rebound. These modes of damage are described more in detail in the “Damage Mechanisms” section.

The average bending stiffness values were calculated using the initial ascending regime of the contact force - displacement responses, and are summarized in Figure 6.6(a). At all impact energies, the bending stiffness increases with reducing temperature, which is expected based on the description given in section 6.3.1. The first maximum contact force values shown in Figure 6.6(b) have a decreasing trend with reducing temperatures under higher impact energies of 15 J, 30 J

and 60 J, which is attributed to facesheet failure due to increased embrittlement at low temperatures. However, under lower impact energy of 7.5 J, the peak contact forces oscillate with changing temperature, as the top facesheet is minimally damaged within the prescribed temperature range.

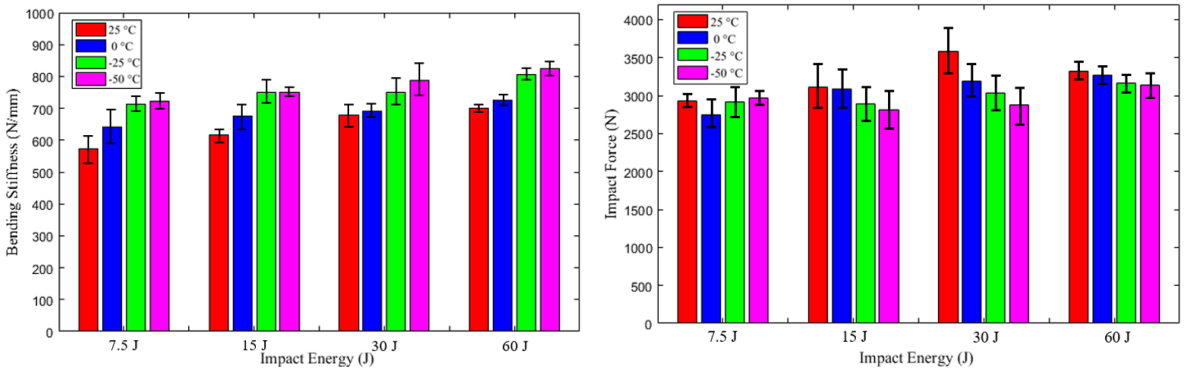

(a) (b)

Figure 6.6: (a) Average bending stiffness and (b) Average first maximum contact force with increasing impact energy and four different temperatures (25 °C, 0 °C, -25 °C and -50 °C).

6.3.3 Absorbed Energy

In addition to the contact force-displacement graphs, the extent of energy absorption and corresponding damage mechanisms presented next are used to characterize the impact behavior of sandwich composites. Figure 6.7(a) shows the energy-time response of a sample tested under an impact energy of 7.5 J at 25 °C. The damage initiation, E_I, is the point where the maximum contact force occurs, beyond which the top facesheet and core are damaged. The maximum impact energy, E_{max}, corresponds to the impacted energy. The post-peak response labeled as E_{abs} (plateau region) corresponds to the energy absorbed by the sample through internal deformation and damage, which in this case (7.5 J at 25 °C) is predominantly delamination in the top facesheet. The difference between E_{max} and E_{abs} is the elastic energy $E_{elastic}$, which is the energy not absorbed by the specimen and is returned to the system by the rebound of the striker. Figures 6.7(b), 6.7(c) and 6.7(d) show the energy-time response of a sample tested at 15 J, 30 J and 60 J each at 25 °C.

In contrast to the energy-time response of the samples impacted at 7.5 J, the samples impacted at 15 J absorbed more energy and the slope of this curve reduced beyond E_I. This is attributed to the damage mechanisms such as fiber fracture and core crushing observed at 15 J. In this case,

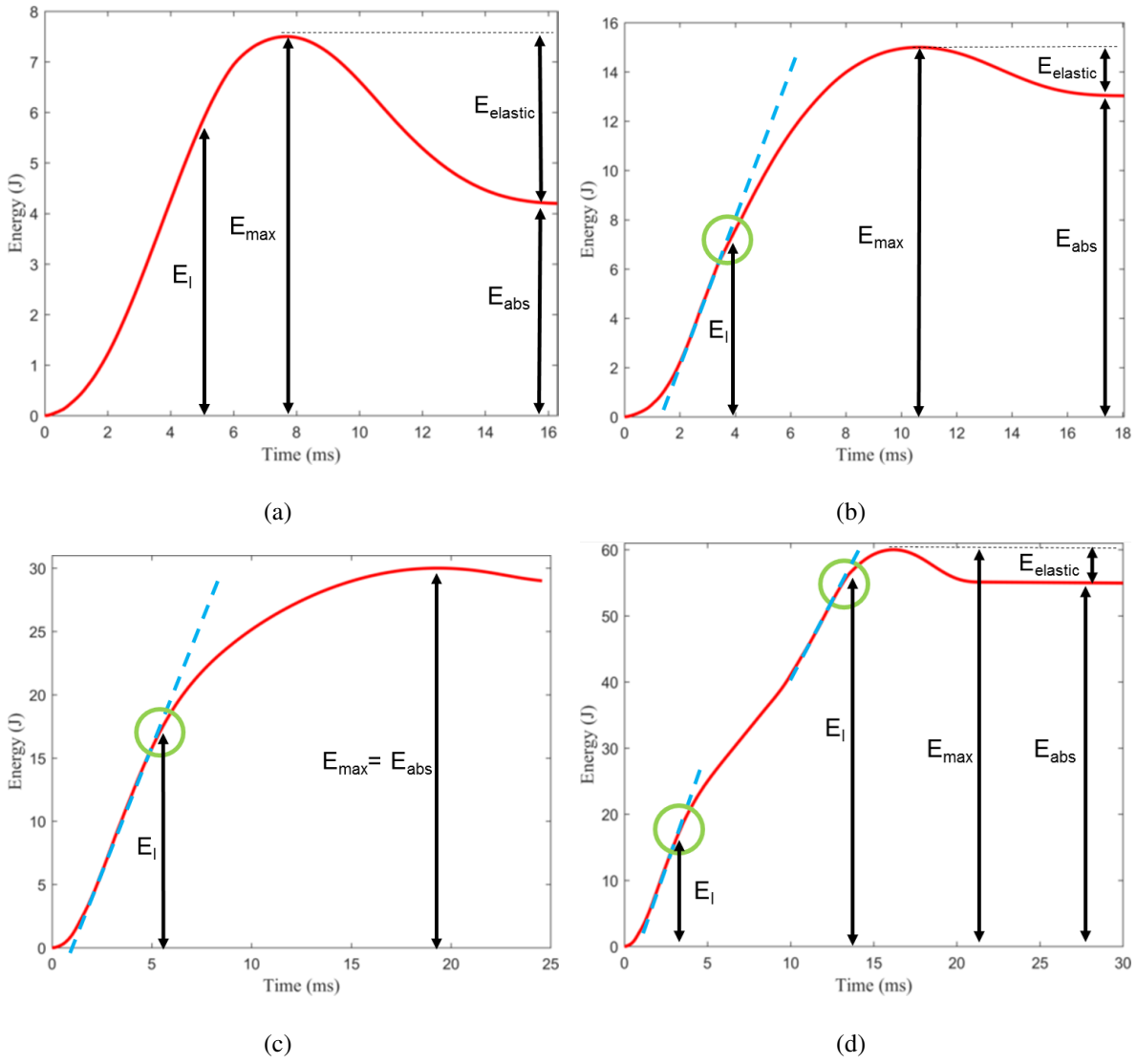

Figure 6.7: Representative energy-time responses for samples impacted at 25 °C at:(a)7.5 J, (b) 15 J, (c) 30 J and (d) 60 J.

the striker rebounded from the sample which can be observed by the elastic energy, $E_{elastic}$. In Figure6.7(c) at 30 J, $E_{max} = E_{abs}$, which implies that the sample completely absorbed the impacted energy. The reduced slope beyond E_I indicates that the top facesheet was completely perforated and the core was penetrated by the striker. Next, recall that two peak forces were observed in the force-displacement responses at 60 J (Figure 6.5(d)) due to damage in the top and bottom facesheets along with the core. Therefore, in Figure6.7(d) at 60 J, the first regime with reduced slope corresponds to the perforation of the top facesheet and core penetration, while the second reduced slope corresponds to fiber fracture at the bottom facesheet and debonding between the core and the bottom facesheet. A small amount of elastic energy is remaining as a result of the striker rebounding from the bottom facesheet.

Energy-time responses of samples tested under impact energy of 7.5 J, 15 J, 30 J and 60 J each at -50 °C are shown in Figures 6.8(a), 6.8(b), 6.8(c) and 6.8(d), respectively. Under 7.5 J, a distinct reduction in the slope of the curve after E_I is observed in contrast to the samples at room temperature. This implies that even at under 7.5 J of impact energy at -50 °C, fiber fracture and delamination in the top facesheet was observed and minimal core crushing. Figure 6.8(b) shows the energy-time response of a sample tested at 15 J at -50 °C. Again, the slope of the curve reduced beyond E_I due to fiber fracture and delamination at the top facesheet and core fracture. Both at 7.5 J and 15 J, the striker rebounded from the samples, which is manifested as the remaining elastic energy in the plateau regions of the graphs. The energy-time response of a sample tested under 30 J of impact energy at -50 °C is shown in Figure 6.8(c), where, E_{max} = E_{abs} which implies that the impacted energy was completely absorbed and the striker did not rebound from the specimen. This is similar to that observed at room temperature. The reduced slope beyond E_I indicates complete perforation of the top facesheet and core penetration by the striker.

Under 60 J of impact energy, the sandwich composite samples experienced two peaks in their force-displacement responses in all in-situ test temperatures including -50 °C, as was previously shown in Figure 6.5(d). Correspondingly, the energy-time response at -50 °C manifested two zones of sudden slope reduction represented by E_I as shown in Figure 6.8(d). The first slope reduction indicates complete perforation of the top facesheet and core penetration by the striker, and the second slope reduction corresponds to damage in the bottom facesheet and debonding between the core and bottom facesheet. In contrast to the room temperature case, here E_{max} = E_{abs}, which

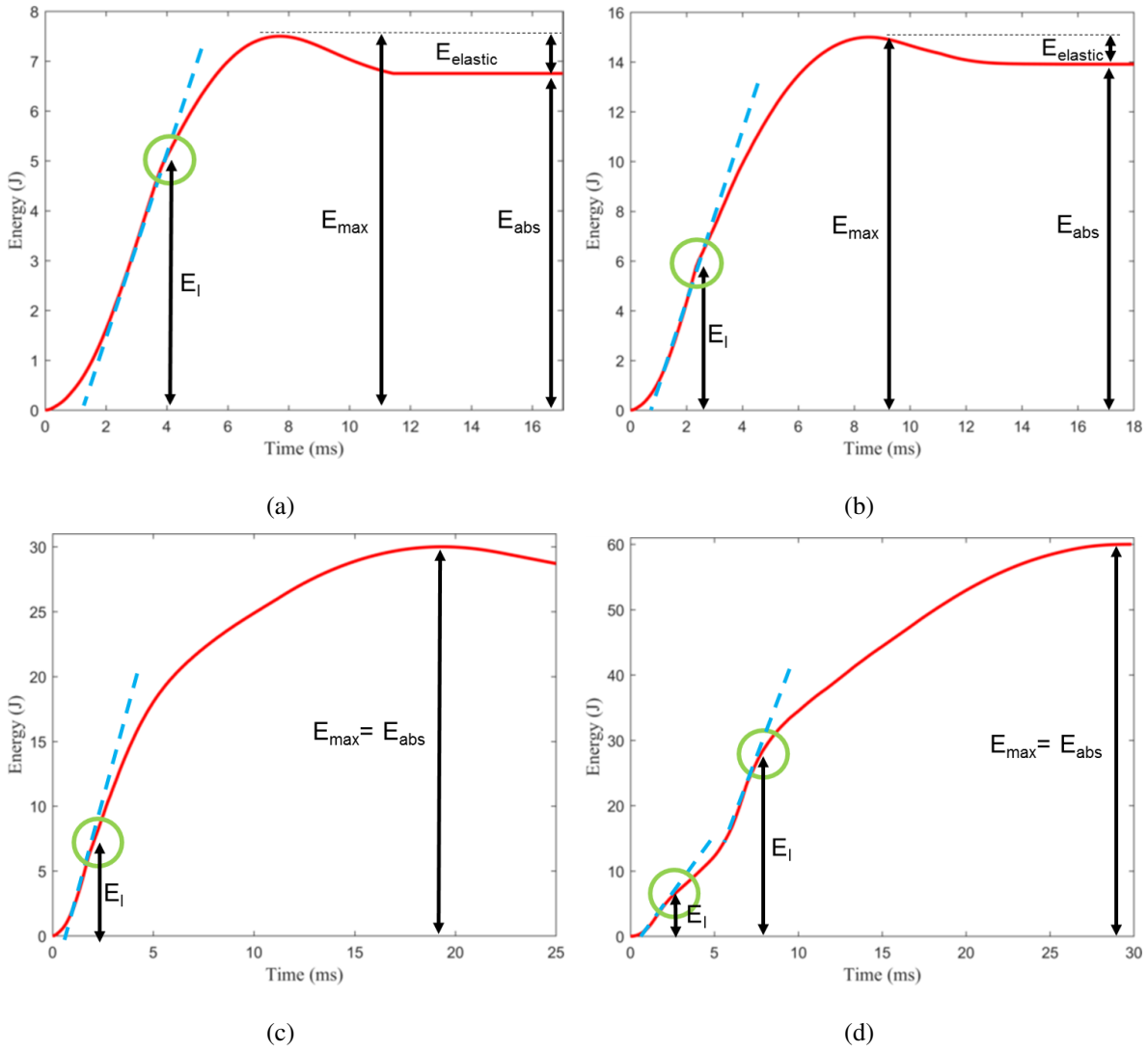

Figure 6.8: Representative energy-time responses for samples impacted at -50 °C at:(a)7.5 J, (b) 15 J, (c) 30 J and (d) 60 J.

implies that the striker did not rebound as it perforated the bottom factsheet of the sample. It can be concluded that the samples tested at low temperatures (that is, 0 °C, -25 °C and -50 °C) experienced more damage than those at 25 °C. This is manifested by an increase in absorbed energy at low temperatures under all the impact energies.

6.3.4 Energy profile diagram

To better understand the energy absorption process, an energy profile diagram was generated that shows the relationship between the absorbed energy E_{abs} and the impacted energy E_{max} [123].

The absorbed energy was obtained by integrating the area under the curve of the contact force-displacement responses for each test conducted. Figure 6.9 shows the energy profile diagram, where each point on the graph represents the average value of the absorbed energy corresponding to an impacted energy at a particular temperature. The yellow line connects the points when the impact energy is equal to the absorbed energy. "I" represents the perforation threshold for the top facesheet. Regardless of the in-situ test temperature under 30 J, the striker completely perforated the top facesheet. "II" represents the perforation threshold for the bottom facesheet only at low temperatures. That is, the striker only caused minimal fiber breakage at the bottom facesheet at 25 °C. Hence, the absorbed energy was less than the impacted energy, resulting in the rebound of the striker. At 0 °C, the samples absorbed almost all the energy due to an increase in debonding between the bottom facesheet and the core. At -25 °C and -50 °C, the striker got lodged into the bottom facesheet, resulting in perforation of the bottom facesheet.

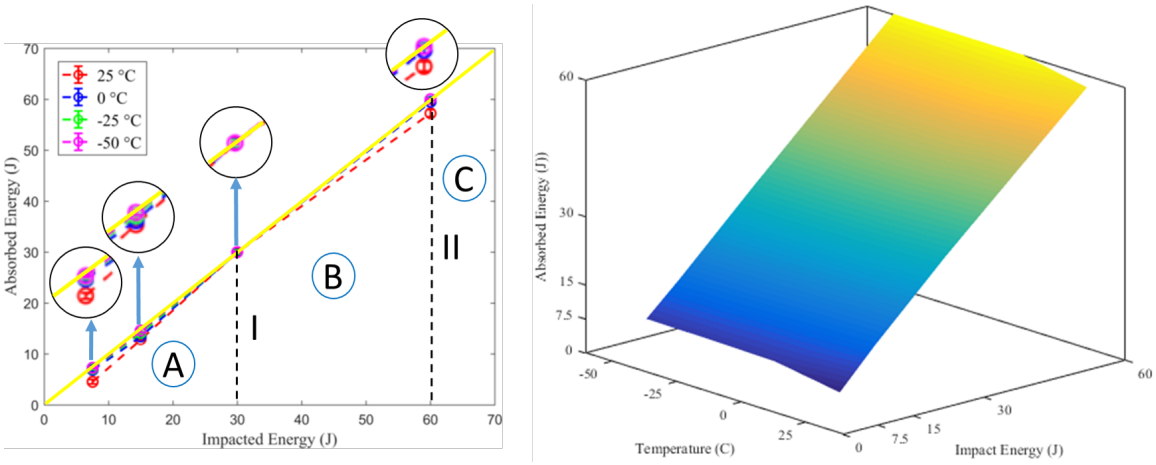

Figure 6.9: Energy profile diagram for the sandwich composite specimens.

In summary, there are three zones in the energy profile diagram: A, B and C. Zone A represents the impact energy where the main damage mechanisms were fiber fracture, delamination and matrix cracking at the top facesheet and core crushing. Zone B represents the impact energy where the main damage mechanisms were perforation of the top facesheet and core fracture. Zone C represents the impact energy where the main damage mechanisms were perforation of the top facesheet, transverse shear fracture in the core, core crushing, debonding between the bottom facesheet and the core, and fiber fracture at the bottom facesheet.

6.3.5 Damage mechanisms

Micro-CT scans of the interior regions of samples and optical images of the impacted and back face were obtained to characterize the damage mechanisms in the sandwich composite samples after dynamic impact loading. Figures 6.10(a), 6.10(b), 6.11(a) and 6.11(b) show the impacted face of the top facesheet, back face of the bottom facesheet and cross-sectional view for the samples impacted at 7.5 J, 15 J, 30 J and 60 J, respectively, at all temperatures. The only impact energy that damaged the bottom facesheet was 60 J, due to which the images of the bottom facesheet of samples impacted at 7.5 J, 15 J and 30 J are not shown. The regions with different damage mechanisms are highlighted as matrix cracking, fiber fracture, delamination, core fracture, transverse shear fracture and facesheet/core debonding in these images.

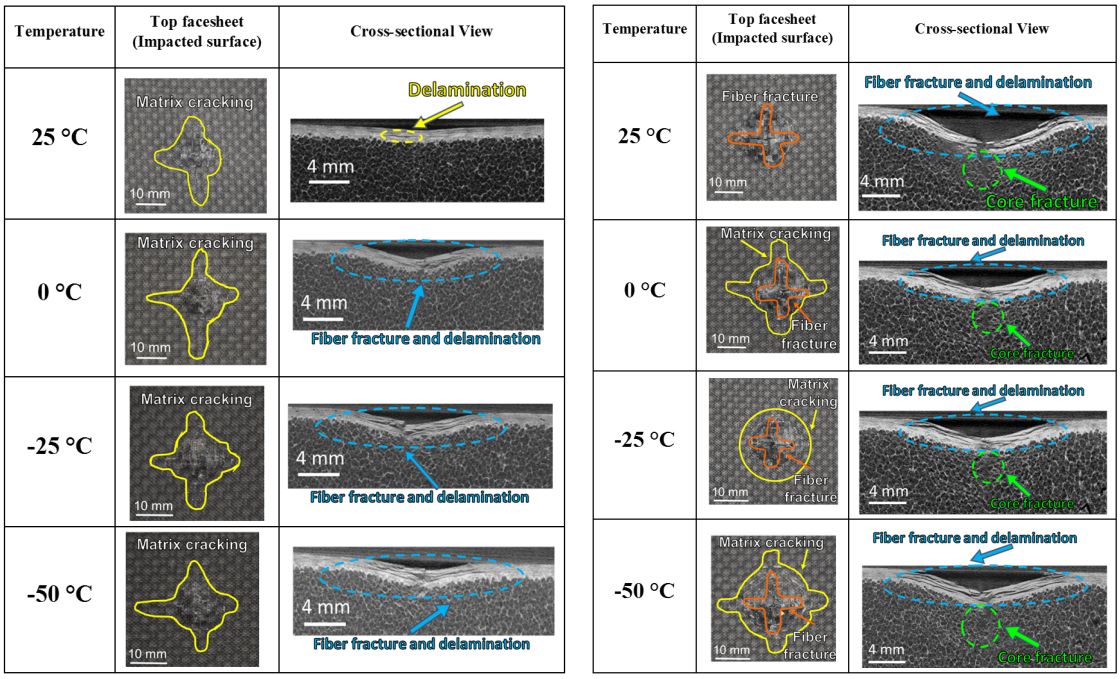

Figure 6.10: Top facesheet and cross-sectional view of the sandwich composite specimens impacted at (a) 7.5 J at 25 °, 0 °C, -25 °C and -50 °C, and (b) 15 J at 25 °, 0 °C, -25 °C and -50 °C.

The samples impacted under 7.5 J of energy at 25 °C predominantly experienced delamination and matrix cracking at the top facesheet as shown in Fig. 6.10(a). At 0 °C, -25 °C and -50 °C, the dominant damage mechanisms were matrix cracks, fiber fracture and delamination at the top

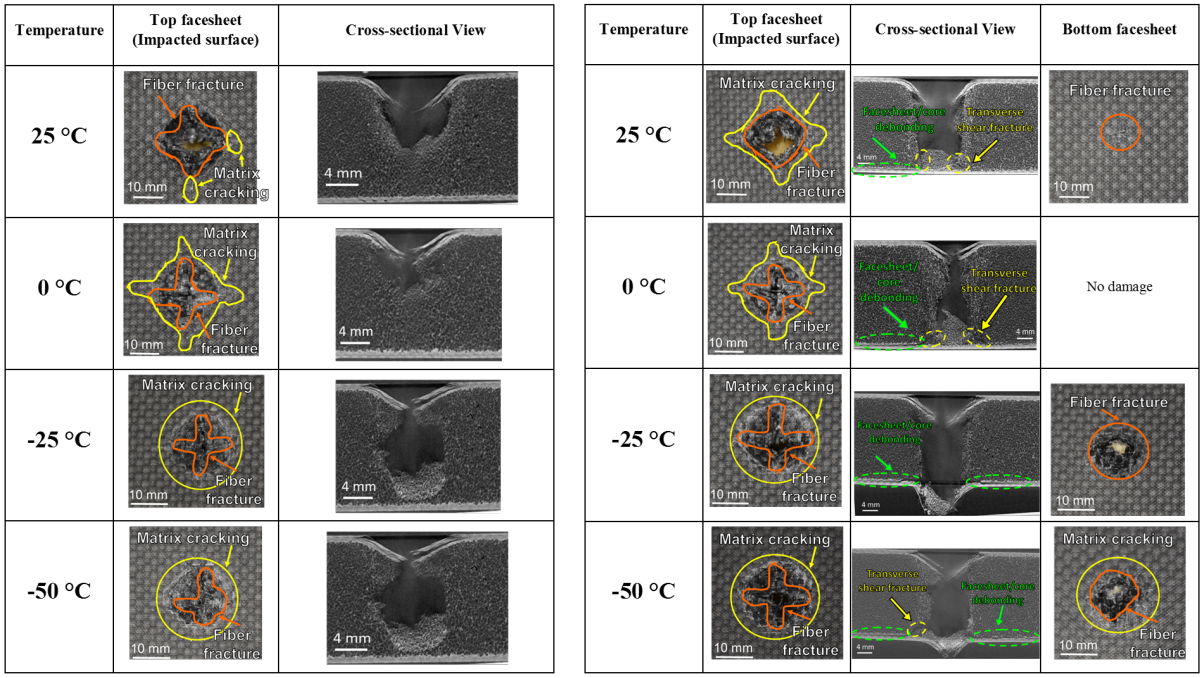

Figure 6.11: Top facesheet and cross-sectional view of the sandwich composite specimens impacted at (a) 30 J at 25 °, 0 °C, -25 °C and -50 °C, and (b) 60 J at 25 °, 0 °C, -25 °C and -50 °C.

facesheet while the core experienced small localized compression. The bottom facesheet was not damaged. The fiber fracture and delamination are manifested as a sudden drop in load in the contact force-displacement responses beyond the peak contact force. The samples impacted under 15 J of energy at all temperatures experienced fiber fracture, matrix cracking and delamination at the top facesheet and localized core crushing/fracture as shown in Figure 6.10(b). Again, the bottom facesheet did not exhibit any damage. The samples impacted under 30 J of energy at all temperatures exhibited penetration of the striker into the core as shown in Figure 6.11(a). The top facesheet was perforated with evident matrix cracking surrounding this area. As the temperature decreased, the penetration of the striker into the core increased. This is attributed to the brittleness of the top facesheet and the matrix at low temperatures, which enabled the striker to perforate the top facesheet easily and to cause more damage to the core. There was no evident damage at the bottom facesheet at 30 J. The samples impacted under 60 J of energy at all temperatures exhibited varying extent of damage at the back facesheet, with almost complete perforation of the bottom facesheet at -25 °C and -50 °C as displayed in Figure 6.11(b) . At 25 °C, the top facesheet was

completely perforated, the foam core was crushed up to the bottom facesheet. This resulted in debonding between the facesheet/core and transverse shear fracture in the core. With reducing temperatures, the laminates became stiffer resulting in less deflection and bending. Therefore, at 0 °C, there was not visible damage at the bottom facesheet. However, there was debonding between the core and the bottom facesheet, transverse shear fracture of the core, and perforation of the top facesheet. At -25 °C and -50 °C, the sandwich composite samples were almost completely perforated by the striker, accompanied by the striker getting lodge into the back facesheet. At -50 °C, it is expected that the sample became more brittle resulting in higher debonding between the bottom facesheet and the core as compared to those tested at -25 °C.

6.4 Conclusion

Dynamic impact behavior of woven carbon/vinyl ester composites at 25 °C, 0 °C, -25 °C and -50 °C were investigated in this paper in view of increasing interest in Arctic explorations and the need to characterize these sandwich composites for future arctic applications. Four different impact energies of 7.5 J, 15 J, 30 J, and 60 J were considered for dynamic impact testing at these temperatures. Key observations regarding the contact force, absorbed energy and damage mechanisms were reported and discussed in this paper. Key conclusions are summarized as follows:

1. Sandwich composites were rendered stiffer and brittle at low temperatures (0 °C, -25 °C and -50 °C) as compared to room temperature (25 °C). The average bending stiffness values increased with reducing temperatures.

2. The peak contact forces reduced with reducing temperatures under higher impact energies of 15 J, 30 J and 60 J, which is attributed to facesheet failure due to increased embrittlement at low temperatures. However, the peak contact forces oscillated under lower impact energy of 7.5 J with reducing temperatures, which is due to minimal damaged imparted to the facesheets under low impact energy.

3. Damage mechanisms contributed significantly to the amount of energy absorbed at low temperatures. That is, higher degree of damage manifested as the temperature decreased. The corresponding damage modes were more pronounced with increasing impact energies.

4. The influence of low temperatures on PVC foam core carbon/vinyl ester sandwich composites at lower impact energies (7.5 J) is not as significant as at higher impact energies (15 J, 30 J and 60 J).

In conclusion, temperature has a significant influence on the dynamic impact behavior of sandwich composites and can further have a detrimental effect on the residual strengths and durability of composite structures. Further studies to elucidate the influence of other sandwich composite parameters, including composite thickness, varying facesheet/core bonding, stiffness of the core, etc. with varying temperatures and impact energies need to be conducted for reliably using these sandwich composites in low temperatures like the arctic.

Chapter 7

Improving the Damage Tolerance of Sandwich Composites through Additive Manufacturing under Low-Velocity Impact

7.1 Introduction

Economic and environmental demands have forced different industries such as marine, aerospace, and automobile to use lightweight structures to reduce their fuel consumption. At the same time, these structures must maintain their stiffness, strength, and damage tolerance. Lightweight structures require the use of high-performance materials, such as sandwich composites [3]. Sandwich composites consist of two thin but very stiff facesheets that sandwich a thick lightweight core between them. The facesheets carry transverse loads or bending moments while the core carries transverse shear loads [12], they are usually made of fiber reinforced polymer composites (FRPCs). The separation of the facesheets increases the moment of inertia of the panels with little increase in weight, which results in an efficient structure that can resist bending and buckling loads [13]. Despite several advantages of sandwich composites, a major drawback is their low resistance to impact damage. Dynamic impact on structures can occur under different scenarios, for example, tool drop during maintenance and repair, wave slamming, iceberg collisions, bird or hail strikes [14, 28, 29]. Low-velocity impacts typically occur at velocities below 10 m/s [17], which may produce barely visible damage (BVD) on composite surfaces (facesheets), but with the possibility of significant internal damage. This is deemed very dangerous, as BVD could result in catastrophic failure of the structure without warning. Extensive delamination and core damage have been observed in sandwich composites with no visible surface damage [124]. Therefore, low-velocity impact studies on sandwich composites with interlaminar reinforcement is critical for material certification and establishing allowable for structural design. There is a wealth of research

studies available that have focused on the dynamic impact behavior of foam core sandwich composites [103, 104, 105, 106, 107, 108, 109, 110, 111, 112, 113, 114]. Most of these prior studies have focused on low-velocity impact loading without reinforcement in the facesheets. Ozdemir et al. [107] investigated the effect of core material and thickness (5, 10 and 15 mm) of unidirectional E-glass/epoxy sandwich composite panel with PVC and poly(ethylene terephthalate) (PET) core with impact energies ranging from 10 J to 70 J at room temperature. They reported that the specimens absorbed more energy as the core thickness increased. Also, PVC cores had higher bending stiffness compared to PET cores. Schubel et al. [108] studied the quasi-static and low-velocity (1.6 to 5 m/s) impact behavior of woven carbon/epoxy sandwich composites with PVC foam core. They concluded that the low-velocity impact response of plates could be characterized as quasi-static based on the load-strain response and damage evaluation. Loganathan et al. [109] explored the effect of core thickness (10 and 14 mm) and density (70, 100 and 200 kg/m^3) of bi-directional woven E-glass/epoxy sandwich composite with polyurethane foam core under three different impact velocities (1.401, 2.426 and 3.123 m/s). They observed that the samples absorbed more energy with increasing core density and thickness. Park et al. [110] evaluated the impact damage resistance of unidirectional carbon/epoxy and glass epoxy sandwich composites with Nomex® honeycomb core at room temperature. They concluded that the damage resistance of sandwich structures is dependent on the facesheet material and core thickness. There has been a considerable effort on enhancing the damage tolerance of sandwich composites under compression [125, 126, 127, 128, 129] and on improving the impact resistance of sandwich composites through stitching, Z-pinning or tufting (sewing the facesheets and core by Z-directional or through-thickness reinforcement) [130, 131, 132]. Although Z-pinning, stitching or tufting have shown to increase the compression after impact (CAI) response, they tend to decrease the in-plane properties of the facesheets due to undesired effects, such as fiber breakage and the creation of large resin pockets around a z-pin or a thread [92]. Therefore, new reinforcement techniques which do not compromise the in-plane mechanical properties of the facesheets must be proposed. Al-Shamary et al. [122] studied the effect of sandwich composite panels with internal facesheets under low-velocity impacts, with impact energies ranging from 10 to 50 J, on unidirectional E-glass/epoxy sandwich composites with polyvinyl chloride foam core. They reported that the sandwich composite with the new foam core design exhibited higher energy absorption than the samples without

it. Ramakrishnan et al. [133] evaluated the effect of low-velocity impact response of a Kevlar ®/epoxy sandwich composite with Rohacell ® foam under impact energies of 8, 12, 16 and 20 J. Nanostrength ®, an acrylate triblock copolymer was added to the epoxy matrix. They reported that the reinforced sandwich composites required higher energy to fail, and the damage in the foam core was spread across a significant part of the structure. Avila et al. [134] investigated the influence of exfoliated nano-structures on fiberglass/nano-modified epoxy sandwich composite with polystyrene foam core under low-velocity impact energies ranging from 5 J to 75 J. Nanoclay (Cloisite 30B) content varied from 0 wt.% to 10 wt.% was added to the polymeric matrix. They reported that the facesheet stiffness and the sandwich composite bending rigidity increased. Reis et al. [135] studied impact response of woven glass fibre/nano-modified epoxy resin sandwich composite with balsa wood core under low-velocity impact energies of 4, 8, 12, 16, 20, 24, 28, 32 and 36 J. Sandwich composites with nano-clays presented higher maximum impact loads, lower displacements and best performance in terms of elastic recuperation and maximum residual flexural strength. However, nano-clays do not have a homogeneous dispersion within the polymer matrix and additional treatment is needed.

To avoid damage in the in-plane mechanical properties of the facesheets and achieve a homogeneous dispersion of the interlaminar reinforcement throughout the polymer matrix, polymer additive manufacturing (PAM) interlaminar reinforcement is explored in this current study. Vinay et al. [136] use PAM to improve the Mode-II interlaminar fracture toughness of polymeric matrix composites. Besides in Chapter in this thesis, it has been shown that Mode-I and Mode-II fracture toughness increased by 30% and 87%, respectively. In the current study, the mechanical response and damage mechanisms of woven carbon/PAM reinforced epoxy sandwich composites with Polyvinyl chloride (PVC) foam core subjected to a range of low-velocity impacts at room temperature are investigated.

A computational model was developed to evaluate the effect that four different PAM interlaminar reinforcement designs had on the stresses of the interlaminar regions. The PAM reinforcement design that showed lower stress concentrations was selected. After that, a damage model was added to the interlaminar regions to identify the regions more susceptible to damage during a low-velocity impact event. Then the PAM reinforcement design selected was added to all the interlaminar regions that experienced failure, and the spread of damage was evaluated. Finally, the

sandwich composite panels were manufactured and were tested. The variation in impact response in terms of force, displacement, energy and damage mechanisms are studied in detail. In addition, a detailed visual damage investigation was conducted using micro-Computed tomography to identify fundamental damage mechanisms and support the observed responses of these sandwich composites.

7.2 Methods

7.2.1 Impact Model

Figure 7.1 shows the approach taken on selecting the optimal PAM reinforcement design for the sandwich composite through computational modeling.

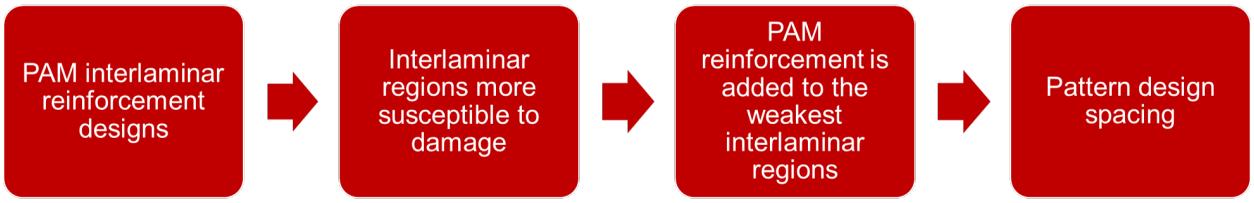

Figure 7.1: Selection of the optimal PAM interlaminar reinforcement.

The first step was to evaluate different PAM interlaminar reinforcement designs. The chosen design was able to minimize stress concentrations on the interlaminar regions, which could lead to matrix cracks or delamination initiators. This computational model only consisted of a quasi-static linear-elastic response. The second step was to develop a dynamic computational model with a damage model (Cohesive Zone Modeling) added to the interlaminar regions to identify the regions more susceptible to damage during a low-velocity impact event. The third step was to add the selected PAM reinforcement to the interlaminar regions more susceptible to damage in the computational model of step 2. After that, the damaged area was measured using Fiji, which is an open source image processing package based on imageJ (www.imageJ.net). The last step was to select the optimal space between PAM interlaminar reinforcements. The impact force, damage area, and deflection from the computation model were considered to select the best space between the reinforcements.

The sandwich composite model consisted of two facesheets made of woven/carbon epoxy which were bonded to the PVC foam by 9430 Hysol epoxy. Due to the symmetry of the sandwich composite, only a quarter of the sample was modeled (75 mm x 50 mm) as seen in Figure 7.2(a). The boundary conditions for symmetry implies that the displacement vector component perpendicular to the plane is zero and the rotational vector components parallel to the plane are zero. Hence, for the YZ plane Ux=0, Uy=free, Uz=free, Rx=free, Ry=0 and Rz=0. For the XZ plane, Ux=free, Uy=0, Uz=free, Rx=0, Ry=free and Rz=0. The impact fixture base has an opening of 76 mm x 127 mm. This aperture was modeled as a partition on the bottom of the sandwich composite as seen in Figure 7.2(b), in which all the degrees of freedom (DOF) were free, except for motion on the Z-direction.

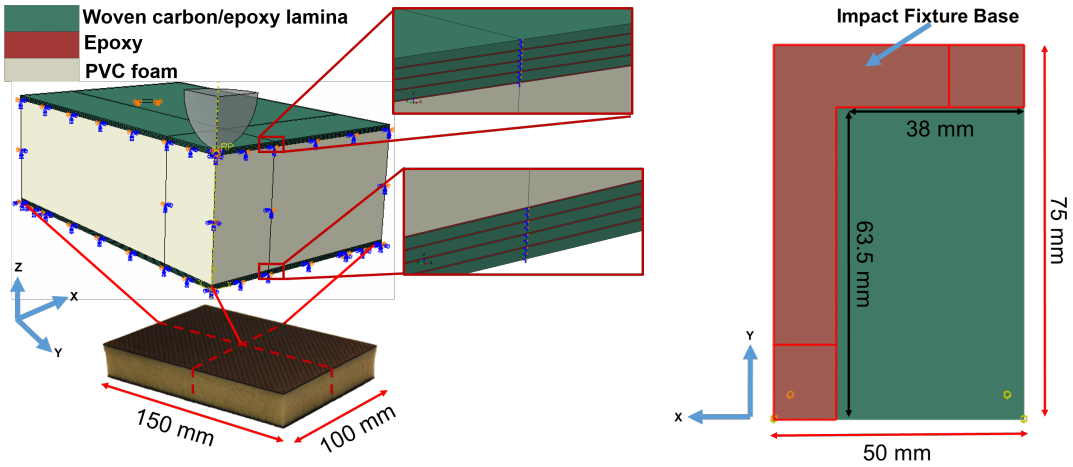

(a) (b)

Figure 7.2: (a) Modeling domain of the sandwich composite; (b) Boundary condition for the base fixture

The toggle clamp was modeled as a circular partition on the sandwich composite with fixed motion on the Z-direction. The striker was modeled as a rigid body with a diameter of 12.7 mm and a mass of 10 kg. The striker DOFs were all fixed, except for the displacement in the Z-direction. The element type used for the striker was R3D4 (rigid element in ABAQUS). The facesheets of the sandwich composite were modeled as four layers of woven carbon/epoxy and four layers of epoxy. Each woven carbon layer was modeled as a homogenized lamina with a thickness of 0.2375 mm. The thickness dimension was obtained by measuring the average thickness of each woven carbon/epoxy layer from a sample cross-section as seen in Figure 7.3. The mechanical properties

used for the laminas are listed in Table 7.1. The element type used for the lamina was C3D8 (8-node linear brick with hourglass control in ABAQUS).

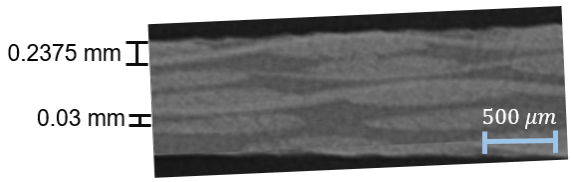

Figure 7.3: Cross-section of a woven carbon/epoxy facesheet.

Table 7.1: Mechanical properties of the woven/epoxy lamina

$E_{11}(GPa)$	$E_{22}(GPa)$	$E_{33}(GPa)$	ν_{12}	ν_{13}	ν_{23}	$G_{12}(GPa)$	$G_{13}(GPa)$	$G_{23}(GPa)$
37	37	4.7	0.3	0.3	0.3	8.2	3.5	3.5

The PVC foam core was modeled as a block with a thickness of 25.4 mm. The mechanical properties used for the core are listed in Table 7.2. The element type used for the lamina was C3D8 (8-node linear brick with hourglass control in ABAQUS).

Table 7.2: Mechanical properties of the PVC foam core

$E_{11}(MPa)$	$E_{22}(MPa)$	$E_{33}(MPa)$	ν_{12}	ν_{13}	ν_{23}	$G_{12}(MPa)$	$G_{13}(MPa)$	$G_{23}(MPa)$
350	350	350	0.3	0.3	0.3	35	35	35

For the computational models where PAM reinforcement was added, the PAM reinforcements were modeled as long strips with a thickness of 0.25 mm. Figure 7.4 shows the cross-section dimensions of the selected reinforcement. The PLA mechanical properties used for the reinforcements are listed in Table 7.4. The element type used for the reinforcement was C3D8 (8-node linear brick with hourglass control in ABAQUS).

For the computational model where the matrix-rich region was linear-elastic without interlaminar reinforcement, the matrix thickness was 0.03 mm as seen in Figure 7.3. The mechanical properties used for interlaminar region are listed in Table 7.4. The element type used for the matrix was C3D8 (8-node linear brick with hourglass control in ABAQUS).

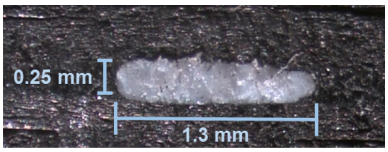

Figure 7.4: PAM reinforcement cross-sectional dimensions

Table 7.3: PLA mechanical properties [2]

$E(GPa)$	ν
3.5	0.3

Table 7.4: Epoxy mechanical properties [1]

$E(GPa)$	ν
2.8	0.3

7.2.1.1 Contact Interactions

The interaction between the striker and the sandwich composite was modeled using the general contact algorithm: surface-to-surface interaction available in ABAQUS/Explicit. This interaction requires two surfaces: a slave and master surface. The master surface was the striker, and the slave surface was the top surface of the sandwich composite. Coincident meshes were used for the models without PAM reinforcement. Non-coincident meshes were used for the models with PAM interlaminar reinforcements due to the different spacing and different geometries used. To reduce the mesh dependency and to improve prediction of matrix crack paths [137], tie constraints were used between the layers of lamina and the reinforced interlaminar regions. Tie constraints are available in ABAQUS/Explicit, and it allows to bond two surfaces together by making the translational and rotational motion equal for both surfaces.

7.2.1.2 Damage criteria and properties for the matrix

As mentioned before, the only damage mechanism considered is delamination. Therefore, for the layers of the matrix, a cohesive damage model was introduced to account for delamination. The

element type used was COH3D8 (an 8-node three-dimensional cohesive element in ABAQUS). Cohesive zone elements modeled the interlaminar regions. The damage model consisted of a linear-elastic response until the onset of damage. After the damage onset, the delamination process was controlled by a bilinear cohesive constitutive relation. The linear-elastic input parameters were defined as follow: t_e is the thickness of the interface cohesive element, so the penalty stiffness were approximated as: $K_3 = E/t_e$ and $K_{sh} = G/t_e$. The linear-elastic mechanical properties are shown in Table 7.5. The interface strengths dictated the damage onset for pure mode I (t_n^0) and shear modes II (t_s^0) and III (t_t^0), which are shown in Table 7.6.

Table 7.5: Linear-elastic mechanical properties of Epoxy [1]

$E(GPa)$	ν	$G(GPa)$
2.8	0.3	1.2

Table 7.6: Epoxy Interface Strengths

$t_n^0(MPa)$	$t_s^0(MPa)$	$t_t^0(MPa)$
53.78	86.88	86.88

A quadratic stress failure criterion was used for the prediction of damage onset with the following equation:

$$\left(\frac{t_n}{t_n^0}\right)^2 + \left(\frac{t_s}{t_s^0}\right)^2 + \left(\frac{t_t}{t_t^0}\right)^2 = 1 \tag{7.1}$$

The interface fracture toughness (critical strain energies) for pure mode I G_{IC} and shear modes II (G_{IIC}) and III (G_{IIIC}) are given in Table 7.7. The mode interaction parameter chosen was η=1.45 as proposed by Crews and Reeder [74].

7.2.1.3 PAM interlaminar reinforcement design

The failure pattern of woven composites is a plus sign as seen in Figure 7.5. This is attributed to the in-plane reinforcement that the yarns offer (X- and Y-direction). Hence, the PAM interlaminar

Table 7.7: Epoxy Interface Fracture Toughness

$G_{IC}(N/mm)$	$G_{IIC}(N/mm)$	$G_{IIIC}(N/mm)$
0.4845	0.4845	0.4845

reinforcement must provide support for the X- and Y-direction. The pattern designs selected were: concentric squares (Figure 7.6(a)), 45° lines (Figure 7.6(b)), concentric circles (Figure 7.6(c)) and squares (Figure 7.6(d)). The blue part represents the Epoxy, and the red part represents the PAM reinforcement (polylactic acid (PLA)).

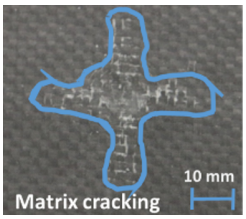

Figure 7.5: Failure pattern under low-velocity impact of a woven carbon laminate

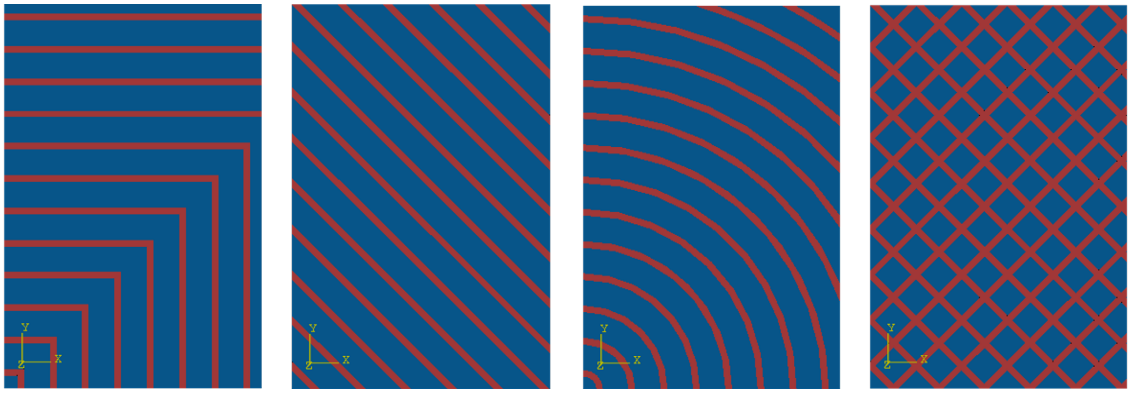

(a) (b) (c) (d)

Figure 7.6: *Only a quarter of the interlaminar regions were modeled. Interlaminar reinforcement: (a) Concentric Squares; (b) 45° lines; (c) Concentric circles; (d) Squares.

After selecting the PAM interlaminar reinforcement that showed lower stress concentrations, a damage model was added to the interlaminar regions to identify the regions more susceptible to damage during a low-velocity impact event. Then the PAM reinforcement design selected was

added to all the interlaminar regions that experienced failure, and the spread of damage was evaluated.

7.2.2 Printing on Prepegs

Once the selected PAM reinforcement was selected, fused deposition modeling (FDM) technique was used to print the reinforcement onto the prepreg layers with a LulzBot TAZ 6. The plastic protector was peeled from the top of the prepreg. Then the prepreg layer was attached to the printer with thermal tape as shown in Figure 7.7(a). The thermal tape secured the prepreg from moving while printing. PLA was melted in a heated liquefier at a temperature of 210 °C and printed on top of the prepreg through a printing nozzle. This temperature was high enough to initiate partial melting of the prepreg resin in order for the PLA reinforcement to adhere to the prepreg. This machine typically prints a raft on the printer baseplate, which acts as a support on which the actual computer-aided design (CAD) 3D model is printed. A code was developed to print only the interlaminar reinforcement. The PAM interlaminar reinforcement design chosen for this study was concentric circles, as shown in Fig.7.7(b). Figure 7.7(c) shows the final printed reinforcement on the prepreg.

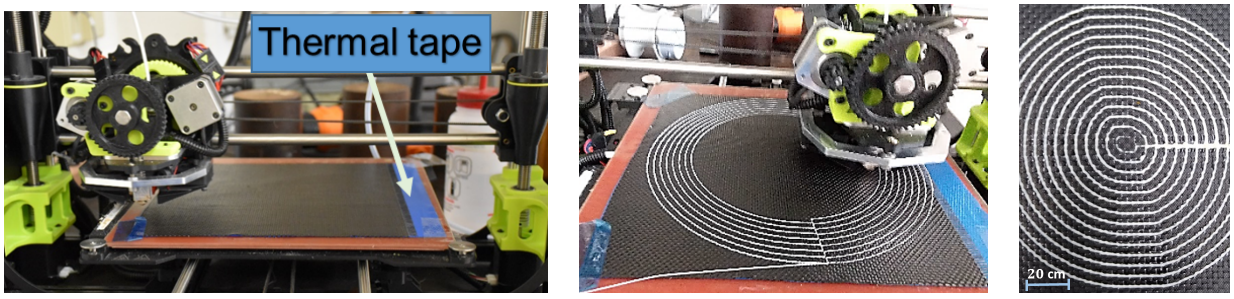

(a) (b) (c)

Figure 7.7: (a) 3D printing on prepreg by LulzBot TAZ 6 ; (b) 3D printing on prepregs; (c) Prepreg layer with PAM interlaminar reinforcement

The cross-sectional dimensions of the printed reinforcement were 1.3 mm wide x 0.25 mm thick at 2.5 mm spacing. Further details on the selection of the reinforcement and its dimensions are given in the “Results and Discussion Section.

7.2.3 Panel Fabrication

Woven carbon fiber/epoxy composite sandwiches with PVC core were manufactured by hand layup with and without PAM interlaminar reinforcements. Plain weave carbon fiber prepreg 3K [1] was purchased from Fibre Glast (ww.fibreglast.com) with a resin content of 38%, and the H100PVC foam was purchased from Aircraft Spruce (www.aircraftspruce.com). Table 7.8 shows the mechanical properties of the sandwich composite constituents. PVC was considered due to their low cost, low density, fire retardancy and high insulation and damping properties [117].

Table 7.8: Mechanical properties of the sandwich composite constituent materials

Mechanical properties	Woven carbon fiber	Epoxy resin	PLA	H100 foam	
				In-Plane	Out-of-plane
Tensile Modulus (MPa)	-	3500	3800	111	126
Tensile Strength (MPa)	-	50	82.7	3	3.3
Density (kg/m^3)	-	1.24	1.800	100	100
Nominal thickness (mm)	0.3048	-	-	25.4	25.4
Fabric Areal weight (gsm)	193	-	-	-	-

For fabricating a sandwich composite panel, PVC foam was sandwiched between two facesheets with [$(0/90)_4$/core/$(0/90)_4$] stacking sequence as per the instructions in ASTM D7766/D7766M-16 [118]. Here, $(0/90)_4$ implies four layers of plain weave carbon fabrics. The facesheets were manufactured first because their curing temperature was 154 °C and it damaged the foam core. All the layers were cut to dimensions of 305 mm x 305 mm. To achieve proper compaction of the facesheets, a process called "debulking" was followed. This process has shown to result in higher quality laminates by ensuring that the layers are compacted sequentially as they are being placed. The debulking step involved placing release fabric and a breather layer on top of four layers of prepreg, followed by drawing and holding it to vacuum for 15 minutes. This step was repeated for all facesheets. After the debulking process, the facesheets were placed between two layers of peel ply and one layer of breather. This whole arrangement of fabrics was placed over an aluminum mold, then wrapped with a Stretchlon 800 bagging film and sealed with vacuum-sealant tape, ensuring a space for the vacuum connector as seen in Figure 7.8(a). The entire setup was then placed

inside an oven for curing with a constant pressure of ≈80 MPa. The temperature in the oven was ramped up to 90 °C at a rate of 1.5 °C per minute and held for 20 minutes to release any trapped air. After that, the temperature was increased to 154 °C and held for 1 hour. Finally, the laminate was cooled to 66 °C before removing it from the oven as suggested by the manufacturer. The facesheets were bonded to the core by using a 9430 Hysol Epoxy adhesive. This epoxy consists of a two-part epoxy adhesive with a mix ratio of 100:23 by weight. The adhesive was spread on the facesheets. Then the facesheets sandwiched the core, and the configuration was placed between two peel plies. This complete arrangement was placed over an aluminum mold, then wrapped with a Stretchlon 800 bagging film and sealed with vacuum-sealant tape, ensuring a space for the vacuum connector as seen in Figure 7.8(b). The entire setup was then placed inside an oven for curing with a constant pressure of ≈80 MPa. The temperature in the oven was ramped up to 80 °C at a rate of 1.5 °C per minute and held for 1 hour. Finally, the sandwich composites were cooled to 66 °C before removing it from the oven as suggested by the manufacturer. A total of 8 panels of 305 mm length x 305 mm width were manufactured (four panels with interlaminar reinforcement and four panels without reinforcement). Six samples were cut with a saw from each panel. Impact test samples were randomly chosen from the set of all the samples fabricated to distribute any manufacturing induced effects on the impact response. Four samples were selected for testing for each impact energy.

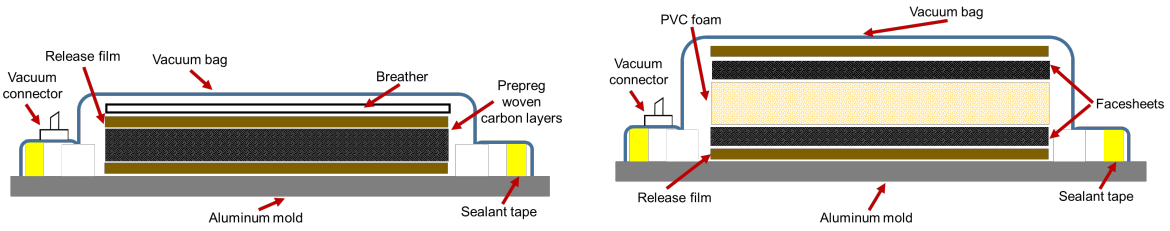

(a) (b)

Figure 7.8: (a) Facesheets manufacturing configuration; (b) Sandwich composite manufacturing configuration

7.2.4 Impact Tests

Drop-weight impact tests were performed using a CEAST 9350 Drop Tower Impact System with a load cell capacity of 22.4 kN and an in-built environmental chamber as shown on Figure 7.9. A metal fixture with a rectangular opening of 76 mm x 127 mm and toggle clamps was used. These clamps apply pressure in the vicinity of the four corners of the samples to prevent their motion during an impact event. The rectangular sandwich samples had dimensions of 150 mm length x 100 mm width (refer to Figure 7.9) with an average thickness of 27.43$\pm$0.16 mm. The core thickness was 25.4 mm, and each facesheet had an approximate thickness of 1 mm. A hemispherical striker with a fixed mass of 10 kg and a diameter of 12.7 mm was used for impacting the samples at the center of the top facesheet in the out-of-plane direction [42]. Impact velocities of 0.7 m/s, 1 m/s, 1.22 m/s and 1.4 m/s were chosen which correspond to kinetic impact energies of 2.5 J, 5 J, 7.5 J, and 10 J, respectively. All these tests were conducted at low-velocities, that is, below 10 m/s [119, 43]. The kinetic energies corresponding to these velocities were calculated based on the mass of the striker and the impact velocities using the equation:

$$E_k = \frac{1}{2}m^2 = mgh \tag{7.2}$$

Here, E_k is the impact energy or kinetic energy, v is the impact velocity, and m is the mass of the impacting striker, h is the height of the striker measured from the surface of a sample in the impact drop tower, and g is the gravitational acceleration.

Robinson et al. [44] investigated the influence of impactor mass and velocity on the low velocity impact performance of woven carbon and glass fiber reinforced laminates for impact energy range from 0.25 J to 12 J. The impactor mass was varied from 1.15 kg to 2.10 kg and the velocity was adjusted to obtain the desired impact energies. They reported that the extent of impact damage predominantly depended on the magnitude of the impact energies and less on the mass or velocity individually. Based on this study, the impactor mass was held constant and the impact energy was varied for the prescribed velocities in the current paper.

Force-time, displacement-time and energy-time responses were recorded by the data acquisition system "CEAST DAS 8000 Junior" of the impact machine for each test. Four samples were impacted for each impact energy.

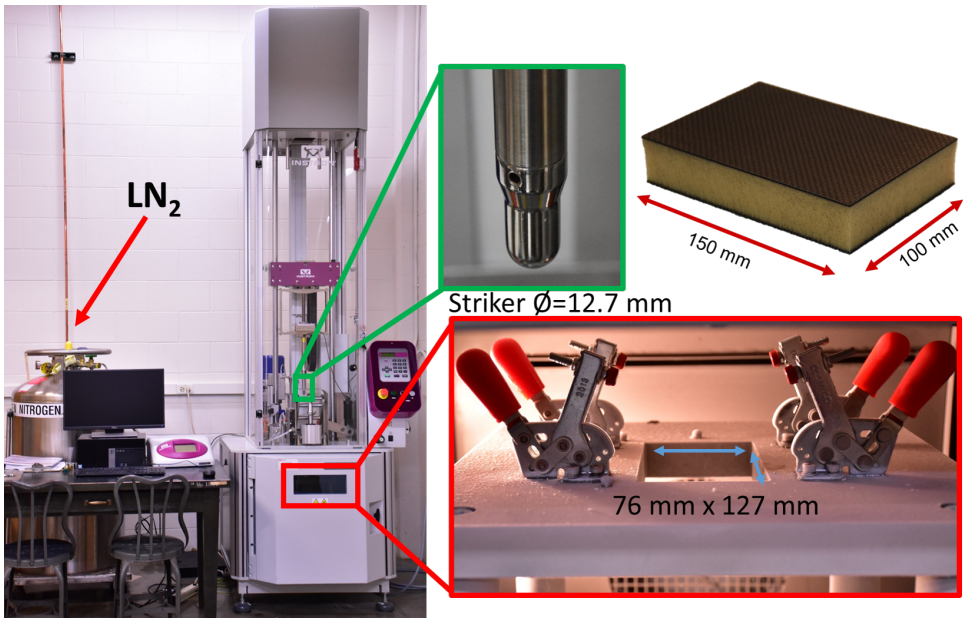

Figure 7.9: CEAST 9350 Drop Tower Impact System

7.2.5 Micro-CT Scanning

Sandwich composite samples were examined under a micro-computed tomography (micro-CT) scanner, which is a non-destructive technique (NDT), upon subjecting to impact loading. The goal was to evaluate the internal damage incurred at different temperatures and impact energies. The samples were scanned within a Zeiss Metrotom OS 800 scanner at UW-Madison. For each sample, 1500 projections were made by rotating them until a complete revolution was obtained. The X-ray tube voltage and current were set to 80 keV and 120 μA, respectively. Reconstruction of the 3D virtual object was done with METROTOM OS software, and were further analyzed with VG Studio Max 22 software. A flat correction was applied for each scan.

7.3 Results and Discussion (*Preliminary)

The mechanical response and damage mechanisms of woven carbon/PAM reinforced epoxy sandwich composites with Polyvinyl chloride (PVC) foam core subjected to a range of low-velocity impacts at room temperature were investigated. A computational model was developed to evaluate the effect that four different PAM interlaminar reinforcement designs had on the stresses of the interlaminar regions. The PAM reinforcement design that showed lower stress concentrations was

selected. After that, a damage model was added to the interlaminar regions to identify the regions more susceptible to damage during a low-velocity impact event. Then the PAM reinforcement design selected was added to all the interlaminar regions that experienced failure, and the spread of damage was evaluated. Finally, the sandwich composite panels were manufactured and were tested. The variation in impact response in terms of force, displacement, energy and damage mechanisms are studied in detail. In addition, a detailed visual damage investigation was conducted using micro-Computed tomography to identify fundamental damage mechanisms and support the observed responses of these sandwich composites.

7.3.1 Impact model

7.3.1.1 PAM interlaminar reinforcement designs

A computational model was developed to evaluate the effect that four different PAM interlaminar reinforcement designs had on the stresses of the interlaminar regions. A displacement of 10 mm was applied to the striker. Figure 7.10(a) shows the Maximum Principal Stresses of the interlaminar regions without reinforcement. M8 M7, M6, and M5 corresponds to the interlaminar regions in the top facesheet (TIR). M8 represents the interlaminar region closer to the striker, and M5 is the interlaminar region between the top facesheet and the core as seen in Figure 7.10(b). M4, M3, M2, and M1 corresponds to the interlaminar regions in the bottom facesheet. M4 is the interlaminar region that connects the bottom facesheet and the core as seen in Figure 7.10(b). The interlaminar regions that exhibited higher stresses were at the top facesheet (TIR). The bottom interlaminar regions did not experience significant stress concentrations as compared to the TIR. Therefore, the PAM interlaminar reinforcements were only added to the TIR.

The concentric squares and 45° lines reinforcements exhibited stress concentrations on M8 and M7 similar to the ones present when no reinforcement was added. The square reinforcement exhibited some decrease in the stress concentrations of M8 and M7. The concentric circles exhibited very low-stress concentrations on M8. Therefore, the concentric circles were the selected reinforcement.

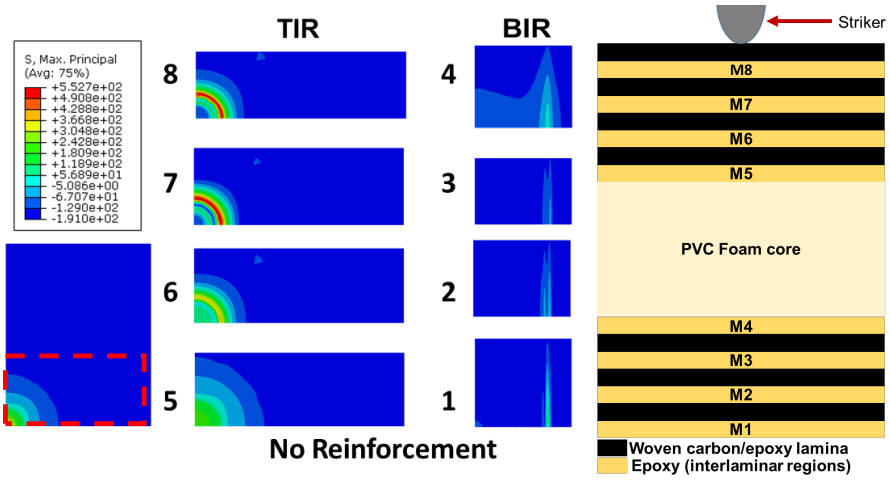

(a) (b)

Figure 7.10: (a) Interlaminar regions with higher stress concentrations; (b) Coniguration of the interlaminar regions

7.3.1.2 Damage interlaminar regions

Figure 7.12(a) shows the force-time curve of the dynamic (low-velocity impact) sandwich composite model panel without any reinforcement. A damage model (cohesive elements) was added to all the interlaminar regions. Due to computational time, the impact modeling was captured only a few milliseconds (ms) after the maximum force was obtained. After the maximum force was reached, the striker rebounding took place. Therefore, no more damage was induced to the sandwich composite. The damage on the interlaminar regions (matrix regions) was captured where the maximum force took place. Figure 7.12(b) shows the damage on the interlaminar regions at the maximum impact force. M5 experienced more damage as compared to the other interlaminar regions (M8, M7, and M6). This was attributed to the mismatch on stiffness between the top facesheet and the core. The damage area was calculated for using Fiji, which is an open source image processing package based on image J (www.imageJ.net). Table 7.9 shows the calculated damage area (red region) of the TIR. Therefore, the PAM interlaminar reinforcement was added to M8, M7, M6 and M5.

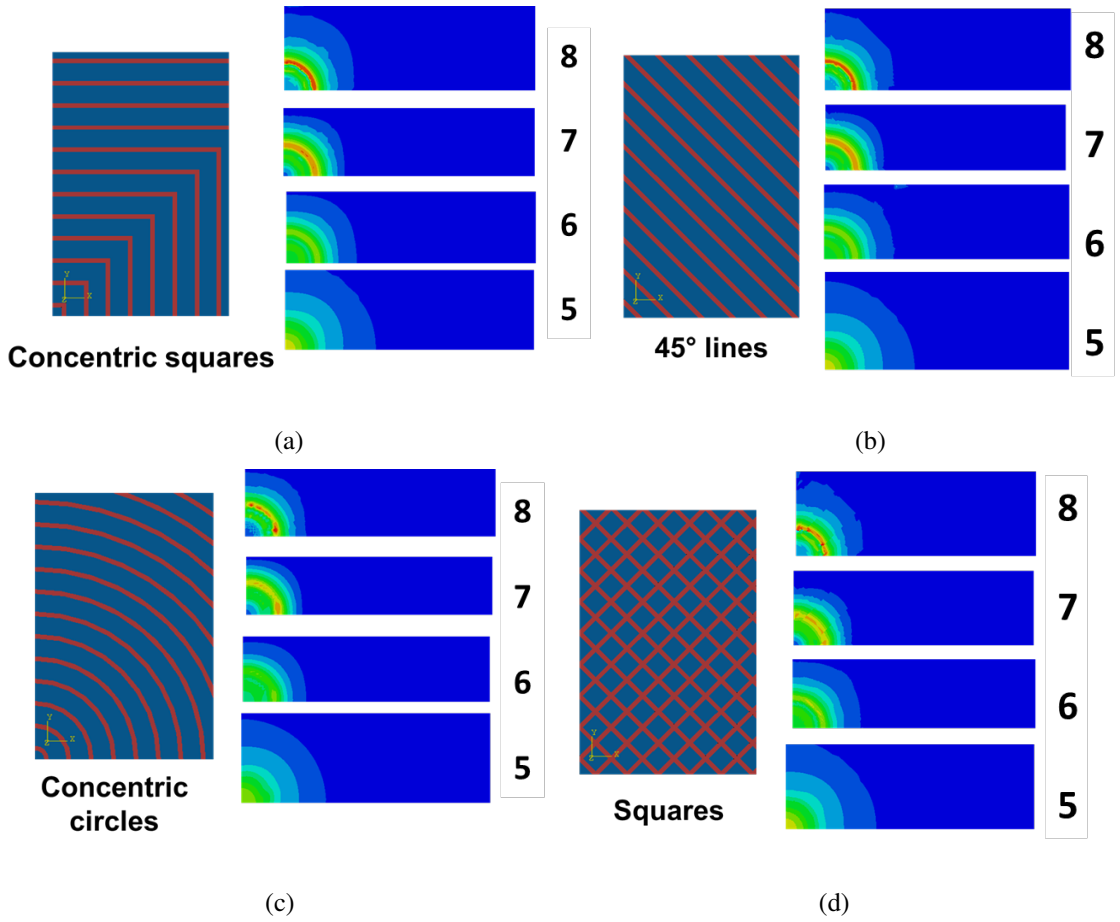

Figure 7.11: TIR max. principal stresses: (a) Concentric squares; (b) 45° lines; (c) Concentric circles; (d) Squares.

Table 7.9: Damage area of the TIR without reinforcement

Interlaminar Region	Area mm^2
M8	257.5
M7	270
M6	316
M5	468

7.3.1.3 PAM interlaminar Reinforcement Cross-Sectional Dimensions

The cross-section dimensions of the printed reinforcement is determined by the clearance between the printer nozzle and the layer of prepreg and the nozzle diameter. A higher print height

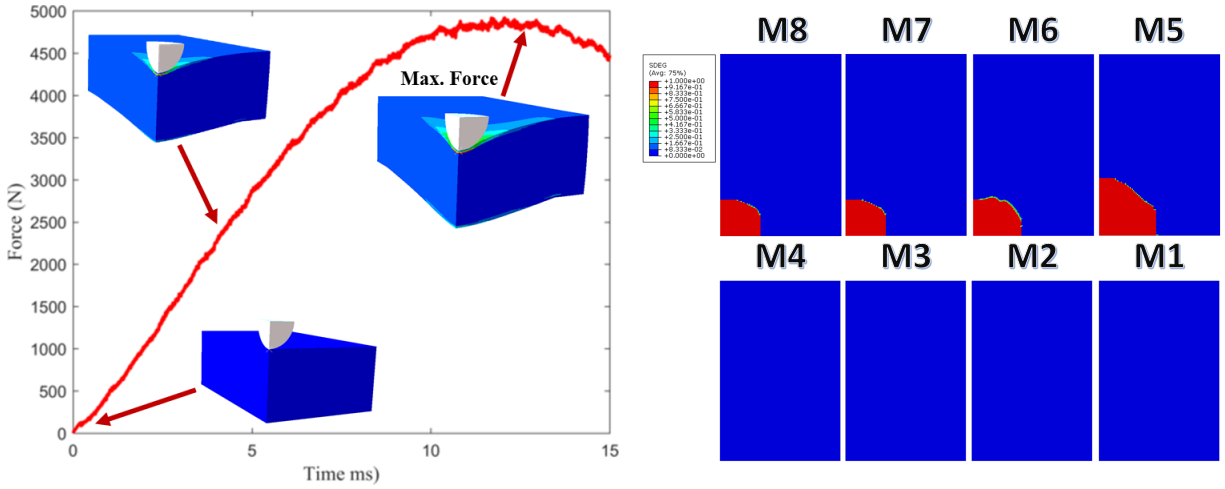

(a) (b)

Figure 7.12: (a) Representative force-time graph of a sandwich composite under a low-velocity impact event; (b) Damage interlaminar regions.

increase the distance between the nozzle and the prepreg, yielding reinforcements with higher thickness to width ratio. Damodaran et al.[136] reported that the flexural modulus reduced with increasing height of the printed interlaminar reinforcement. Hence, they used the smallest printing offset from the prepreg layer to the nozzle and the smallest nozzle diameter (0.3 mm). For this work, the same nozzle diameter was used. As mentioned before a code was developed to print concentric circles. Therefore, some of the parameters that could be modified were the spacing, the printing height of the nozzle with respect to the printing bed (Z) and the Epmm (length of filament extruded per unit length of head travelled). The smallest printing offset was chosen based on the smallest distance of the printing reinforcement to adhere to the prepreg layer. The thickness of the prepreg layer was 0.3 mm. Therefore, the Z value was increased by 0.1 mm until a good adhesion of the printed reinforcement was achieved. Due to the weave pattern of the prepreg layer, Z values of 0.4 and 0.5 mm tended to tangle between the fibers as the nozzle is printing and to peel off the prepreg layer from its printing position. Therefore, in order to avoid all contact with the prepreg layer, a Z=0.6 mm was the selected height of the nozzle. The Epmm value was calculated by the distance traveled between a start and an end point of the nozzle from previous code. The Epmm start value was 0.0438 mm/mm. By increasing the Epmm value, more material was printed, and the thickness increased. When the Epmm value decreased, the reinforcement thickness decreased.

However, a very low Epmm value resulted in no printed reinforcement. Figure 7.13 shows a representative graph of some Epmm values tested and the final cross-sectional dimensions of the selected reinforcement. For any Epmm value equal or lower to 0.015 mm/mm, the machine was not able to print any reinforcement. Section A represents the Epmm values between 0.016 and 0.025 mm/mm. At the beginning of the printing, the material extruded value was very low that the middle circle of the reinforcement was missing. Therefore, the Epmm was increased to 0.027 mm/mm where all the concentric circles were printed. The final cross-sectional dimensions of the reinforcements were 1.25 mm wide by 0.29 mm thick. Section B represents the Epmm values between 0.028 and 0.08. At these values, the thickness reinforcement increased, resulting in a decrease of the flexural modulus. Therefore, they were not considered.

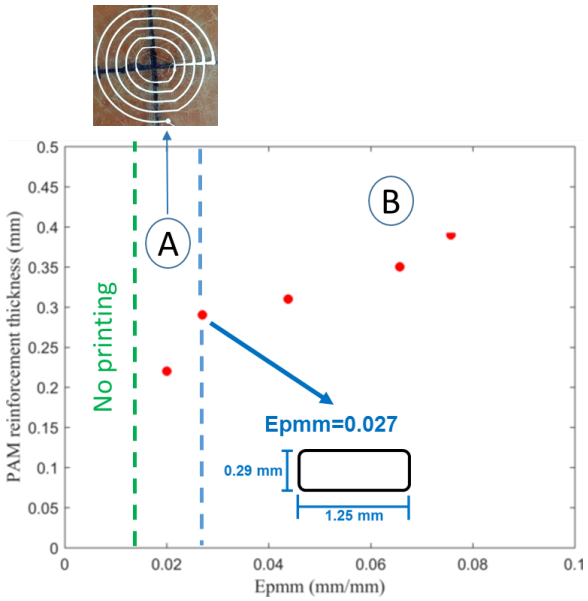

Figure 7.13: Representative PAM reinforcement thickness-Epmm graph.

7.3.1.4 PAM interlaminar Reinforcement Spacing

Figure 7.14(a) shows the force-time curve of a sandwich composite with PAM interlaminar reinforcement (Concentric circles) with different spacing under low-velocity impact (7.5 J). The bottom interlaminar regions did not exhibit any damage when there was no reinforcement. Thus, only the interlaminar regions at the top facesheet were reinforced, and cohesive elements were added

only to the TIR. Due to computational time, the impact modeling was captured only a few milliseconds (ms) after the maximum force was obtained. As the spacing of the reinforcement reduced, the peak force increased. This is expected because the interlaminar reinforcement is stiffer (3.5 GPa) than the pure matrix (2.8 GPa). As the spacing started to increase, the graphs tended to behave as the pristine graph (no reinforcement). The displacement of the sandwich composite started to decrease as the spacing reinforcement reduced as seen in Figure 7.14(b). Figure 7.14(c) showed the force-displacement graph of a sandwich composite with different reinforcement spacing. Typically, contact force-deflection responses have an initial linear ascending region from which the initial bending stiffness [121] is determined. The bending stiffness is shown in Table 7.10. Due to the increase in rigidity of the samples with the reduction of the reinforcement spacing, the samples with lower spacing experienced more significant bending stiffness.

Table 7.10: Bending stiffness of a sandwich composites impacted at 7.5 J

Spacing (mm)	Bending Stiffness (N/mm)
No Reinforcement	390
1.25	661
2.5	614
7.5	484
10	475
12.5	454

From these results, it can be concluded that the best spacing was 1.25 mm. However, the selected reinforcement spacing was 2.5 mm. Before manufacturing the sandwich composite samples, a laminate of two layers of plain weave woven carbon/epoxy with printed reinforcement at the middle interlaminar region was manufactured. The objective was to determine if the resin on the layers of prepreg was enough to infill the regions where the interlaminar reinforcement was printed. Figure 7.15 shows the cross-section of some manufactured laminates with different spacing between them. For the spacing of 1.25 mm and 2.25 mm, the epoxy in the prepreg was not enough to fill the regions around the reinforcement. Resin pockets are formed around the reinforcements (red

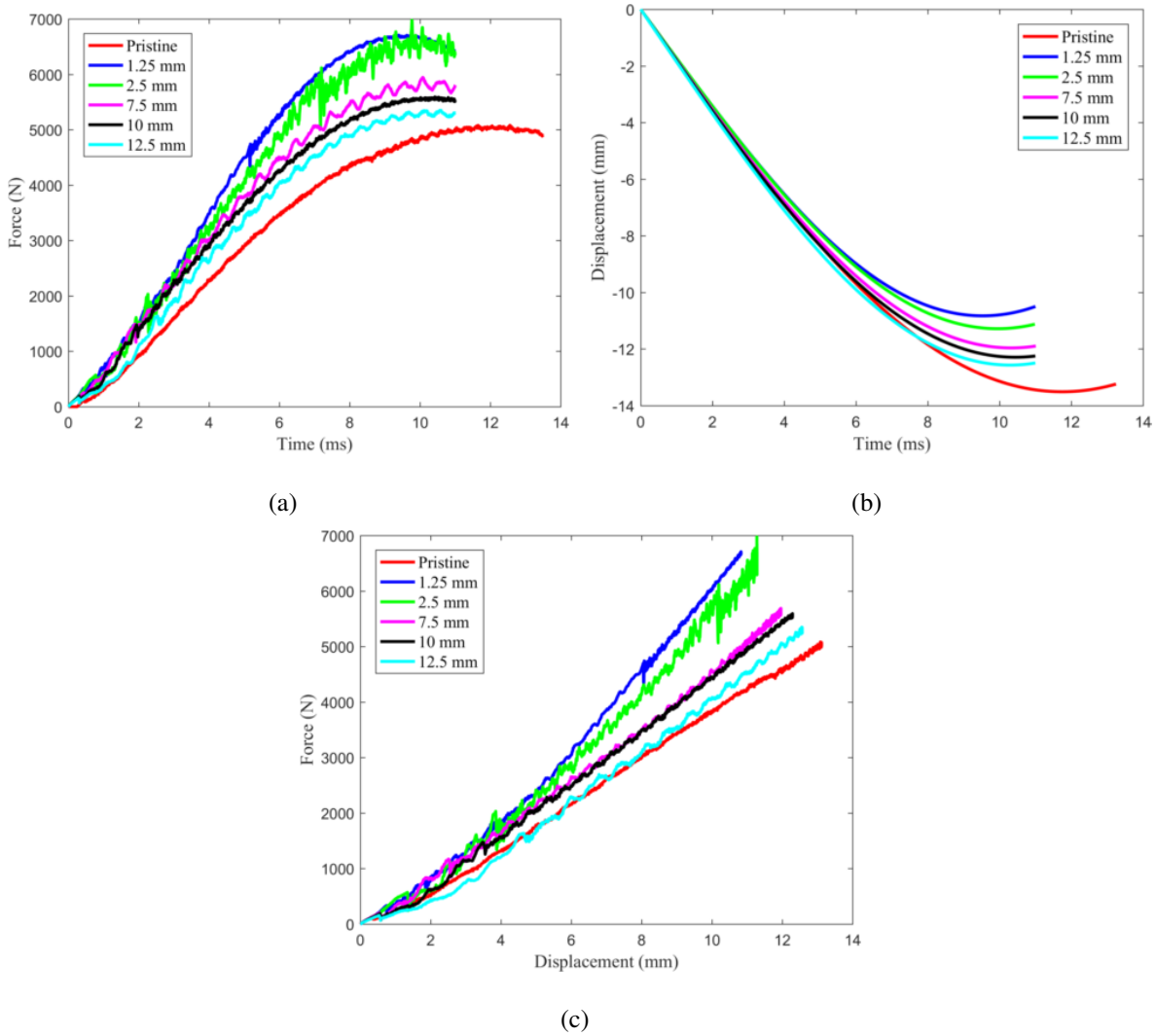

Figure 7.14: Representative responses of a sandwich composite under a low-velocity impact event (7.5 J): (a) Force-time graph; (b) Displacement-time graph; (c) Force-displacement graph

circles), which could act as delamination initiators. For the sample with a 2.5 mm spacing, the resin completely covered the interlaminar reinforcement. Thus 2.5 mm was the selected spacing.

7.3.2 Dynamic Impact Tests

Contact force-time, energy-time, and deformation-time responses were recorded by the data acquisition system of the impact machine for each impact energy (2.5 J, 5 J, 7.5 J and 10 J). In addition, the response of the laminates in terms of visual damage and damage mechanisms were established, which are discussed in detail in the following sections.

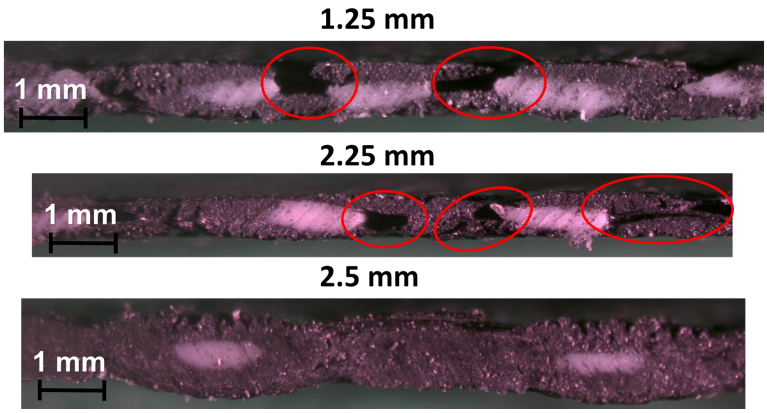

Figure 7.15: Cross-sectional region of a woven carbon/epoxy laminate with different PAM interlaminar reinforcement spacing

7.3.2.1 Contact Force-Displacement Response

Contact of the impact striker with the impacted face of a sandwich composite sample (top facesheet) generates the contact force and deflection during an impact test, which is recorded by the data acquisition system of the impact machine. Typically, contact force-deflection responses have an initial linear ascending region from which the initial bending stiffness [121] is determined. Two characteristic dynamic impact responses are shown in Figure 7.16, where the post-peak regimes upon reaching the maximum contact force have very different behaviors. There can be three possibilities: rebounding, penetration, and perforation of the striker. In Figure 7.16(a), the striker rebounds from the sample upon reaching a maximum contact force. A rebounding case is characterized by a gradual decrease in the displacement while the contact force diminishes to zero. Figure 7.16(b) shows a typical response of a descending regime that combines loading and unloading (rebounding). Here, there is a sudden drop in load after the maximum contact force is reached, which is typically due to damage in the top facesheet (impacted surface), such as fiber fracture, delamination or matrix cracks. This is followed by a small increase in load as the displacement increases, which is due to the crushing of the core by the striker. Finally, the striker rebounds without damaging the bottom facesheet. Figure 7.16(c) shows a representative case of striker penetration, where the striker perforates the top facesheet and the core of the sandwich composites, with no damage in the bottom facesheet. The displacement continues to increase with reduction in

contact force, which implies that there is no rebound. Figure 7.16(d) shows a representative case of perforation of the sandwich composite by the striker. The striker perforates the top facesheet and penetrates the core beyond which the contact force increases resulting in a second peak contact force which is larger than the first. This is attributed to the stiffness of the bottom facesheet which is locally subjected to local in-plane tensile loading. If the bottom facesheet is damaged, a sudden drop in contact force follows the second peak, which is typically due to fiber fracture. This is followed by an increase in displacement with reduction in contact force, which implies complete perforation of the sandwich composite.

For this current work, only the responses of Figure 7.16(a) and Figure 7.16(b) were observed.

7.3.2.2 Contact force-displacement responses

In this section, the contact force-displacement responses were used to characterize the damage caused by an impact event at four different impact energies (2.5 J, 5 J, 7.5 J, and 10 J). Figure 7.17 shows the representative force-displacement response of a sample tested at 7.5 J with and without reinforcement.

A drop in load is seen in both cases upon reaching the maximum contact force, which indicates damage in the top facesheet. This was also accompanied by core crushing, which is indicated by the small increase in the contact force after the first vertical drop in the contact force. The striker rebounded from the specimen with reinforcement (red curve) without further penetration into the sample. The sample without interlaminar reinforcement experienced complete perforation of the top facesheet and penetration of the striker through the foam, which is indicated by a decrease in the contact force with increasing displacement upon core crushing.

7.3.2.3 Absorbed Energy

In addition to the contact force-displacement graphs, the extent of energy absorption and corresponding damage mechanisms presented next are used to characterize the impact behavior of sandwich composites. Figure 7.18 shows the energy-time response of samples tested under an impact energy of 7.5 J with and without reinforcement.

The damage initiation, E_I, is the point where the maximum contact force occurs, beyond which the top facesheet and core are damaged. The maximum impact energy, E_{max}, corresponds to

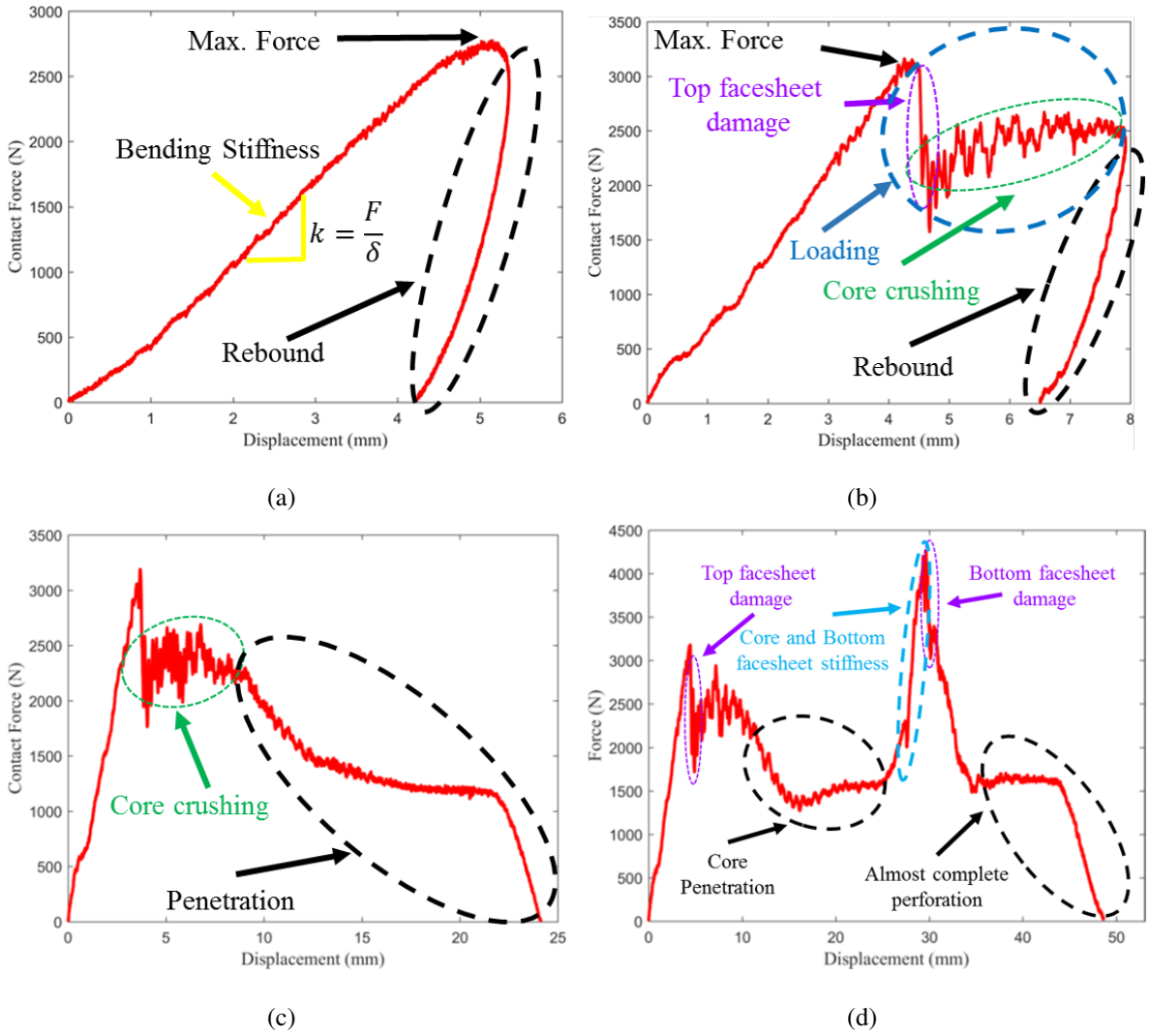

Figure 7.16: Typical load deflection responses of foam core sandwich composites under low-velocity impact loading: (a) Rebounding, (b) Partial loading and rebound, (c) Partial Perforation and (d) Complete Perforation

the impacted energy. The post-peak response labeled as E_{abs} (plateau region) corresponds to the energy absorbed by the sample through internal deformation and damage, which in the case of the both samples was predominantly fiber fracture and core crushing. The difference between E_{max} and E_{abs} is the elastic energy $E_{elastic}$, which is the energy not absorbed by the specimen and is returned to the system by the rebound of the striker. This is the case for the sample with reinforcement. The sample without any reinforcement absorbed all the impacted energy. Thus, this sample experienced more damage.

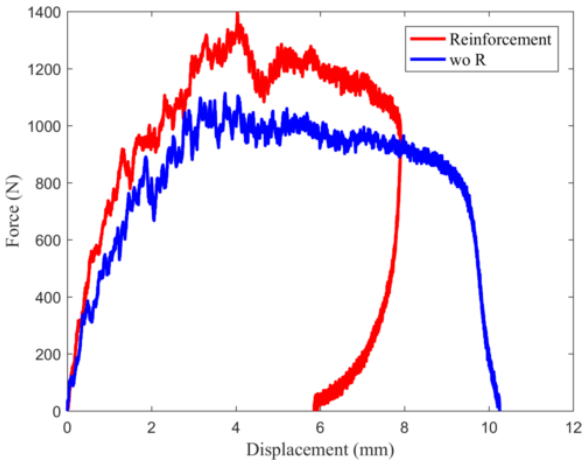

Figure 7.17: Representative force-displacement response of a sample tested at 7.5 J with and without PAM reinforcement

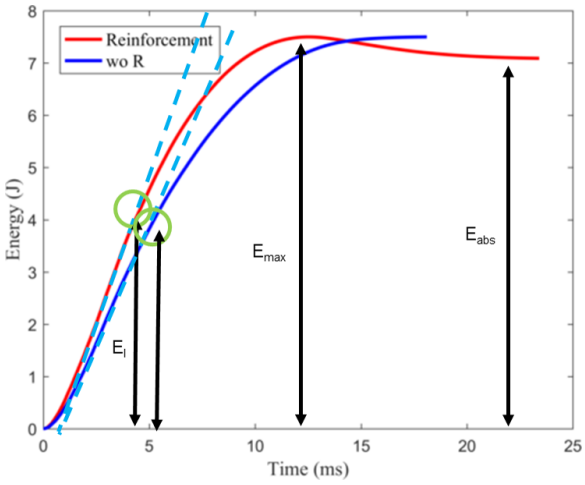

Figure 7.18: Representative energy-time response of a sample tested at 7.5 J with and without PAM reinforcement

7.3.2.4 Damage Mechanisms

Micro-CT scans of the interior regions of samples and optical images of the impacted and back face were obtained to characterize the damage mechanisms in the sandwich composite samples after dynamic impact loading. The cross-sectional views for the samples impacted at 7.5 J with and without reinforcement are shown in Figure 7.19(a) and Figures 7.19(b). The main failure mechanism in both cases was fiber fracture, matrix cracking and delamination a the top facesheet

and localized core crushing/fracture. However, the samples with reinforcement experienced fiber bridging. The bottom facesheet did not exhibit any damage.

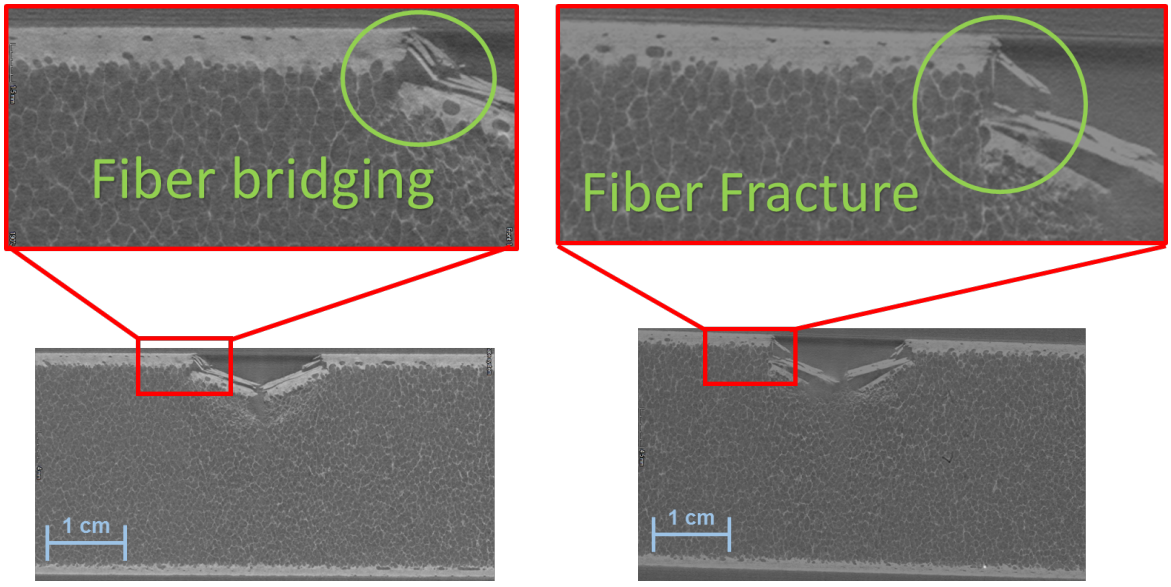

(a) (b)

Figure 7.19: Cross-sectional view of the sandwich composite impacted at 7.5 J: (a) with PAM interlaminar reinforcement; (b) without reinforcement

7.4 Conclusion

Dynamic impact behavior of woven carbon/epoxy composites with interlaminar reinforcement was investigated in this paper in view of increasing the damage tolerance of these sandwich composites for marine, automobile and aerospace applications. Four different impact energies of 2.5 J, 5J, 7.5 J, and 10 J were considered for dynamic impact testing. A computational model was developed to find the optimal PAM reinforcement shape and spacing to mitigate impact damage on the sandwich composites. Critical observations regarding the computational model, printing parameters, contact force, absorbed energy and damage mechanisms were reported and discussed in this paper. Major conclusions are summarized as follows:

1. The interlaminar reinforcement that spread the stresses through the interlaminar regions and reduced stress concentrations were the concentric circles.

2. The peak contact forces reduced with increasing the spacing of the reinforcement.
3. The displacement of the sandwich composite decreased by decreasing the spacing of the reinforcement.
4. The nozzle height selected as Z=0.6 and the Epmm value was 0.027mm.
5. The peak impact force of the sample tested at 7.5 J with PAM reinforcement was higher as compared to the sample tested without reinforcement.
6. Damage mechanisms contributed significantly to the amount of energy absorbed. That is a higher degree of damage manifested for the sample without reinforcement.

In conclusion, PAM interlaminar reinforcement has a significant influence on the dynamic impact behavior of sandwich composites and can increase the damage tolerance of composite structures. This could increase the residual strengths and durability of composite structures.

Chapter 8

Conclusion and Original Contributions

In this thesis, it was addressed the fundamental challenges of damage mitigation, failure mechanisms and life of composites in extreme environments. The low-temperature effects on sandwich composites and facesheets were investigated. The dynamic single and repeated impact behavior of woven carbon/vinyl ester laminates at room (25 °C) and arctic (-50 °C) temperatures were investigated because of the increasing interest in Arctic explorations for future arctic applications. The failure mechanism shifts from matrix failure towards fiber failure at arctic temperature. Even though the measured degree of damage from the impact tests provide lower values at AT as compared to RT, this shift in failure mechanism can have a significant detrimental effect on the residual strengths and durability of the composite. A computational model was developed to predict fiber failure and matrix damage during a single impact on woven carbon/vinyl ester composites. The predictions of the model had good agreement with the experimental results. The model was able to capture fiber fracture, delamination and the "plus sign failure pattern on the laminate. A novel reinforcing for the interlaminar regions (resin-rich regions) by introducing PAM reinforcement in carbon fiber/epoxy composites was proposed. Meaningful improvement in the interlaminar fracture toughness under Mode-I and Mode-II was observed. This new reinforcement does not degrade the in-plane mechanical properties of the laminates as the currently available methods. After that, the dynamic impact behavior of woven carbon/vinyl ester composites at 25 °C, 0 °C, -25 °C and -50 °C was investigated in view of increasing interest in Arctic explorations and the need to characterize these sandwich composites for future arctic applications. The temperature has a significant influence on the dynamic impact behavior and can further have a detrimental effect on the residual strength and durability of lightweight composites. In the last part of the thesis, the dynamic impact behavior of reinforced woven carbon/epoxy composites was investigated in view on increasing

the damage tolerance of lightweight composites. A PAM interlaminar reinforcement pattern was studied to mitigate the damage during a low-velocity impact event. Future suggestions:

1. Further studies to elucidate the influence of other sandwich composite parameters, including composite thickness, varying facesheet/core bonding, stiffness of the core, etc. with varying temperatures and impact energies need to be conducted for reliably using these sandwich composites in low temperatures like the Arctic.

2. Further studies on the impact modeling of woven carbon/vinyl ester composites need to be conducted to account for failure mechanisms such as bending and fiber/matrix crushing.

3. The adhesion of the PAM interlaminar reinforcement with the epoxy can be improved by adding cenospheres that has good affinity with the carbon fiber, such as ZnO.

LIST OF REFERENCES

[1] Fibre Glast Developments Corporation. Prepreg 3k, plain weave carbon fiber 6-months. *Product Data Sheet*, page 1, 2019.

[2] Makeitfrom. Polylactic acid. *Makeitfrom*, page 1, 2019.

[3] S. Kazemahvazi. *Impact Loading of Composite and Sandwich Structures*. KTH, 2010.

[4] E. Barbero. *Introduction to Composite Materials Design*. Taylor & Francis, 6000 Broken Sound Parkway, 1 edition, 1998.

[5] S. Bagherpour. *Polyester*. InTech Prepress, Janeza Trdine 9, 51000 Rijeka, 1 edition, 2012.

[6] A. Kaw. *Mechanics of Composite Materials*. Taylor & Francis Group, 6000 Broken Sound Parkway, 2 edition, 2006.

[7] R.G. Budynas, J.K. Nisbett, and J.E. Shigley. *Shigley's mechanical engineering design*. McGraw-Hill series in mechanical engineering. McGraw-Hill, 2008.

[8] P. Tan, L. Tong, and G. P. Steven. Modelling for predicting the mechanical propertoes of textile composites. *Composites Part A: Applied Science and Manufacturing*, 28(11):903–922, 1997.

[9] D. R. Bortz, C. Merino, and I. Martin-Gullon. Mechanical characterization of hierarchical carbon fiber/nanofiber composite laminates. *Composites: Part A*, 42:1584–1591, 2011.

[10] B. Lars, J. Sumfleth, H. Hedemann, and K. Schulte. Improvement of fatigue life by incorporation of nanoparticles in glass fibre reinforced epoxy. *Composites: Part A*, 41:1419–1424, 2010.

[11] D. Tenney, J. Davis, R. Byron, and N. Johnston. NASA composite materials development: Lessons learned and future challenges. *Conference Paper LF99-9370*, pages 1–58, 2009.

[12] G. Li and N. Jones. Development of rubberized syntatic foam. *Composites: Part A*, 38:1483–1492, 2007.

[13] A. Petras. Design of sandwich structures. *Cambridge University*, 1998.

[14] A. Julias and V. Murali. Effect of carbon fiber position on the impact behavior og glass/carbon fiber hybrid composite laminates. *Internationa Journal of Applied Engineering Research*, 9(26):9103–9106, 2014.

[15] A. Malhotra and F. J. Guild. Impact damage to composite laminates: effect of impact location. *Applied Composite Materials*, 21:165–177, 2014.

[16] R. Karakuzu, E. Erbil, and A. Mehmet. Impact characterization of glass/epoxy composite plates: An experimental and numerical study. *Composites: Part B*, 41:388–395, 2010.

[17] P. O. Sjoblom, J. T. Hartness, and T. M. Cordell. On low-velocity impact testing of composite materials. *Composite Materials*, 22:30–52, 1988.

[18] K.N Shivakumar, W. Elber, and W. Illg. Prediction of impact force and duration due to low velocity impact on circular composite laminates. *Journal of Applied Mechanics*, 52:674–680, 1985.

[19] S.N.A. Safri, M.T.H. Sultan, N. Yidris, and F. Mustapha. Low velocity and high velocity impact test on composite materials - a review. *International Journal of Engineering and Science*, 3(9):50–60, 2014.

[20] S. Abrate. Impact on laminated composites: recent advances. *Applied Mechanics Reviews*, 47(11):517–544, 1994.

[21] V. Caprino, V. Lopresto, C. Scarponi, and G. Briotti. Effect of ZnO nanowire morphology on the interfacial strength of nanowire coated carbon fibers. *Composites Science and Technology*, 59:2279–2286, 1999.

[22] A. Szekrenyes. Overview on the experimental investigations of the fracture toughness in composite materials. *Journal of Engineering materials and technology*, 100:1–19, 2011.

[23] T-W. Shyr and Y-H. Pan. Impact resistance and damage characteristic of composite laminates. *Composite Structures*, 62:193–203, 2003.

[24] S. Babu and H. K. Shivanand. Impact analysis of laminated composite on glass fiber and carbon fiber. *International Journal of Emerging Technology and Advanced Engineering*, 4(6):824–829, 2014.

[25] U.S. Geological Survey. Circum-arctic resource appraisal: Estimates of undiscovered oil and gas north of the arctic circle. *Fact Sheet*, pages 1–4, 2008.

[26] Arctic Councill. Arctic marine shipping assessment. *Report*, pages 1–194, 2009.

[27] A. Krzyzak, M. MAzur, M. Gajewski, K. Drozd, A. Komorek, and P. Przybylek. Sandwich structured composites for aeronautics: methods of manufacturing affecting some mechanical properties. *International Journal of Aerospace Engineering*, pages 1–10, 2016.

[28] J. P. Dempsey. Research trends in ice mechanics. *International Journal of Solids and Structures*, 37:131–153, 2000.

[29] L. Zhu and D. Faulkner. Damage estimate for plating ships and patforms under repeated impacts. *Marine Structures*, 9:697–720, 1996.

[30] V. P. W. Siow, Y. P. Shim. An experimental study of low velocity impact damage in woven fiber composites. *Journal of Composite Materials*, 32:1178–1202, 1998.

[31] D. Liu and L. E. Malvern. Matrix cracking in impacted glass/epoxy plates. *Journal of Composite Materials*, 21:594–609, 1987.

[32] M. T. Sultan, K. Worden, W. J. Staszewski, and A. Hodzic. Impact damage characterization of composite laminates using a statistical approach. *Composite Science Technology*, 72:1108–1120, 2012.

[33] B. I. S. Murat and A. A. A. Rahman. Study of impact damage beahvior in coven carbon fiber plates. *Engineering physics international conference, EPIC 2016*, pages 47–54, 2017.

[34] T. Gomez-del Rio, R. Zaera, E. Barbero, and C. Navarro. Damage in cfrps due to low velocity impact at low temperature. *Composites: Part B*, 36:41–50, 2006.

[35] A.A.M. Badawy. Impact behavior of glass fibers reinforced composite lamnates at different temperatures. *Ain Shams Engineering*, 3:105–111, 2012.

[36] B. M. Icten, C. Atas, M. Aktas, and R. Karakuzu. Low temperature effect on impact response of quasi-isotropic glass/epoxy laminated plates. *Composites Structures*, 91:318–323, 2009.

[37] B. M. Icten. Repeated impact behavior og glass/epoxy laminates. *Polymer Composites*, 30:1545–1715, 2009.

[38] A. Salehi-Khojin, R. Bashirzadeh, M. Mahinfalah, and R. Nakhaei-Jazar. The role of temperature on impact properties of kevlar/fiberglass composite laminates. *Composites: Part B*, 37:593–602, 2006.

[39] L. L. Sobrinho, M. Ferreira, and F. L. Bastian. The effect of water absorption on an ester vinyl resin system. *Materials Research*, 12:353–361, 2009.

[40] A. W. Signor and J. W. Chin. Effects of ultraviolet radiation exposure on vinyl ester matrix resins: chemical and mechanical characterization. *Polymer degradation and stability*, 79:1–12, 2003.

[41] K. Chittajallu. Computational modeling of the vacuum assisted resin transfer molding (VARTM) process. *Thesis Clemson University*, 2004.

[42] ASTM D7136/D7136M-15. . standard test method for measuring the damage resistance of a fiber-reinforced polymer matrix composite to a drop-weight impact event. *Journal of ASTM International D7136/D7136M-15*, pages 1–16, 2015.

[43] W.J. Cantwell and J. Morton. Impact perforation of carbon-fiber reinforced plastics. *Composites Science and Technology*, 38:119–141, 1990.

[44] P. Robinson and G. A. O. Davies. Impactor mass and specimen geometry effects in low velocity impact of laminated composites. *International Journal of Impact Engineering*, 12(2):189–207, 1992.

[45] ASTM D695-15. Standard test method for compressive properties of rigid plastics. *Journal of ASTM International D695-15*, pages 1–8, 2015.

[46] P. K. Dutta. Low-temperature compressive strength of glass-fiber-reinforced polymer composites. *Journal of Offshore Mechanics and Arctic Engineering*, 116:167–172, 1994.

[47] X. X. Chu, Z. W. Wu, R. J. Huang, Y. Zhou, and L. F. Li. Mechanical and thermal expansion properties of glass fibers reinforced peek composites at cryogenic temperatures. *Cryogenics*, 50:84–88, 2010.

[48] R. Garcia, A. G. Castellanos, and P. Prabhakar. Influence of arctic seawater exposure on the flexural behavior of woven carbon/vinyl ester composites. *Journal of Sandwich Structures and Materials*, pages 1–19, 2017.

[49] G. Belingardi and R. Vadori. Influence of the laminate thickness in low velocity impact behavior of composite material plate. *Composiite Structures*, 61:27–38, 2003.

[50] E. Greene. Use of fiber reinforced plastics in the marine industry. *Home-Transport Research International Documentation*, SSC-360, 1990.

[51] S. Selvaraju and S. Illaiyavel. Application of composites in marine industry. *Journal of Engineering Research and Studies*, 2:89–91, 2011.

[52] D. W. Chalmers. The potential for the use of composite materials in marine structures. *Marine Structures*, 7:441–456, 1994.

[53] A. G. Gibson. The cost effective use of fibre reinforced compopsites offshore. *Report for the Health and Safety Executive 2003*, 2003.

[54] *A review on composite materials for offshhore structures*, volume 5 of *Materials Technology*, California, USA, 2014. ASME.

[55] C. Guedes Soares and Y. Garbatov. *Progress in the Analysis and Design of Marine Structures*. Proceedings of the 6th International Conference on Marine Structures (MARSTRUCT 2017). CRC Press/Balkema, 2017.

[56] N. Jones. Recent studies on the response of structures subected to large impact loads. *The Society of Naval Architects and Marine Engineers and the Ship Structure Committee*, pages 1–22, 1993.

[57] N. K. Naik, Y. Chandreshakarkhar, and S. Mduri. Polymer matrix woven fabric composites subjected to low velocity impact: Part i. damage initiation studies. *Journal of Reinforced Plastics and Composites*, 19:912–943, 2000.

[58] G. R. Rajkumar, M. Krishna, H. N. Narasimha, S. C. Sharma, and K. R. Vishnu. Experimental ivestigation of low-velocity repeated impacts on glass fiber metal composites. *Journal of Materials Engineering and Performance*, 21:1485–1490, 2012.

[59] M. Sayer, N. B. Bektas, and O. Sayman. An experimental investigation on the impact behavior of hybrid composite plates. *Composite Structures*, 92:1256–1262, 2010.

[60] S. N. Morais, W. A. Monteiro and J. R.M. d'Almeida. Evaluation of repeated low energy impact damage in carbon-epoxy composite materials. *Composite Structures*, 91:318–323, 2009.

[61] X. K. Li and P. F. Liu. Expperimental analysis of low-velocity impact beaviors of carbon fibre composite laminates. *Journal of Failure Analysis and Prevention*, 17:1126–1130, 2017.

[62] S. Nguyen, T. James, and Ianucci L. Low, medium and high velocity impact on composites. *16th International Conference on Compostite Structures*, pages 1–2, 2016.

[63] B. M. Icten. Low temperature effect on single and repeated impact behavior of woven glass-epoxy composite plates. *Journal of Composite Materials*, 49:1171–1178, 2015.

[64] S. I. Ibekwe, P. F. Mensah, G. Li, S. S. Pang, and M. A. Stubblefield. Impact and post impact response of laminated beam beams at low temperatures. *Composite Structures*, 79:12–17, 2007.

[65] J. Lopez-Puente, R. Zaera, and C. Navarro. The effect of low tempertures on the intermediate and high velocity impact response of cfrps. *Composites: Part B*, 33:559–566, 2002.

[66] K. Im, C. Cha, S. Kim, and I. Yang. Effects of temperature on impact damages in cfrp composite laminates. *Composites: Part B*, 32:669–682, 2001.

[67] ASTM D3039M-17. Standard test method for tensile properties of polymer matrix composite materials. *Journal of ASTM International D3039M-17*, pages 1–13, 2017.

[68] G. Hartwig and S. Knaak. Fibre-epoxy xomposites at low temperatures. *Cryogenics*, pages 639–647, 1984.

[69] M. Kim, S. Kang, C. Kim, and C. Kong. Tensile response of graphite/epoxy composites at low temperatures. *Composite Structures*, 79:84–89, 2007.

[70] X. F. Wang and J. H. Zhao. Monte-carlo simulation to the tensile mechanical behaviors of unidirectional composites at low temperature. *Cryogenics*, pages 683–691, 2001.

[71] J. Bienia, B. Surowska, and P. Jakubczak. Influence of repeated impact on damage growth in fibre reinforced polymer composites. *Maintenance and Reliability*, 17:194–198, 2015.

[72] L. Yusriah, M. Mariatti, and A. A. Bakar. The properties of vinyl ester composites reinforced with different types of woven fabric and hollow phenolic micospheres. *Journal of Reinforced Plastics and Composites*, 29(20):3066–3073, 2010.

[73] P. Sjoblom. Simple design approach against low velociy impact damage. *Proc. 32 SAMPE Symposium*, Anaheim, CA:30–52, 1987.

[74] J. H. Crews and J. R. Reeder. A mixed-mode bending apparatus for delamination testing. *NASA/TM-1000662*, Hampton VA, 1988.

[75] C. Lopes, Z. Gurdal, P. P. Camanho, Maimi, and E. V. Gonzalez. Simulation of low-velocity impact damage on composite laminates. *Conference paper: American Institute of Aeronautics and Astronautics*, pages 1–13, 2009.

[76] A. J. Smiley and R. B. Pipes. Rate effects on mode I interlaminar fracture toughness in composite materials. *Composite Materials*, 21:1–18, 1987.

[77] M. Czabaj and J. Ratcliffe. Comparison of intralaminar and interlaminar mode-I fracture toughness of unidirectional IM7/8552 graphite/epoxy composite. *Durability, Damage Tolerance, and Reliability Branch, NASA Langley Research Center.*, 2012.

[78] R. Marat-Mendes and M. Freitas. DCB, ENF and ECT tests for interlaminar fracture of glass/epoxy unidirectioal laminates. *10th Portuguese Conference on Fracture*, pages 2–12, 2006.

[79] A. Arguelles, J. Vina, A. F. Canteli, M. A. Castrillo, and Bonhomme. Interlaminar crack initiation and growth rate in a carbon-fibre epoxy composite under mode I fatigue loading. *Composites Science and Technology*, 68:2325–2331, 2008.

[80] R. Khan, C. D. Rans, and R. Benedictus. Effect of stress ratio on delamination growth behavior in unidirectional carbon/epoxy under mode I fatigue loading. *Conference Paper*, ICCM International Conferences on Composite Materials:1–11, 2008.

[81] K. O'Brian. Characterization of delamination onset and growth in a composite laminate. *NASA Technical Memorandum*, pages 1–63, 1981.

[82] R. Rikards, F. G. Buchholz, A. K. Bledzki, G. Wacker, and Korjakin. Mode I, mode II and mixed-mode I/II interlaminar fracture toughness of gfrp influenced by fiber surface treatment. *Mechanics of Composite Materials*, 32:1–24, 1996.

[83] K. S. Dransfield, K. J. Lalit, and Y. Mai. On the effects of stitching in CFRPs-I mode I delamination toughness. *Composite Science and Technology*, 58:815–827, 1998.

[84] R. Krueger. The virtual crack closure technique: history, approach and applications. *NASA/CR-2002-211628*, 2002.

[85] S. Prasad, C.S. Venkatesha, and T. Jayaraju. Experimental methods of determining fracture toughness of fiber reinforced polymer composites under various loading conditions. *Journal of Minerals & Materials Characterization & Engineering*, 10:1263–1275, 2011.

[86] P. Robinson and S. Das. Mode-I dcb testing of composite laminates reinforced with z-direction pins: a simple model for the investigation of data reduction strategies. *Engineering Fracture Mechanics*, 71:345–364, 2003.

[87] S. Wicks, W. Wang, M. R. Williams, and B. L. Wardle. Multi-scale interlaminar fracture mechanisms in woven composite laminates reinforced with aligned carbon nanotubes. *Composite Science and Technology*, 100:128–135, 2014.

[88] A.G. Castellanos, Md. S. ISlam, M.A.I Shuvo, Y. Lin, and P. (in press) Prabhakar. Nanowire reinforcement of woven composites for enhancing interlaminar fracture toughess. *Journal of Sandwich Structures and Materials*, Advance online publication:doi:10.1177/1099636216650989, 2016.

[89] J. Ren, K. Kim, and J. Rice. Comparing the fracture toughness of 3-D braided preform composites with z-fiber reinforced laminar composites. *Textile Research Journal*, 81(4):335–343, 2011.

[90] A. P. Mouritz and B. N. Cox. A mechanistic interpretation of the comparative in-plane mechanical properties of 3D woven, stitched and pinned coomposites. *Composites: Part A*, 41:709–728, 2010.

[91] S. Deng, P. Rosso, L. Ye, and K. Firedrich. Interlaminar fracture of cf/ep composites modified with nano-silica. *Solid State Phenomena*, 121-123:1403–1406, 2007.

[92] R. J. Sager, P. J. Klein, D. C. Davis, D. C. Lagoudas, G. L. Warren, and H. Sue. Interlaminar fracture toughness of woven fabric composite laminates with carbon nanotube/epoxy interleaf films. *Wiley Online Library*, DOI 10.1002/app.33479:1–12, 2010.

[93] X. Tian, T. Liu, C. Yang, Q. Wang, and D. Li. Interface and performance of 3D printed continuous carbon fiber reinforced pla composites. *Composites: Part A*, 88:198–205, 2016.

[94] T. Halil, V. Kunc, G. M. Velez-Garcia, C. E. Duty, L. J. Love, A. K. Naskar, and et al. Highly oriented carbon fiber-polymer composites via additive manufacturing. *Composites Science and Technology*, 105:144–150, 2014.

[95] W. Zhong, F. Li, Z. Zhang, L. Song, and Z. Li. Short fiber reinforced composites for fused deposition modeling. *Materials Science and Engineering: A*, 301:125–120, 2001.

[96] Netcomposites. Volume-weight-fraction, Retrieved:2017.

[97] C. L. Nogueira, J. M. Faultstich de Paiva, and M. C. Rezende. Effect of the interfacial adhesin on the tensile and impact properties of carbon fiber reinforced polypropylene matrices. *Mat. Rec*, 8(1), 2003.

[98] ASTM D5528-13. Astm international. standard test method for mode I interlaminar fracture toughness of unidirectional fiber-reinforced polymer matrix composites. *D5528 13*, pages ASTM International, West Conshohocken, PA, DOI: 10.1520/D5528, www.astm.org., 2013.

[99] ASTM D7905/D7905M-14. Astm international. standard test method for mode II interlaminar fracture toughness of unidirectional fiber-reinforced polymer matrix composites. *D7905/D7905M-14*, pages 1–18, 2014.

[100] Y. Zhu. Characterization of interlaminar fracture toughness of a carbon/epoxy composite material. Master's thesis, The Pennsylvania State University, 2009.

[101] C. Makabe, A. Murdani, K. Kuniyoshi, Y. Irei, and A. Saimoto. Crack-growth arrest by redirecting crack growth by drilling holes and inserting pins into them. *Engineering Failure Analysis*, 16:475–483, 2009.

[102] Y. Li and M. Zhou. Prediction of fracture toughness scatter of composite materials. *Computational Materials Science*, 116:44 – 51, 2016. Articles from EUROMECH Colloquium 577 "Micromechanics of Metal Ceramic Composites".

[103] N. Jover, B. Shafiq, and U. Vaidya. Ballitic impact analysis of bala core sandwich composites. *Composites: Part B*, 67:160–169, 2014.

[104] V. L. Tagarielli, V. S. Deshpande, and N. A. Fleck. The dynamic response of composite sandwich beamc to transverse impact. *International Jpurnal of Solids and Structures*, 44:2442–2457, 2008.

[105] L. Torre and J. M. Kenny. Impact testing and simulation of composite sandwich structures for civil transportation. *Composite Structures*, 50:257–267, 2000.

[106] J. Wang, B. Chen, H. Wang, and Waas A. M. Experimental study on the compression-after-impact behavior of foam-core sandwich panels. *Jpurnal of Sandwich Structures and Materials*, 17(4):446–465, 2015.

[107] O. Ozdemir, R. Karakuzu, and A. K. J. Al-shamary. Core-thickness effect on the impact response of sandwich composites with poly(vinyl chloride) and poly(ethylene terephthalate) foam cores. *Journal of Composite Materials*, 49:1315–1329, 2015.

[108] P. M. Schubel, J. Luo, and I. M. Daniel. Low velocity impact behavior of composite sandwich panels. *Composites: Part A*, 36:1389–1396, 2005.

[109] S. B. Loganathan and H. K. Shivanand. Effect of core thickness and core density on low velocity impact behavior of sandwich panels with pu foam core. *Journal of Minerals and Materials Characterization and Engineering*, 3:164–170, 2015.

[110] J. H. Park, S. K. Ha, K. W. Wang, C. W. Kim, and H. S. Kim. Impact damage resistance of sandwich structures subjected to low velocity impact. *Journal ofmaterials processing technology*, 201:425–430, 2008.

[111] S. Gupata and A. Shukla. Blast performance of marine foam core sandwich composites at extreme temperatures. *Experimental Mechanics*, 52:1521–1534, 2012.

[112] Gibson. L. and M. Ashby. *Cellular Solids: Structure and Properties (Cambridge Solid State Science Series)*. Cambridge: Cambridge University Press, 1997.

[113] M. D. Erickson, A. R. Kallmeyer, and K. G Kellogg. Effect of temperature on the low-velocity impact behavior of composite sandwich panels. *Journal of Sandwich Structures and Material*, 7:245–264, 2005.

[114] A. Salehi-Khojin, M. Mahinfalah, R. Bashirzadeh, and B. Freeman. Temperature effects on kevlar/hybrid and carbon fiber composite sandwiches under impact loading. *Composite Structures*, 78:197–206, 2007.

[115] A. G. Castellanos, K. Cinal, K. Guven, and P. Prabhakar. Low-velocity impact response of woven carbon composites in arctic conditions. *Journal of Dynamic Behavior of Materials*, 4:308–316, 2018.

[116] A. G. Castellanos and P. Prabhakar. Durability and failure mechanics of woven carbon composites under repeated impact loading in arctic conditions. *Multiscake annd Multidisciplinary Modeling, Experiments and Design*, 1:157–170, 2018.

[117] M. M. Jamel, P. Khoshnoud, S. Gunashekar, and N. Abu-Zahra. Enhancement of dimensional stability of rigid pvc foams using e-glass fibers. *Journal of Minerals and MAterials Charazterization and Engineering*, 3:65–75, 2015.

[118] ASTM. ASTM D7766/D7766M-16. standard practice for damage resistance testing of sandwich constructions. *Journal of ASTM International D7766/D7766M-16*, pages 1–9, 2016.

[119] B. Yang, Z. Wang, L. Zhou, L. Tong, and W. Liang. Study on the low-velocity impact response and cai behavior of foam-filled sandwich panels with hybrid facesheet. *composite Structures*, 132:1129–1140, 2015.

[120] ASTM. ASTM D3039/D3039M-17.standardd test method for tensile properties of polymer matrix composite materials. *Journal of ASTM International D3039/D3039M-17*, pages 1–13, 2017.

[121] Serge Abrate. *Impact on Composite Structures*. Cambridge University Press, 1998.

[122] A. K. J. Al-Shamary, R. Karakuzu, and O. Ozdemir. Low-velocity imact response of sandiwch composites with different foam core configurations. *Journal of Sandwich Structures and Materials*, 18:754–768, 2016.

[123] C. Atas and C. Sevim. On the impact response of sandwich composites with cores of balsa wood and pvc foam. *Composite Structures*, 93:40–48, 2010.

[124] M. L. Bernard and P. A. Lagace. Impact resistance of composite sandwich plates. *J Reinf Plast Compos*, 8(5):432–45, 1989.

[125] A. Nanayakkara, S. Feih, and A.P. Mouritz. Experimental analysis of the through-thicknes compression properties of z-pinned sandwich composites. *Compos A Appl Sci Manuf*, 42:1673–1680, 2011.

[126] B. Abdi, S. Azwan, and M. R. Abdullah. Flatwise compression and flexural behavior of foam core and polymer pin-reinforced foam core composite snadwich panels. *Int J Mech Sci*, 88:138–144, 2014.

[127] B. Abdi, S. Azwan, and M. R. Abdullah. Comparison of foam core sandwich panel and though-thickness polymer pin-reinforced foam core sandwich panel subjected to indentation and flatwise compression loadings. *Polym Compos*, 37:612–619, 2016.

[128] A. I Marasco, D. D. R. Cartie, and I. K. Partridge. Mechanical properties balance in novel z-pinned sandwich panels: out-of-plane properties. *Compos A Appl Sci Manuf*, 32:295–302, 2006.

[129] B. T. HWallace, B. V. Sankar, and P. G. Ifju. Pin reinforcement of delaminated sandwich beams under axial compression. *J Sandwich Struct Mater*, 3:117–129, 2001.

[130] U. K. Vaidya, M. V. Kamath, and M. Hosur. Low-velocity impact response of cross-ply laminated sandwich composites with hollow and foam-filles z-pin reinforced core. *J compo Technol Res*, 21:84–97, 1999.

[131] F. Han, Y. Yan, and J. Ma. Experimental study and progressive failure analysis of stitched foam-coe sandwich composites subjected to low-velocity impact. *Polym compos*, 39:624–635, 2016.

[132] A. Heano, R. G. De Villoria, and J. Cuartero. Enhanced impact energy absorption characteristic of sandwich composites though tuftiing. *Mech Adv Mater Struct*, 22:1016–1023, 2015.

[133] K. R. Ramakrishnan, S. Guerard, P. Viot, and K. Shankar. Effect of block nano-reinforcement on the low velocity impact response of sandwich structures. *Composite Structures*, 110:174–182, 2010.

[134] A. F. Avila, M. G. R. Carvalho, E. C. Dias, and D. T. L. da Cruz. Nano-structured sandwich composite response to low-velocity impact. *Composite Structures*, 92:745–751, 2010.

[135] P. N. B. Reis, P. Sandtos, J. A. M. Ferreira, and M. O. W. Richardson. Impact response of sandwich composites with nano-enahnced epoxy resin. *Journal of reinforced plastics and composites*, 32:898–906, 2013.

[136] W. Damodaran, A. G. Castellanos, M. Milostan, and P. Prabhakar. Improving the mode-ii interlaminar fracture toughness of polymeric matrix composites though additive manufacturing. *Materials and Design*, 157:60–73, 2018.

[137] M. Jirazek. Lecture notes: Modelling of localized inelastic deformation. *Short course given by Milan Jirazek at the Czech Technical Unve5rsity in Prague*, September 24-28, 2007.